Development of temperature-responsive and photo-reactive polymers for biomedical applications

Mahmoud Hassan Mahmoud Othman

Department of Biological Sciences

Tokyo Metropolitan University

2023

東京都立大学　博士（理学）学位論文（課程博士）

論 文 名: 生医学応用を目指した温度応答性と光反応性高分子の開発 (英文)

著　者: マフムード　ハッサン　マフムード　オスマン

審査担当者

主　査

委　員

委　員

委　員

上記の論文を合格と判定する

年　　月　　日

東京都立大学大学院理学研究科教授会

研究科長

DISSERTATION FOR A DEGREE OF DOCTOR OF PHILOSOPHY IN SCIENCE TOKYO METROPOLITAN UNIVERSITY

TITLE : **Development of temperature-responsive and photo-reactive polymers for biomedical applications**

AUTHOR : Mahmoud Hassan Mahmoud Othman

EXAMINED BY

Examiner in chief

Examiner

Examiner

Examiner

QUALIFIED BY THE GRADUATE SCHOOL OF SCIENCE
TOKYO METROPOLITAN UNIVERSITY

Dean

Date

Table of contents

Abstract

In order to develop devices for biomedical applications, various functional polymers are required. Stimuli-responsiveness is an important property for the design of medical devices. First, as a temperature-responsive material, a hydrogel was prepared using the dynamic covalent bonds (DCBs) of a boronic ester formed by phenylboronic acid (PBA) and the diols of poly(vinyl alcohol) (PVA) through mixing PBA-incorporated nanoparticles (PBA-NPs) with PVA. PBA-NPs underwent three-dimensional (3D)-crosslinking with PVA and exhibited a reversible gel−sol phase transition at 39.7 °C. The phenylboronic acid-diol DCBs were controlled at temperatures slightly higher than body temperature. The prepared thermo-hydrogel is promising for the development of smart materials in biomedical applications.

Secondly, template polymerization was applied for the preparation of strong hydrogel. As the result, PBA-NPs can be fixed inside the hydrogel, to form a strong hydrogel and improve its temperature-dependent viscoelasticity. The NP-type crosslinker with highly efficient conjugation was prepared with backbone polymer (trishydroxymethyacrylamide). The template polymerization was a useful approach for the recombination of crosslinking points of self-healing and thermoplastic smart hydrogels. In this study, the smart hydrogel, with high hysteresis, efficient thermal-plasticity, and self-healing properties was successfully prepared using the DCB-introduced NPs as crosslinkers.

Thirdly, polyethylene glycol (PEG)-grafted photoreactive PEG polymers bearing azidophenyl groups were synthesized and immobilized on the polystyrene surfaces by photoirradiation, for the preparation of anti-biofouling surfaces which are important for biomaterials. The prepared polymers were soluble in water and the photo-immobilization was confirmed by micropatterning using a photomask. The polymers suppressed nonspecific interactions with proteins and cells on the substrate. Considering that photo-immobilization can be applied for covalent bond modification of various surfaces, the water-soluble and highly anti-biofouling polymers will be very useful for biomedical applications.

List of abbreviation

ACMO	4-Acryloylmorpholine
AIBN	2,2′-Azobisisobutyronitrile
Alexa488-IgG	Alexa488-cnjugated immunoglobulin G
APBA	3-(Acrylamido) phenylboronic acid
APS	Ammonium persulfate
ARS	Alizarin red S
AzPEG	Photoreactive PEG-grafted PEG polymer
AzPheEO	4-(Glycidyloxymethyl)azidobenzene
BMA	n-Butyl methacrylate
$CDCl_3$	Chloroform
CPDT	2-Cyano-2-propyl dodecyl trithiocarbonate
CST	Critical-solution temperature
D–A reaction	Diels–Alder reaction
DCB	Dynamic covalent bond
DDS	Drug delivery systems
DLS	Dynamic light scattering
DMAPAAm	N,N-dimethylaminopropyl acrylamide
DSC	Differential scanning calorimetry
DTC	Dodecyltrithiocarbonate
EO	Ethylene oxide
FBS	Fetal bovine serum
G′	Storage modulus
G″	Fluidity modulus
GPC	Gel permeation chromatography
i-Bu_3Al	Triisobutyl aluminum
LCST	Lower critical-solution temperature
MixGel(NP)	Nanoparticle crosslinker mixed hydrogel
mPEG-EPO	Methoxy-PEG epoxide
NIPAAm	N-isopropyl acrylamide
NPs	Nanoparticles
PBA	Phenylboronic acid
PBMA	Poly(n-Butyl methacrylate)

PDMAPAAm	Poly(N,N-dimethylaminopropyl acrylamide)
PEG	Polyethylene glycol
PVA	Poly(vinyl alcohol)
RAFT	Reversible addition-fragmentation chain transfer
SEM	Scanning electron microscopy
TBAB	Tetrabutylammonium bromide
TCEP	Tris(2-carboxyethyl) phosphine hydrochloride
TDCB	Thermal-responsive dynamic covalent bond
TEM	Transmission electron microscopy
TEMED	N,N,N′,N′-tetramethyl ethylenediamine
TempGel(LN)	Linear crosslinker template polymerized hydrogel
TempGel(NP)	Nanoparticle crosslinker template polymerized hydrogel
THMAAm	N-[Tris(hydroxymethyl)methyl]acrylamide
3D	Three dimensional
UCST	Upper critical-solution temperature
UV	Ultraviolet

CHAPTER I

GENERAL INTRODUCTION

1. Stimuli-responsive polymers

Stimuli-responsive polymers have raised major attention in digital technology, sensors, and biomedical applications owing to their quick response towards external stimuli, for example, light, voltage, pressure, temperature, mechanical friction, and pH. Nevertheless, the action of external stimuli on organic materials affects their internal physicochemical properties and facilitates improved thermal/photostability, tuning detection sensitivity, accuracy, and biocompatibility. They show a dramatic change in their physical and/or chemical properties upon exposure to external stimuli. This unique and interesting property allows them to be applied in smart and intelligent responsive materials [1].

In general, stimuli can be classified into three categories: physical, chemical, and biochemical. Physical stimuli usually alter chain dynamics, including temperature, light, magnetic stress, and ultrasound. Chemical stimuli such as pH, redox, and ionic strength modulate molecular interactions. Some examples of biological stimuli include enzymes, proteins, ligands, and glucose [2].

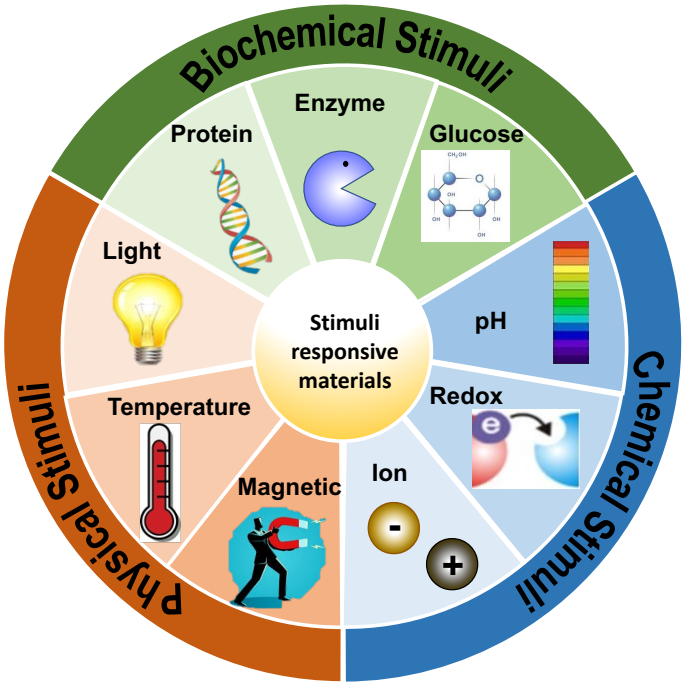

Figure 1. Classification of stimuli based on physical, chemical, and biochemical triggers

Traditional organic polymer-based materials have shown great applications in sensors and digital technologies during the past few decades. These polymers are found to be non-renewable and resistant to environmental changes due to the presence of irreversible covalent bonds. As a result, it is more practicable to alter the intrinsic properties of polymers by external

stimuli, making them suitable for use in artificial machines, biocomputers, and medicinal applications [3].

The "Stimuli" phenomenon is ubiquitous in current technology because tuning the physicochemical properties affects the electronic nature of materials thereby improving the detection sensitivity and biocompatibility for *in-vitro/vivo* clinical testing [4]. Nonetheless, stimuli-responsive polymers exhibit miscellaneous applications such as memory devices, drug delivery/release, and electrochromic/photochromic materials that respond to external stimuli in an intelligent manner [5]. For example, pressure, temperature, light, mechanical friction, and chemical stimulus are utilized for the generation of mixed valence species, viologens formation, sol-gel transformation, and varying pH of the smart materials [6,7].

Considering the biomedical fields, temperature variations can be applied through thermal heating or photoillumination. Contrary to other stimuli like changes in pH and redox potential, these strategies do not involve altering the medium composition. Because of this, temperature-responsive polymers are the ideal choice when the stimulus needs to be delivered artificially rather than by utilizing the particular characteristics of the targeted tissues or organs [8]. Photo-technology significantly contributes to multifield including biotechnology and the manufacturing of medical devices. By using the photo-immobilization method, various types of biological components can be immobilized on the surface. The applications of photo-sensitive polymers for biomaterials to create bio-inactive and bioactive surfaces that provide a platform for the fabrication of new biomaterials for surface modifications, including immobilization, functionalization, and modification [2].

2. Temperature-responsive polymers

Among the several stimuli, the temperature is the most versatile stimulus for medical and engineering applications. Temperature-responsive polymers are very useful in biomaterial applications since the average human body temperature is constantly about 37 °C. Additionally, because it is so simple to adjust the external temperature using a variety of heating devices, the temperature is a stimulus that is used frequently in the biomedical sector [8].

Temperature-responsive polymers exhibit a phase transition temperature in correspondence with which a drastic change in solubility occurs. Temperature-responsive polymers exhibit a unique property called critical-solution temperature (CST). Typically, there are two critical-solution temperatures: the upper critical-solution temperature (UCST) and the lower critical-solution temperature (LCST). Thermo-responsive polymers that show a UCST

behavior are less common compared to the LCST ones because of their higher sensitivity to environmental properties such as ionic strength and concentration [9].

The LCST is the temperature at which phase separation occurs. Among water-soluble temperature-responsive polymers, those showing an LCST are the most common. Polymers exhibiting LCST can suddenly change their hydrophilicity at a certain temperature, which can be explained based on hydrogen bonding between the polymer chain and the surrounding water molecules. However, when the temperature is increased, the hydrogen bonds weaken and the polymer chains begin to dehydrate, resulting in the aggregation of polymer chains. Moreover, above the LCST, the hydrogen bonding between polymers and water becomes unfavorable, and a transition occurs and quickly dehydrates and changes into a hydrophobic. For example, the temperature-responsive polymer, Poly(N-isopropyl acrylamide) (PNIPAAm) exhibits an LCST behavior at 32 °C. It has been widely studied because its LCST is close to the body temperature [9,10].

2.1. Medical applications of temperature-responsive polymers

In the last few decades, temperature-responsive polymers have recently come under increasing consideration for their use in the biomedical field as nanovectors for controlled drug delivery, scaffolds promoting cell growth, and biomedical hydrogels. Thus, they impart a “smart” behavior to the final product to give it a specific dynamic and an advanced function [8].

One of the most extensively studied applications of thermo-responsive polymers in the biomedical area is the development of “smart” micelles to encapsulate pharmaceuticals and control their release both in space and time. The instability of the thermo-responsive micelles in response to temperature accelerates the release rate of the payload. This technique may be utilized to conveniently localize the medicine release to the target tissue. This would increase the bioavailability of the drugs and minimize the side effects connected with taking drugs that are encapsulated [11–14].

Examples are given by temperature-responsive polymers for the formulation and controlled release of therapeutics. These devices can be in the form of nanoparticles (NPs) for intravenous administration [15,16], microparticles for oral delivery [17,18], and hydrogels for subcutaneous and localized delivery [19–21]. The aim in each situation is to adjust the pharmacokinetics and pharmacodynamics of the payload to keep its concentration between therapeutic and toxic levels. By doing so, both repeated administrations and undesirable side effects would be avoided, and patient compliance would increase [22]. In particular, medical

treatments, such as cartilage regeneration and support, which were considered extreme complications, have become feasible thanks to the advance of these temperature-responsive materials. As an example, a thermo-responsive formulation of doxorubicin has reached Phase I and II clinical trials [23].

Recently, thermo-responsive polymers are utilized for thermo-responsive surfaces for cell culture. Cell sheet engineering enables the growth of continuous cell films that can be further layered to obtain tissue-like and organ-like structures. Numerous studies have shown that cell sheet transplantation is superior to single-cell injection in the treatment of a variety of illnesses, including lung air leak sealants, limbal stem-cell deficiency, bone fractures, and cardiac repair [24–27]. A new development in the field consists of the exploitation of thermo-responsive modified microcarriers for the smart culturing of cells in 3D. Microcarriers provide a higher specific surface compared to conventional 2D cell culture and make the culturing process easier to monitor, favoring the scaling up to industrial processes. The functionalized microcarriers offered the perfect environment for cell growth, and the cells multiplied similarly kinetically to the control group while maintaining high viability [28].

The unique properties and versatile tailored structures of temperature-responsive polymers allow them to be applied in a wide range of biomedical fields for various applications, including drug delivery, biosensing, and tissue engineering, and for fabricating wound-healing hydrogels [22].

2.2. Temperature-responsive polymers for preparation of thermo-hydrogels

One of the most important medical applications of temperature-responsive polymers is the preparation of temperature-responsive hydrogels. Hydrogel is a hydrophilic polymer with a three-dimensional crosslink network. It can absorb the surrounding water from 10 percent to a thousand times its net weight without degrading. Hydrogel has unique properties that make it resemble human soft tissues even though it is technically neither a solid nor a liquid. These characteristics include the capacity to maintain volume and shape like a solid while also exhibiting solute diffusion and liquid exchange. As a result, the hydrogel has become one of the most popular subjects in the modern biomedical research [29]. Traditional hydrogels are typically crosslinked chemically or physically from their crosslinking structure (e.g., hydrogen bonds, π-π stacking force, hydrophobic effect, electrostatic interaction, molecular chain winding, etc) or chemical crosslinking (i.e., crosslinking via covalent bonds) [30].

Physically crosslinked hydrogels utilize weak intermolecular forces and are randomly arranged at crosslinking points, so they are structurally unstable and have poor mechanical properties [31].

Chemical crosslinking, as opposed to physical crosslinking, significantly enhances the stability and mechanical properties of hydrogels by introducing strong homogeneous covalent bonds; however, these bonds cannot be recovered spontaneously after being irreversibly broken. Therefore, their life span expectancy is drastically reduced due to the structural irreversibility [32].

In both cases, the main drawback is their irreversibility, which prevents a non-invasive subcutaneous application or the easy recovery of the cells when these gels are used as scaffolds for cell housing [33].

In addition, numerous drawbacks such as lack of robustness, lethargic response, weak gesture recognition, and limited capability to self-healing properties in the temperature-responsive polymeric-based hydrogel. Moreover, sensitivity and stability are the important parameters that determine the temperature response of action. Consequently, the latest development in material and biological areas of temperature response hydrogels and their applications suggest that research progress in this area helps to resolve the existing issues/drawbacks and find the solutions for futuristic challenges such as improvement in sensing performance, enhanced stability, better exploitation of self-healing for biomedical applications [34,35].

In the case of conventional thermo-responsive polymers such as PNIPAAm, a significant drawback is the broad hysteresis between the heating and the cooling behaviors, justified by the formation of intramolecular hydrogen bonds after the polymer collapse above the transition temperature, which in turn hampers the polymer rehydration and dispersion when the temperature is lowered [36,37]. Additionally, PNIPAAm notoriously shows acute cytotoxicity, which requires a careful purification of the synthesized polymer, especially when aimed at biomedical applications [38,39]. These aspects are currently limiting the interest towards PNIPAAm, in favor of other categories of thermo-responsive biomaterials.

I can solve these current drawbacks, enhance the thermo-sensitivity, and improve the stability as well as the self-healing of hydrogels by applying dynamic covalent bonds (DCBs).

2.3. Dynamic covalent bonds (DCBs) for the advancement of hydrogels

Dynamic covalent bonding (DCB) can endow hydrogels with very special characteristics, such as self-healing, responsiveness, injectability, and mechanical strength recoverability. DCBs conceived to be applied in various biomedical areas own not only the sensitivity and reversibility but also the improved stability and prolonged life span of the hydrogel [32].

Dynamic bonds reversibly break and reform, which can occur autonomously or in response to external stimuli (Figure 2). DCBs are usually static at ambient conditions but dynamic under stimuli such as light, temperature, or pH. As a result, polymeric materials with DCBs are both robust and adaptable. The dynamic nature of these bonds has been used in organic synthesis, material science, and biomedical applications [40].

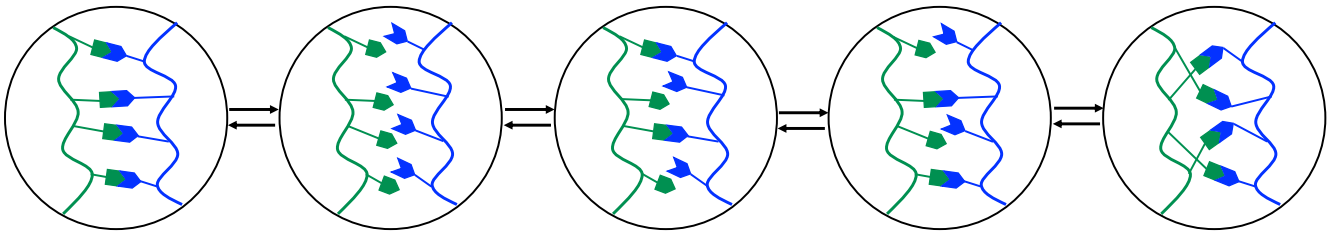

Figure 2. Dynamic association/dissociation equilibrium of the crosslinks upon application of external stimuli

Thermal-responsive dynamic covalent bonds (TDCBs) have received significant interest over the past decade. These are covalent bonds, which are capable of exchanging or switching between several molecules by temperature changes. Particular focus has recently been on utilizing these TDCBs in polymeric materials. Polymer materials gain strong thermoresponsive properties when TDCBs are added to them. These properties include self-healing capacity, shape memory, increased toughness, capacity to relax stresses, and capacity to switch from one macromolecular architecture to another [41].

Recently, many advances in polymeric materials containing TDCBs have been developed, introducing unprecedented properties such as malleability, self-healing, shape-memory, adaptability, stress relaxation, and responsiveness [42,43]. Due to the ability to tune the response of TDCBs and the resulting structure through specific chemistry, various TDCBs have been integrated into macromolecules and materials. Interestingly, many of these bonds are formed via widely known simple organic reactions, which are often “click” in nature [41].

Self-healing and responsiveness make the TDCB-based hydrogels unique, which lay the foundation for the relations between TDCB hydrogels and their biomedical application prospects. Additionally, these characteristics are correlated in some way with the physiological or pathological surroundings of the human body. Therefore, it is still an intriguing topic to research how to use these qualities to promote the actual application [44]. Moreover, TDCB improves the self-healing capability that makes the TDCB-based hydrogel injectable, which is of great significance considering its application [45,46].

However, considering the biomedical applications, the thermal dissociation of TDCB is difficult to achieve in mild conditions because high temperature is generally required to dissociate these bonds (e.g., ester bond (> 100 °C). Moreover, covalent bonds that dissociate at low temperatures (e.g., azo and peroxide bonds) are generally unstable. Therefore, a stable thermal cleavage bond that dissociates under a mild environment such as body temperature is extremely difficult to develop [45]. Furthermore, the unexpected exchange of TDCBs facilitates these materials often being unstable and they can creep [46].

Therefore, in this study, I developed a new thermal-cleavage polymer using boronic ester dynamic covalent bonding (PBA-DCB). The PBA-DCB-based polymer was applied for the fabrication of thermo-responsive hydrogel that dissociates at a mild temperature near body temperature. The prepared smart hydrogel can be promising for the development of many applications in several biomedical fields.

3. Photo-responsive polymers

Light is another important external stimulus because it can be precisely controlled in terms of its wavelength and intensity, which affects the electronic properties of photoresponsive systems. Additionally, light exhibits an ability as restricted to time and area of interest and is essential to trigger the dynamic photo-switching process due to the generation of photoinduced radicals. The chromophore attached to the system also contributes to photoisomerization and polymerization. Azobenzene, spiropyran, o-nitrobenzoyl esters, and diarylethene have all been widely applied up to this point. Additionally, smart materials with shape memory capabilities have been produced, allowing them to return to their initial state when the characteristics used in photo-actuators, sensors, microfluidic chips, and bioseparations are modulated [47,48].

Light stimulus is beneficial in polymer chemistry because it can induce various physicochemical changes in polymers. It enables bond formation, degradation, functionalization, and structural change of polymers, and even brings out a response from smart materials. The most distinctive advantage of light stimulus is that it can be applied instantaneously with high accuracy. In addition, temporal control can be achieved by simply switching the light on and off as required. Owing to the distinctive properties imparted by the spatiotemporal control of gels, photoreactions are widely used in numerous applications varying from lithography to *in-vivo* polymerized biomedical applications [49]. Light is also a noncontact and noninvasive stimulus. Hence, it affords easier access to body parts such as the eyes and skin as a transdermal DDS [50].

To design the photo-responsive polymers, a photo-responsive or photo-reactive functional group is needed to be introduced into polymer chains. Depending on the type of the photoreactive group, the photoresponsive system can be classified into a reversible or irreversible (photo-reactive) system. Several photo-sensitive moieties, such as o-nitrobenzylesters, may undergo irreversible transformations during irradiation, whereas others can react reversibly (e.g., azobenzenes) [51].

Photoreaction is considered an effective method to prepare a polymer-coated surface through grafting. The photo-reactive polymers can react with light stimuli and can easily and covalently immobilize various types of organic molecules and biomolecules on the surface. Photoimmobilization enables random immobilization of all molecules; hence, the activity of such an immobilized surface can be calculated by determining the average of each immobilized molecule [51,52].

Azidophenyl groups have gained considerable attention because of their high reactivity. UV light irradiation of azidophenyl groups generates nitrenes, which react with various organic materials to form covalent bonds (Figure 3). Highly active nitrene molecules can react with saturated or unsaturated hydrocarbon chains or undergo cycloaddition reactions with alkynes. Hence, azidophenyl groups are useful for application in the fields of chemistry and material science for preparing functionalized surfaces. For example, a methacrylate-based polymer containing an azidophenyl group in the side chains was prepared for a photo-immobilized surface modification [50].

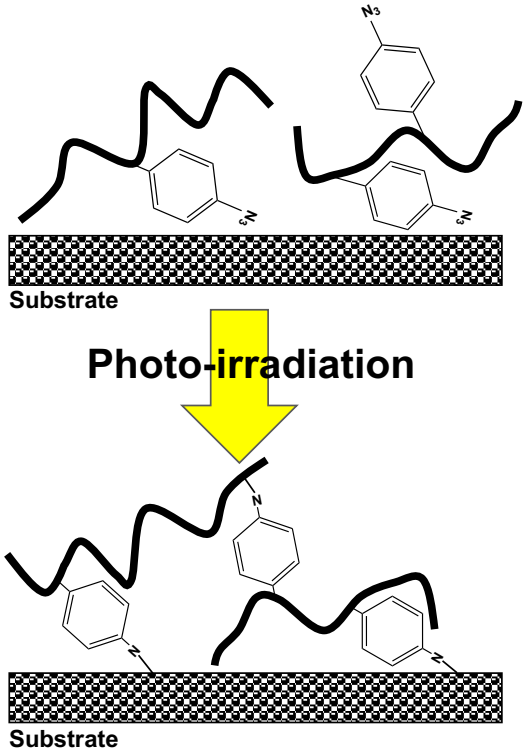

Figure 3. Photoimmobilization of azidophenyl group containing polymers

3.1. Medical applications of photo-reactive polymers

Photo-reactive polymers are being widely utilized and continuously developed for a variety of biological and medical applications. In fact, they have revolutionized the field of medicine, including the subject areas of oncology, molecular biology, drug delivery, and surgery. For instance, photo-reactive polymers used to create bioadhesives and biosealants have made significant progress. In general, the amount of light delivered can be used to regulate the degree of crosslinking, and the light can be turned off to halt the process. For example, they offer the potential to be used as a tissue sealant in situ during surgery [53].

In the development of drug delivery systems, photo-reactive polymers have been exploited for the encapsulation of drugs in matrices as well as their photo-controlled release. photo-reactive polymers can be used for both "targeted release," in which the space is regulated, and the other is "controlled release," wherein materials are regulated in response to time [54–56]. Additionally, for preparation of photo-cross-linkable hydrogels which can be utilized as localized drug delivery depots, cell encapsulation materials, and tissue engineering scaffolds [57]. One of the distinct applications in this field is the fabrication of medical microdevices [58,59].

Photo-reactive polymers are utilized to prepare a wide variety of materials that have been studied in terms of diagnostic purposes, as well as therapeutic purposes. All these types of materials have been examined chiefly for cancer treatments (be they therapeutic, diagnostic, or both) such as dendrimers [60], liposomes [61], and polymeric micelles [62].

The photo-immobilization has been used for the immobilization of various photo-reactive polymers on various substrates extending from protein immobilization to cell and virus immobilizations [63]. Another good example is various types of allergen microarrays that have been prepared [64]. The detection of autoantibodies that act as diagnostic markers, surrogate markers, and prognostic factors has also been used to characterize autoimmune diseases like rheumatoid arthritis, multiple sclerosis, and autoimmune diabetes through autoantigen microarray technology [65].

Additionally, an important biomedical application of photo-reactive polymers is the preparation of biologically active surfaces. These surfaces have been used for cell adhesion enhancement [66] and also have been utilized for cell growth enhancement through immobilization of growth factors [67,68].

3.2. Photo-reactive polymers as antibiofouling agents

Fouling is an undesirable adhesion of molecules, living organisms, and suspended particles on a surface. It is a serious issue in many industries, including marine, food, and medical industries, and causes problems such as high energy consumption and high maintenance costs [69]. Fouling becomes even more serious for biomedical applications because it can cause various health problems. Nonspecific interactions are also a problem because they reduce the sensitivity of biosensors and affect the efficiency of microarray chips and diagnostic systems. In addition, protein adhesion caused by nonspecific interactions between biological components and the device surface is another major problem in the development of blood-

contacting biomaterials and medical devices. These issues may result in the formation of a thrombus, which leads to platelet formation and ultimately to the failure of the implanted device failures and fatal complications [70].

Advanced polymer synthesis and technologies have enabled the development of several polymer-coating methods to fabricate antifouling surfaces. Surface coating using has been widely used to prevent biofouling in medical devices and implants. Surface modification, immobilization, and functionalization can be achieved [50,71].

Because biofouling is mediated by proteins, prevention of protein adsorption has been proposed as an effective solution to the biofouling [72]. Many antifouling strategies have been developed, which can be categorized into three groups: fouling-degrading/killing, fouling-release, and fouling-resistant [73,74] (Figure 4). Initially, antifouling systems were designed to have antimicrobial properties, which can be explained as a fouling-degrading mechanism. It uses biocides or antibacterial materials, such as silver nanoparticles or quaternary ammonium compounds, which can kill microorganisms. However, due to the complicated, time-consuming synthetic conditions and high cost, it remains a challenge to create an efficient antimicrobial surface for the anti-biofouling [75]. In addition, the disadvantages such as biocompatibility and biosafety, and stability have not been further studied [76]. The fouling-release mechanism requires the application of external force which require expensive techniques and uncontrollable leaching of microbial growth and multiplication [69]. Thus, the fouling-resistant should be considered a superior strategy and has gained significant attention for antibiofouling surface modifications.

A PEG-coated hydrophilic surface is the most common example of a fouling-resistant. The PEG-coated surface shows resistance to protein adsorption because of the low interfacial energy between the polymer and water. The ethylene glycol repeating unit in the PEG chain can strongly bind to water molecules and form a highly hydrated water layer that hinders the approaching protein and other biomolecules. When a protein approaches the hydrated layer, the compression of the layer decreases the entropy of the polymer chains, resulting in the

repulsion of the approaching proteins. The high mobility of the PEG chain also contributes to the overall antifouling properties [50,77].

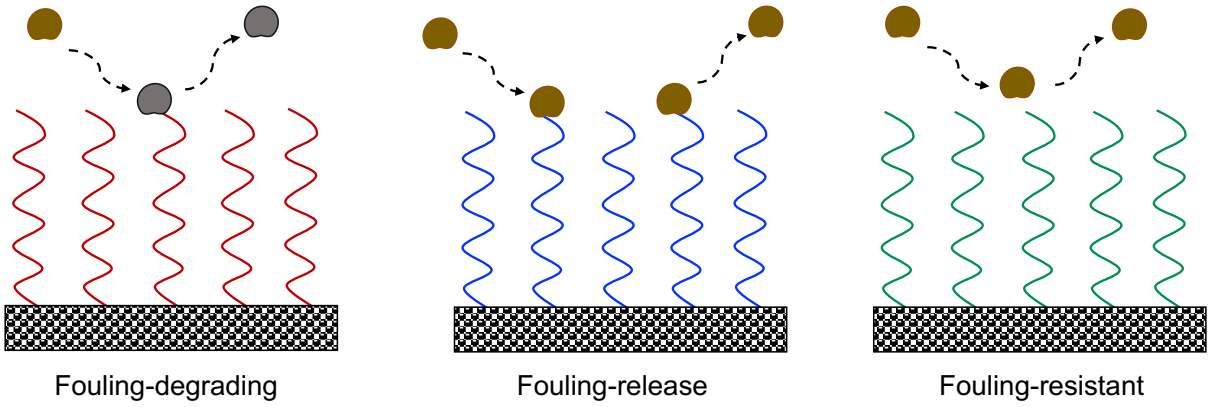

Figure 4. Illustration of antifouling strategies based on different mechanisms

Photoimmobilization is considered an effective method to prepare a polymer-coated anti-biofouling surface modification. The photoreactive PEG can react with light stimuli and can easily covalently immobilize various types of organic molecules and biomolecules on the surface [49,51,78,79].

In a previous study, methacrylate-PEG and acryloyl 4-azidobenzene were copolymerized to create photo-reactive PEG. However, the water solubility of these polymers was relatively low due to the minor hydrophilicity of the polymethacrylate backbone, and it further declines as the number of azidophenyl groups increases [50,80]. In order to increase the water solubility and photoreactivity, coimmobilization with PEG-carrying ethylene oxide was done in this thesis. The resulting antibiofouling properties were then investigated. The created photo-reactive grafted PEG polymer can therefore be used for surface modification in biomedical applications because it has desirable antibiofouling properties.

4. Objectives and outlines

The objectives of this study were to design and synthesize new stimuli-responsive and fabricate stimuli-reactive polymers, which can provide a platform for the development of new biomaterials. For this purpose, temperature-responsive and photo-reactive polymers were designed and synthesized, and their properties were evaluated for their potential biomedical applications.

The first target was the preparation of temperature-responsive systems. As mentioned earlier in this chapter, a stable thermal cleavage bond that dissociates under a mild environment such as body temperature is extremely difficult to develop. This is because a higher temperature is generally required to dissociate covalent bonds (> 100 °C). Moreover, bonds that dissociate at low temperatures are generally unstable. Furthermore, the acute cytotoxicity of conventional temperature-responsive polymers such as PNIPAAm polymer. These aspects are currently limiting the interest towards conventional thermo-responsive polymers in favor of other categories of thermo-responsive materials especially when aimed at biomedical applications. In addition, numerous drawbacks such as lack of robustness, lethargic response, weak gesture recognition, and limited capability to self-healing properties in the temperature-responsive polymeric-based hydrogel.

In this study, I solved these current drawbacks, enhanced the sensitivity and stability, and improved the self-healing of hydrogels by applying DCB. DCB endows hydrogels with very special characteristics, such as self-healing, responsiveness, injectability, and mechanical strength recoverability. I described the design and synthesis of temperature-responsive polymers using boronic ester dynamic covalent bonding. The DCB-based polymers were applied for the fabrication of thermo-responsive hydrogel that dissociated at a mild temperature near body temperature.

To meet the practical requirements in biomedical applications such as drug delivery, wound dressing, tissue engineering, 3D cell culture, biosensors, and others, DCB hydrogels are being built. DCB hydrogels may be the next paradigm as a result of their demand-oriented design.

The next target was the preparation of photo-reactive polymers. In some previous studies, photo-reactive PEG was synthesized via the copolymerization of methacrylate-PEG and acryloyl 4-azidobenzene. However, owing to the low hydrophilicity of the polymethacrylate backbone and the hydrophobic nature of the azidophenyl group, the water solubility of these polymers is low and decreases further upon an increase in the number of

azidophenyl groups. These aspects are currently limiting the effective surface modification and lowering the antibiofouling-capabilities of azidophenyl-containing polymers.

In this study, to enhance the water solubility thus enhancing the surface coating and anti-biofouling effect, I designed azidophenyl-modified and PEG-grafted PEGs as photoreactive polymers for surface anti-biofouling modifications. The PEG-grafted photo-reactive polymers were successfully synthesized and significantly reduced the interactions with biological components, such as proteins and cells. Hence, PEG-grafted photo-reactive polymers, with desirable antibiofouling properties, can be used for surface modification in biomedical applications.

Finally, this thesis discusses the application of the polymeric material developed and provides a platform for the fabrication of new materials based on stimuli-responsive and stimuli-reactive polymers. This study demonstrated the advantages of thermal and photo-induced systems for future biomedical applications. Each system can be used as a temperature-responsive polymer for developing self-healing hydrogels and photo-reactive polymers for surface chemistry, including immobilization, functionalization, and modification.

5. References

1. Mrinalini, M.; Prasanthkumar, S. Recent Advances on Stimuli-responsive Smart Materials and Their Applications. *Chempluschem* 2019, *84*, 1103–1121.
2. El-Husseiny, H.M.; Mady, E.A.; Hamabe, L.; Abugomaa, A.; Shimada, K.; Yoshida, T.; Tanaka, T.; Yokoi, A.; Elbadawy, M.; Tanaka, R. Smart/Stimuli-Responsive Hydrogels: Cutting-Edge Platforms for Tissue Engineering and Other Biomedical Applications. *Mater. Today Bio* 2022, *13*, 100186.
3. Stupp, S.I.; LeBonheur, V.; Walker, K.; Li, L.-S.; Huggins, K.E.; Keser, M.; Amstutz, A. Supramolecular Materials: Self-Organized Nanostructures. *Science (80-.).* 1997, *276*, 384–389.
4. Huang, F.; Zhang, X.; Tang, B.Z. Stimuli-Responsive Materials: A Web Themed Collection. *Mater. Chem. Front.* 2019, *3*, 10–11.
5. á Zhang, X.; á Chen, L.; á Lim, K.H.; á Gonuguntla, S.; á Lim, K.W. D. ÁPranantyo, WP ÁYong, WJT ÁYam, Z. ÁLow, WJ ÁTeo, HP ÁNien, QW ÁLoh, S. ÁSoh. *Adv. Mater* 2019, *31*, 1804540.
6. Theato, P.; Sumerlin, B.S.; O'Reilly, R.K.; Epps III, T.H. Stimuli Responsive Materials. *Chem. Soc. Rev.* 2013, *42*, 7055–7056.
7. Yan, X.; Wang, F.; Zheng, B.; Huang, F. Stimuli-Responsive Supramolecular Polymeric Materials. *Chem. Soc. Rev.* 2012, *41*, 6042–6065.
8. Sponchioni, M.; Palmiero, U.C.; Moscatelli, D. Thermo-Responsive Polymers: Applications of Smart Materials in Drug Delivery and Tissue Engineering. *Mater. Sci. Eng. C* 2019, *102*, 589–605.
9. Seuring, J.; Agarwal, S. Polymers with Upper Critical Solution Temperature in Aqueous Solution. *Macromol. Rapid Commun.* 2012, *33*, 1898–1920.
10. Roy, D.; Brooks, W.L.A.; Sumerlin, B.S. New Directions in Thermoresponsive Polymers. *Chem. Soc. Rev.* 2013, *42*, 7214–7243.
11. Bae, K.H.; Choi, S.H.; Park, S.Y.; Lee, Y.; Park, T.G. Thermosensitive Pluronic Micelles Stabilized by Shell Cross-Linking with Gold Nanoparticles. *Langmuir* 2006, *22*, 6380–6384.
12. Bhaisare, M.L.; Pandey, S.; Khan, M.S.; Talib, A.; Wu, H.-F. Fluorophotometric Determination of Critical Micelle Concentration (CMC) of Ionic and Non-Ionic Surfactants with Carbon Dots via Stokes Shift. *Talanta* 2015, *132*, 572–578.
13. Piñeiro, L.; Novo, M.; Al-Soufi, W. Fluorescence Emission of Pyrene in Surfactant

Solutions. *Adv. Colloid Interface Sci.* 2015, *215*, 1–12.

14. Li, Y.; Qian, Y.; Liu, T.; Zhang, G.; Liu, S. Light-Triggered Concomitant Enhancement of Magnetic Resonance Imaging Contrast Performance and Drug Release Rate of Functionalized Amphiphilic Diblock Copolymer Micelles. *Biomacromolecules* 2012, *13*, 3877–3886.
15. Petros, R.A.; DeSimone, J.M. Strategies in the Design of Nanoparticles for Therapeutic Applications. *Nat. Rev. Drug Discov.* 2010, *9*, 615–627.
16. Ferrari, R.; Talamini, L.; Violatto, M.B.; Giangregorio, P.; Sponchioni, M.; Morbidelli, M.; Salmona, M.; Bigini, P.; Moscatelli, D. Biocompatible Polymer Nanoformulation to Improve the Release and Safety of a Drug Mimic Molecule Detectable via ICP-MS. *Mol. Pharm.* 2017, *14*, 124–134.
17. Ghaffarian, R.; Pérez-Herrero, E.; Oh, H.; Raghavan, S.R.; Muro, S. Chitosan–Alginate Microcapsules Provide Gastric Protection and Intestinal Release of ICAM-1-Targeting Nanocarriers, Enabling GI Targeting In Vivo. *Adv. Funct. Mater.* 2016, *26*, 3382–3393.
18. Agostini, A.; Palmiero, U.C.; Barbieri, S.D.A.; Lupi, M.; Moscatelli, D. Synthesis and Characterization of PH-Sensitive Drinkable Nanoparticles for Oral Delivery of Ibuprofen. *Nanotechnology* 2018, *29*, 225604.
19. Ahmed, E.M. Hydrogel: Preparation, Characterization, and Applications: A Review. *J. Adv. Res.* 2015, *6*, 105–121.
20. Annabi, N.; Tamayol, A.; Uquillas, J.A.; Akbari, M.; Bertassoni, L.E.; Cha, C.; Camci-Unal, G.; Dokmeci, M.R.; Peppas, N.A.; Khademhosseini, A. 25th Anniversary Article: Rational Design and Applications of Hydrogels in Regenerative Medicine. *Adv. Mater.* 2014, *26*, 85–124.
21. Caló, E.; Khutoryanskiy, V. V Biomedical Applications of Hydrogels: A Review of Patents and Commercial Products. *Eur. Polym. J.* 2015, *65*, 252–267.
22. Ferrari, R.; Sponchioni, M.; Morbidelli, M.; Moscatelli, D. Polymer Nanoparticles for the Intravenous Delivery of Anticancer Drugs: The Checkpoints on the Road from the Synthesis to Clinical Translation. *Nanoscale* 2018, *10*, 22701–22719.
23. Valle, J.W.; Armstrong, A.; Newman, C.; Alakhov, V.; Pietrzynski, G.; Brewer, J.; Campbell, S.; Corrie, P.; Rowinsky, E.K.; Ranson, M. A Phase 2 Study of SP1049C, Doxorubicin in P-Glycoprotein-Targeting Pluronics, in Patients with Advanced Adenocarcinoma of the Esophagus and Gastroesophageal Junction. *Invest. New Drugs* 2011, *29*, 1029–1037.

24. Sekine, H.; Shimizu, T.; Kosaka, S.; Kobayashi, E.; Okano, T. Cardiomyocyte Bridging between Hearts and Bioengineered Myocardial Tissues with Mesenchymal Transition of Mesothelial Cells. *J. Hear. lung Transplant.* 2006, *25*, 324–332.
25. Sekine, H.; Shimizu, T.; Yang, J.; Kobayashi, E.; Okano, T. Pulsatile Myocardial Tubes Fabricated with Cell Sheet Engineering. *Circulation* 2006, *114*, I–87.
26. Shimizu, T.; Sekine, H.; Isoi, Y.; Yamato, M.; Kikuchi, A.; Okano, T. Long-Term Survival and Growth of Pulsatile Myocardial Tissue Grafts Engineered by the Layering of Cardiomyocyte Sheets. *Tissue Eng.* 2006, *12*, 499–507.
27. Yang, J.; Yamato, M.; Nishida, K.; Ohki, T.; Kanzaki, M.; Sekine, H.; Shimizu, T.; Okano, T. Cell Delivery in Regenerative Medicine: The Cell Sheet Engineering Approach. *J. Control. Release* 2006, *116*, 193–203.
28. Song, K.; Yang, Y.; Wu, S.; Zhang, Y.; Feng, S.; Wang, H.; Wang, Y.; Wang, L.; Liu, T. In Vitro Culture and Harvest of BMMSCs on the Surface of a Novel Thermosensitive Glass Microcarrier. *Mater. Sci. Eng. C* 2016, *58*, 324–330.
29. Rosiak, J.M.; Yoshii, F. Hydrogels and Their Medical Applications. *Nucl. Instruments Methods Phys. Res. Sect. B Beam Interact. with Mater. Atoms* 1999, *151*, 56–64.
30. Chung, H.J.; Park, T.G. Self-Assembled and Nanostructured Hydrogels for Drug Delivery and Tissue Engineering. *Nano Today* 2009, *4*, 429–437.
31. Tang, Y.; Heaysman, C.L.; Willis, S.; Lewis, A.L. Physical Hydrogels with Self-Assembled Nanostructures as Drug Delivery Systems. *Expert Opin. Drug Deliv.* 2011, *8*, 1141–1159.
32. Perera, M.M.; Ayres, N. Dynamic Covalent Bonds in Self-Healing, Shape Memory, and Controllable Stiffness Hydrogels. *Polym. Chem.* 2020, *11*, 1410–1423.
33. Kirkland, S.E.; Hensarling, R.M.; McConaughy, S.D.; Guo, Y.; Jarrett, W.L.; McCormick, C.L. Thermoreversible Hydrogels from RAFT-Synthesized BAB Triblock Copolymers: Steps toward Biomimetic Matrices for Tissue Regeneration. *Biomacromolecules* 2008, *9*, 481–486.
34. Goponenko, A. V; Dzenis, Y.A. Role of Mechanical Factors in Applications of Stimuli-Responsive Polymer Gels–Status and Prospects. *Polymer (Guildf).* 2016, *101*, 415–449.
35. Roy, D.; Cambre, J.N.; Sumerlin, B.S. Future Perspectives and Recent Advances in Stimuli-Responsive Materials. *Prog. Polym. Sci.* 2010, *35*, 278–301.
36. Deshmukh, S.A.; Kamath, G.; Suthar, K.J.; Mancini, D.C.; Sankaranarayanan, S.K.R.S. Non-Equilibrium Effects Evidenced by Vibrational Spectra during the Coil-to-Globule

Transition in Poly (N-Isopropylacrylamide) Subjected to an Ultrafast Heating–Cooling Cycle. *Soft Matter* 2014, *10*, 1462–1480.

37. Sambe, L.; de La Rosa, V.R.; Belal, K.; Stoffelbach, F.; Lyskawa, J.; Delattre, F.; Bria, M.; Cooke, G.; Hoogenboom, R.; Woisel, P. Programmable Polymer-Based Supramolecular Temperature Sensor with a Memory Function. *Angew. Chemie* 2014, *126*, 5144–5148.
38. Mehri, S.; Abnous, K.; Mousavi, S.H.; Shariaty, V.M.; Hosseinzadeh, H. Neuroprotective Effect of Crocin on Acrylamide-Induced Cytotoxicity in PC12 Cells. *Cell. Mol. Neurobiol.* 2012, *32*, 227–235.
39. Vihola, H.; Laukkanen, A.; Valtola, L.; Tenhu, H.; Hirvonen, J. Cytotoxicity of Thermosensitive Polymers Poly (N-Isopropylacrylamide), Poly (N-Vinylcaprolactam) and Amphiphilically Modified Poly (N-Vinylcaprolactam). *Biomaterials* 2005, *26*, 3055–3064.
40. Zhang, W.; Jin, Y. Dynamic Covalent Chemistry: Principles, Reactions, and Applications. 2017.
41. Chakma, P.; Konkolewicz, D. Dynamic Covalent Bonds in Polymeric Materials. *Angew. Chemie* 2019, *131*, 9784–9797, doi:10.1002/ange.201813525.
42. Roy, N.; Bruchmann, B.; Lehn, J.-M. DYNAMERS: Dynamic Polymers as Self-Healing Materials. *Chem. Soc. Rev.* 2015, *44*, 3786–3807.
43. AbdolahZadeh, M.; Van Der Zwaag, S.; Garcia, S.J. Self-Healing Corrosion-Protective Sol–Gel Coatings Based on Extrinsic and Intrinsic Healing Approaches. *Self-healing Mater.* 2016, 185–218.
44. Ye, J.; Fu, S.; Zhou, S.; Li, M.; Li, K.; Sun, W.; Zhai, Y. Advances in Hydrogels Based on Dynamic Covalent Bonding and Prospects for Its Biomedical Application. *Eur. Polym. J.* 2020, *139*, 110024, doi:https://doi.org/10.1016/j.eurpolymj.2020.110024.
45. Othman, M.H.; Ito, Y.; Akimoto, J. Mild-Temperature-Induced Recombination of Crosslinking Structures in Hydrogels Using Phenylboronic-Acid-Functionalized 3D Nanoparticle Crosslinkers. *ACS Appl. Polym. Mater.* 2022, *4*, 5047–5055.
46. Zhang, B.; Digby, Z.A.; Flum, J.A.; Foster, E.M.; Sparks, J.L.; Konkolewicz, D. Self-Healing, Malleable and Creep Limiting Materials Using Both Supramolecular and Reversible Covalent Linkages. *Polym. Chem.* 2015, *6*, 7368–7372.
47. Habault, D.; Zhang, H.; Zhao, Y. Light-Triggered Self-Healing and Shape-Memory Polymers. *Chem. Soc. Rev.* 2013, *42*, 7244–7256.

48. Jochum, F.D.; Theato, P. Temperature-and Light-Responsive Smart Polymer Materials. *Chem. Soc. Rev.* 2013, *42*, 7468–7483.
49. Ito, Y. *Photochemistry for Biomedical Applications: From Device Fabrication to Diagnosis and Therapy*; Springer, 2018; ISBN 9811301522.
50. Akimoto, J.; Park, S.J.; Obuse, S.; Kawamoto, M.; Tamura, M.; Nandakumar, A.; Kobatake, E.; Ito, Y. Synthesis of Photoreactive Poly (Ethylene Oxide) s for Surface Modification. *ACS Appl. Bio Mater.* 2020, *3*, 5941–5947.
51. Ren, X.; Akimoto, J.; Miyatake, H.; Tada, S.; Zhu, L.; Mao, H.; Isoshima, T.; Müller, S.; Kim, S.M.; Zhou, Y. Cell Migration and Growth Induced by Photo-Immobilised Vascular Endothelial Growth Factor (VEGF) Isoforms. *J. Mater. Chem. B* 2019, *7*, 4272–4279.
52. Buwalda, S.; Rotman, S.; Eglin, D.; Moriarty, F.; Bethry, A.; Garric, X.; Guillaume, O.; Nottelet, B. Synergistic Anti-Fouling and Bactericidal Poly (Ether Ether Ketone) Surfaces via a One-Step Photomodification. *Mater. Sci. Eng. C* 2020, *111*, 110811.
53. Ito, Y. Bioadhesives and Biosealants. In *Photochemistry for Biomedical Applications*; Springer, 2018; pp. 195–230.
54. Hoffman, A.S. Hydrogels for Biomedical Applications. *Adv. Drug Deliv. Rev.* 2012, *64*, 18–23.
55. Tai, H.; Howard, D.; Takae, S.; Wang, W.; Vermonden, T.; Hennink, W.E.; Stayton, P.S.; Hoffman, A.S.; Endruweit, A.; Alexander, C. Photo-Cross-Linked Hydrogels from Thermoresponsive PEGMEMA-PPGMA-EGDMA Copolymers Containing Multiple Methacrylate Groups: Mechanical Property, Swelling, Protein Release, and Cytotoxicity. *Biomacromolecules* 2009, *10*, 2895–2903.
56. Zhou, D.; Ito, Y. Visible Light-Curable Polymers for Biomedical Applications. *Sci. China Chem.* 2014, *57*, 510–521.
57. Nguyen, K.T.; West, J.L. Photopolymerizable Hydrogels for Tissue Engineering Applications. *Biomaterials* 2002, *23*, 4307–4314.
58. Tayalia, P.; Mendonca, C.R.; Baldacchini, T.; Mooney, D.J.; Mazur, E. 3D Cell-migration Studies Using Two-photon Engineered Polymer Scaffolds. *Adv. Mater.* 2008, *20*, 4494–4498.
59. Ovsianikov, A.; Malinauskas, M.; Schlie, S.; Chichkov, B.; Gittard, S.; Narayan, R.; Löbler, M.; Sternberg, K.; Schmitz, K.-P.; Haverich, A. Three-Dimensional Laser Micro-and Nano-Structuring of Acrylated Poly (Ethylene Glycol) Materials and

Evaluation of Their Cytoxicity for Tissue Engineering Applications. *Acta Biomater.* 2011, *7*, 967–974.

60. Ideta, R.; Tasaka, F.; Jang, W.-D.; Nishiyama, N.; Zhang, G.-D.; Harada, A.; Yanagi, Y.; Tamaki, Y.; Aida, T.; Kataoka, K. Nanotechnology-Based Photodynamic Therapy for Neovascular Disease Using a Supramolecular Nanocarrier Loaded with a Dendritic Photosensitizer. *Nano Lett.* 2005, *5*, 2426–2431.
61. Hong, H.; Zhang, Y.; Sun, J.; Cai, W. Molecular Imaging and Therapy of Cancer with Radiolabeled Nanoparticles. *Nano Today* 2009, *4*, 399–413.
62. Shiraishi, K.; Kawano, K.; Maitani, Y.; Yokoyama, M. Polyion Complex Micelle MRI Contrast Agents from Poly (Ethylene Glycol)-b-Poly (L-Lysine) Block Copolymers Having Gd-DOTA; Preparations and Their Control of T1-Relaxivities and Blood Circulation Characteristics. *J. Control. release* 2010, *148*, 160–167.
63. Schena, M.; Shalon, D.; Davis, R.W.; Brown, P.O. Quantitative Monitoring of Gene Expression Patterns with a Complementary DNA Microarray. *Science (80-.).* 1995, *270*, 467–470.
64. Vigh-Conrad, K.A.; Conrad, D.F.; Preuss, D. A Protein Allergen Microarray Detects Specific IgE to Pollen Surface, Cytoplasmic, and Commercial Allergen Extracts. *PLoS One* 2010, *5*, e10174.
65. Matsudaira, T.; Tsuzuki, S.; Wada, A.; Suwa, A.; Kohsaka, H.; Tomida, M.; Ito, Y. Automated Microfluidic Assay System for Autoantibodies Found in Autoimmune Diseases Using a Photoimmobilized Autoantigen Microarray. *Biotechnol. Prog.* 2008, *24*, 1384–1392.
66. Heydari, M.; Hasuda, H.; Sakuragi, M.; Yoshida, Y.; Suzuki, K.; Ito, Y. Modification of the Titan Surface with Photoreactive Gelatin to Regulate Cell Attachment. *J. Biomed. Mater. Res. Part A An Off. J. Soc. Biomater. Japanese Soc. Biomater. Aust. Soc. Biomater. Korean Soc. Biomater.* 2007, *83*, 906–914.
67. Ito, Y. Growth Factors on Biomaterial Scaffolds. In *Biological Interactions on Materials Surfaces*; Springer, 2009; pp. 173–197.
68. Zhou, D.; Ito, Y. Inorganic Material Surfaces Made Bioactive by Immobilizing Growth Factors for Hard Tissue Engineering. *RSC Adv.* 2013, *3*, 11095–11106.
69. Zhang, H.; Zhu, S.; Yang, J.; Ma, A. Advancing Strategies of Biofouling Control in Water-Treated Polymeric Membranes. *Polymers (Basel).* 2022, *14*, 1167.
70. Jiang, C.; Wang, G.; Hein, R.; Liu, N.; Luo, X.; Davis, J.J. Antifouling Strategies for

Selective in Vitro and in Vivo Sensing. *Chem. Rev.* 2020, *120*, 3852–3889.

71. Nagasaki, Y. Construction of a Densely Poly (Ethylene Glycol)-Chain-Tethered Surface and Its Performance. *Polym. J.* 2011, *43*, 949–958.
72. Ratner, B.D.; Hoffman, A.S.; Schoen, F.J.; Lemons, J.E. Biomaterials Science: An Introduction to Materials in Medicine. *San Diego, Calif.* 2004, 162–164.
73. Maan, A.M.C.; Hofman, A.H.; de Vos, W.M.; Kamperman, M. Recent Developments and Practical Feasibility of Polymer-based Antifouling Coatings. *Adv. Funct. Mater.* 2020, *30*, 2000936.
74. He, Z.; Lan, X.; Hu, Q.; Li, H.; Li, L.; Mao, J. Antifouling Strategies Based on Super-Phobic Polymer Materials. *Prog. Org. Coatings* 2021, *157*, 106285.
75. Zhao, H.-Z.; Wang, L.; Chang, Y.-Y.; Xu, Y. High-Efficiency Removal of Perfluorooctanoic Acid from Water by Covalently Bound Hybrid Coagulants (CBHyC) Bearing a Hydrophobic Quaternary Ammonium Group. *Sep. Purif. Technol.* 2016, *158*, 9–15.
76. Nikkola, J.; Liu, X.; Li, Y.; Raulio, M.; Alakomi, H.-L.; Wei, J.; Tang, C.Y. Surface Modification of Thin Film Composite RO Membrane for Enhanced Anti-Biofouling Performance. *J. Memb. Sci.* 2013, *444*, 192–200.
77. Kuzmyn, A.R.; Nguyen, A.T.; Teunissen, L.W.; Zuilhof, H.; Baggerman, J. Antifouling Polymer Brushes via Oxygen-Tolerant Surface-Initiated PET-RAFT. *Langmuir* 2020, *36*, 4439–4446.
78. Chen, G.; Ito, Y. Gradient Micropattern Immobilization of EGF to Investigate the Effect of Artificial Juxtacrine Stimulation. *Biomaterials* 2001, *22*, 2453–2457.
79. Ito, Y.; Kondo, S.; Chen, G.; Imanishi, Y. Patterned Artificial Juxtacrine Stimulation of Cells by Covalently Immobilized Insulin. *FEBS Lett.* 1997, *403*, 159–162.
80. Pasut, G.; Veronese, F.M. State of the Art in PEGylation: The Great Versatility Achieved after Forty Years of Research. *J. Control. release* 2012, *161*, 461–472.

CHAPTER II

SYNTHESIS AND CHARACTERIZATION OF TEMPERATURE-RESPONSIVE HYDROGEL USING DYNAMIC COVALENT CROSSLINKING BY MIXING OF 3D NANOPARTICLE

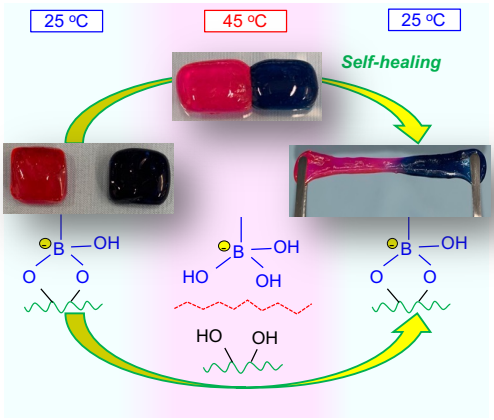

1. Introduction

Smart hydrogels have been used in a variety of fields including biomaterials, polymeric actuators, energy devices, and molecular sensing [1–4]. They exhibit controllable physical properties in response to changes in the external environment, such as different physical and chemical stimuli. Smart gels based on dynamic covalent bonds (DCBs) have recently been developed [5,6]. These gels exhibit reversible bond dissociation in response to changes in the surrounding environment. The covalent properties of DCBs are extremely stable, and they also reach equilibrium and partially dissociate in response to external stimuli (such as heat and light) and subsequently reform bonds when the stimulus is removed. Because external stimuli can encourage their dissociation, DCBs can be used as crosslinkers to change the internal structure of hydrogels [7,8]. Because external stimuli can encourage their dissociation, DCBs can be used as crosslinkers to change the internal structure of hydrogels. After the stimulus is removed, these DCB-derived non-bonding free functional groups can randomly recombine with their gel counterpart functional groups, allowing recombination of the crosslinking points and enabling adhesion between gels due to a self-healing function [9,10].

Different dynamic covalent bondings have different properties and characteristics. These unique properties make dynamic covalent bondings have diverse application prospects in the biomedical field. Several stimuli such as pH and temperature enable the cleavage of DCBs for the preparation of self-healing hydrogel (Figure 1).

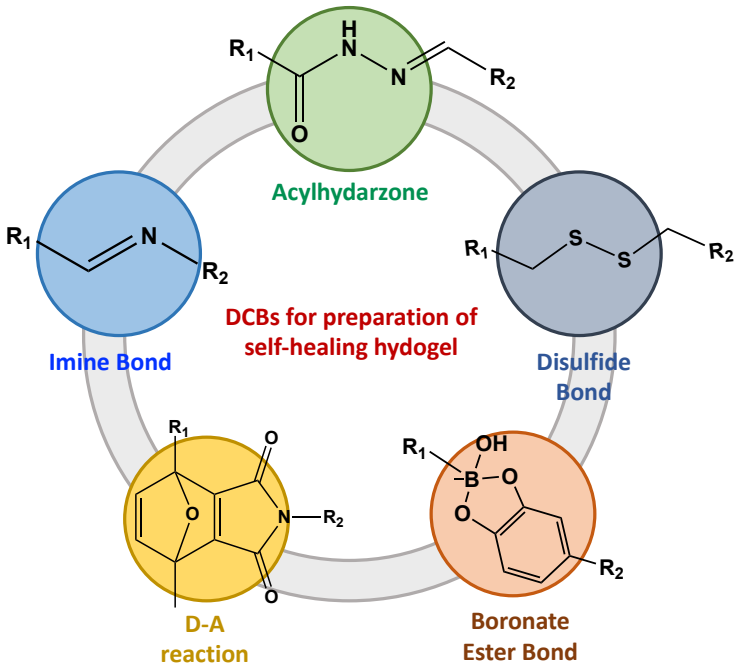

Figure 1. Dynamic covalent bonds used for the preparation of self-healing hydrogel

Temperature is a particularly common stimulus in the biomedical field because of the ease of external temperature control that can be achieved using various heating devices. The Schiff bases (amine-aldehyde) [11,12], acylhydrazone (hydrazine-aldehyde) [13], Diels-Alder reaction (ene-diene) [14,15], dithioesters (thiol-thiol) [16], and alkoxyamines (styryl-radical-nitroxyl-radical) [17] are examples of DCBs that dissociate with heat. The physical properties and structure of a gel can be drastically altered using these DCBs because the crosslinking points that support its morphology can be directly cleaved by heating. Controlling the binding and dissociation caused by thermal stimuli can make it possible for the functional groups that make up the DCBs to recombine, giving the gel self-healing properties [18]. However, high-temperature treatment is typically needed to break these bonds and promote polymer chain mobility in the gel and subsequently allow the crosslinking structure to recombine. For instance, to regulate the functionality of the hydrogel, Schiff bases are only heated to 67 °C or higher, which are thought of as relatively low temperatures [8,12].

The high-temperature processes used to create smart hydrogels have a significant impact on their physical characteristics, particularly concerning surface drying and water evaporation. Therefore, DCBs that are in equilibrium at room temperature and passively exchange their functional groups are used to create hydrogels that have self-healing qualities in ambient environments [19,20]. DCBs should be stable at room temperature and dissociate at mild temperatures to actively induce the exchange of DCB-derived functional groups. However, these DCBs have been rarely reported. As a result, regulating the bonding of DCB-type smart hydrogels at room temperature can greatly facilitate their biomedical applications.

Phenylboronic acid (PBA), which forms boronic ester DCBs with diol compounds [21,22], is extensively used in biomedical applications, especially as a glucose sensor owing to its high binding affinity to sugars [23,24]. Moreover, PBA can form a hydrogel with diol-containing polymers, such as poly(vinyl alcohol) (PVA), at high concentrations; the resulting hydrogel has biomedical applications as glucose sensors and a cell-coating material, for instance [25].

The DCBs of boronic esters are widely used in the biomedical field due to the high biocompatibility of PBA, but it is unknown how temperature affects these boronic esters at this time. The phase transition of the thermoresponsive polymers occurs at temperatures close to room temperature or higher, making it difficult to analyze the thermal effects of boronic esters under ambient conditions even though temperature responsiveness has been added to PBA using these polymers [26,27].

In order to determine whether it would be possible to take advantage of the thermal dissociation of its bonds in the creation of functional hydrogels, the thermochemical properties of a boronic ester were clarified in this study. In particular, PBA was combined with cationic poly(N,N-dimethylaminopropyl acrylamide) (PDMAPAAm) because the presence of cationic polymers significantly increases the dissociation constant of boronic esters [28].

Additionally, PBA was added to the surface of cationic nanoparticles in order to multivalently bind with diol compounds. This multivalence effect enabled control of the bonding and dissociation states of the DCBs via a thermal stimulus, thus permitting the recombination of hydrogel samples in terms of position and crosslink density to impart self-healing properties.

2. Materials and methods

2.1. Materials

The n-butyl methacrylate (BMA), N,N-dimethylaminopropyl acrylamide (DMAPAAm), and 4-acryloylmorpholine (ACMO) were provided by FUJIFILM Wako Pure Chemicals (Tokyo, Japan), and they were subsequently purified by distillation under reduced pressure. PVA (polymerization degree: 1000), 2,2′-azobisisobutyronitrile (AIBN), 2-ethanolamine, alizarin red S (ARS), acetone, hexane, 1,4-dioxane, sodium hydroxide, hydrochloric acid, sulforhodamine B, and glutaraldehyde were also bought from FUJIFILM Wako Pure Chemicals. 3-(acrylamido) phenylboronic acid (APBA; Combi-Blocks, San Diego, CA, USA), 2-cyano-2-propyl dodecyl trithicarbonate (CPDT; Sigma-Aldrich, St. Louis, MO, USA), and tris(2-carboxyethyl) phosphine hydrochloride were used as received (TCEP; Tokyo Chemical Industry, Tokyo, Japan).

2.2. Synthesis of PBA-terminated block copolymer

BMA (75 mmol), CPDT (3 mmol), and AIBN (0.3 mmol) were dissolved in 1,4-dioxane (100 mL) and bubbled with nitrogen gas for 30 min at 25 °C. After that, polymerization was carried out for 24 hours at 80 °C. The resulting mixture was dissolved in acetone and the unreacted monomer was completely evaporated at 100 °C for one hour under vacuum. For use in the ensuing copolymerization, the obtained PBMA was dissolved in 1,4-dioxane. Then, 1,4-dioxane (10 mL) was used to dissolve PBMA (0.1 mmol), DMAPAAm (10 mmol) or ACMO (10 mmol), and AIBN (0.01 mmol). The solution was bubbled with nitrogen gas for 20 min and subsequently reacted at 80 °C for 24 h under a nitrogen atmosphere. Dropwise addition of the reactant solution to an excess of hexane produced the yellow compound, which was then dialyzed for two days against water using a dialysis membrane (Spectra/Por 6, MWCO 3500, Spectrum Laboratories, Rancho Dominguez, CA, USA). By lyophilization, a block copolymer was obtained. Following the dissolution of the diblock copolymer, APBA (10 molar equivalents of the diblock copolymer), and TCEP in 1,4-dioxane (10 mL), the dodecyltrithiocarbonate (DTC) group on the block copolymer's terminus was converted into APBA by slowly adding 2-aminoethanol (10 molar equivalents of the diblock copolymer). The solution was stirred for 12 h at 25 °C. After the reaction, a dialysis membrane (MWCO 3500) was used to dialyze the reactant solution against water for 72 hours, producing polymers that could then be freeze-dried. The cationic PDMAPAAm or nonionic PACMO-containing block polymers with DTC- and PBA-terminations are referred to as PBMA-*b*-PDMAPAAm-DTC,

PBMA-*b*-PDMAPAAm-PBA, and PBMA-*b*-PACMO-PBA, respectively (Scheme 1). The obtained polymers were characterized using a gel permeation chromatography (GPC; JASCO) system outfitted with a refractive index detector (RI-2032, JASCO, Tokyo, Japan) and two columns (SB-803 HQ and SB804 HQ; Showa Denko, Tokyo, Japan), as well as ^{1}H-NMR spectroscopy (JNM-ECZ400R, 400 MHz, JEOL, Tokyo, Japan). A UV-vis spectrometer (model V750, JASCO) was used to measure UV absorbance.

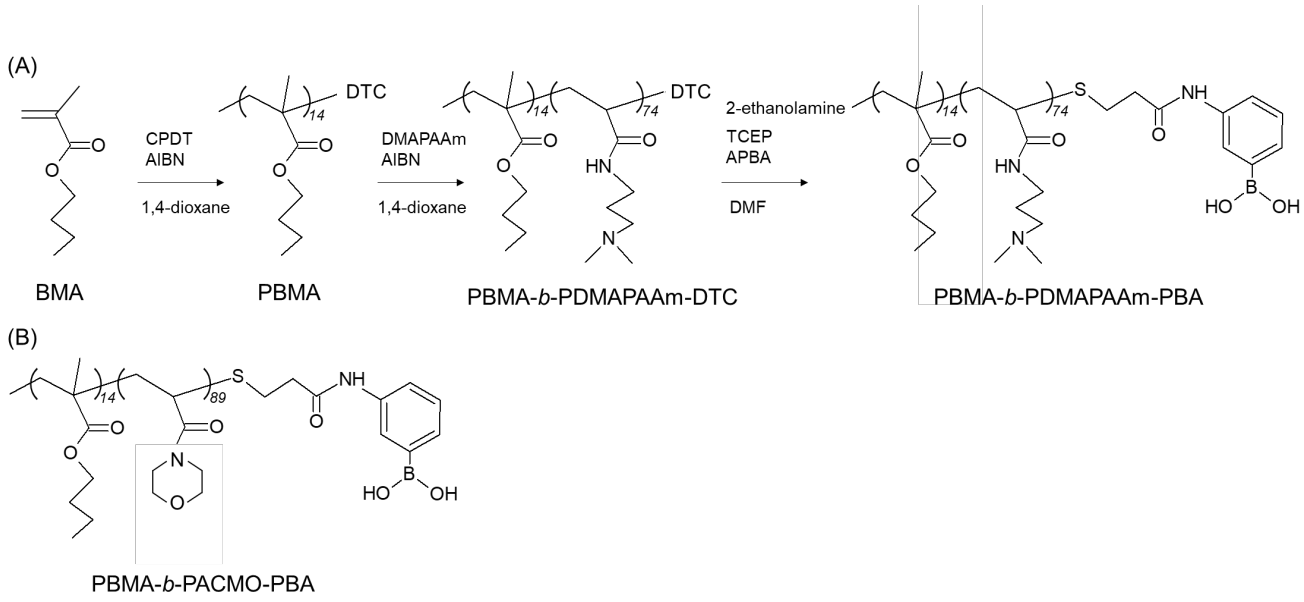

Scheme 1. (A) Scheme for preparing PBMA-*b*-PDMAPAAm-PBA and (B) chemical structure of PBMA-*b*-PACMO-PBA.

2.3. Preparation of nanoparticles

Acetone (1 mL) was added after each block copolymer (1-100 mg) had been dissolved in water (1 mL). Using a rotary evaporator at 100 hPa, the acetone was completely removed under vacuum at room temperature. The block copolymer solution was diluted with water to adjust the polymer concentration from 0.1 to 100 mg/mL. The terms NP(PDMAPAAm)-PBA, NP(PDMAPAAm)-DTC, and NP(PACMO)-PBA, respectively, are used to denote nanoparticles made using PBMA-*b*-PDMAPAAm-PBA, PBMA-*b*-PDMAPAAm-DTC, and PBMA-*b*-PACMO-PBA.

2.4. Transmission electron microscopy (TEM)

One drop of each nanoparticle solution (1 mg/mL) was placed on a carbon-coated TEM grid (COL-C10, 100 μm grid pitch, Okenshoji, Tokyo, Japan). Subsequently, the samples were

negatively stained with 2% samarium acetate, and excess liquid was removed with filter paper. The samples were dried for 1 h and examined by TEM (JEOL).

2.5. Dynamic light scattering (DLS) and ζ-potential measurements

For the DLS and ζ-potential measurements, the NP(PDMAPAAm)-PBA solution was diluted to 1.0 and 0.5 mg/mL, respectively. A NaOH solution (1 mol/L) was used to adjust the pH of the solution. Measurements were performed using the ELSZ-2PL device (Otsuka Electronics, Osaka, Japan).

2.6. Fluorescence measurements

The NP(PDMAPAAm)-PBA solution was mixed with an equimolar mixture of ARS. A fluorimeter (FP-6500, JASCO, Tokyo, Japan) was used to measure the fluorescence intensities in the 480–650 nm range with an excitation wavelength of 468 nm. A sample-cell thermostat was used to regulate the solution's temperature (ETC-717, JASCO).

2.7. Differential scanning calorimetry (DSC)

PVA (5 mg/mL) and NP(PDMAPAAm)-PBA (5 mg/mL) were combined, and the pH of the mixture was adjusted by adding either HCl or NaOH solutions. Water and the sample were placed in the reference and sample cell holder of the micro-CAL VP DSC apparatus, respectively (GE Healthcare, Chicago, IL, USA). The DSC peaks were measured between 15 and 70 °C.

2.8. Changes in thermo-viscoelasticity of PBA-modified-nanoparticle/PVA system

A vial was placed with NP(PDMAPAAm)-DTC, NP(PDMAPAAm)-PBA, or NP(PACMO)-PBA (1–5 wt.%), and the pH of the mixture was adjusted using HCl or NaOH solutions. The same volume of 10 wt.% of PVA solution was then added, and the mixture was gently stirred at 25 °C. At 25 and 45 °C, the vial was inverted to examine how the PBMA-*b*-PDMAPAAm-PBA/PVA mixtures changed in viscosity.

A rheometer (AR-G2, TA Instruments, New Castle, DE, USA) was used to measure the thermo-viscoelastic changes in NP(PDMAPAAm)-PBA/PVA. The NP(PDMAPAAm)-PBA and PVA solution or hydrogel was then put on the rheometer plate after being thoroughly mixed. In order to stop the water from evaporating, silicone oil was applied to it. Time sweep measurements were then taken with a fixed frequency ($\omega = 1$ Hz) and strain ($\gamma = 1\%$).

After the hydrogel had been fixed with 0.3% glutaraldehyde, which was added to the PVA solution to crosslink the PVAs, colored cubic hydrogels were created by adding NP(PDMAPAAm)-PBA and sulforhodamine B or methylene blue to the mixture. On a hot plate, these hydrogels were combined at 45 °C, and the heated hydrogels were subsequently cooled to room temperature. For each procedure, the hydrogel connections were visually verified.

3. Results and discussion

3.1. Synthesis of PBA-terminated block copolymer

Sequential reversible addition-fragmentation chain transfer (RAFT) polymerization was used to synthesize PBMA-*b*-PDMAPAAm-DTC. Hydrophobic PBMA was synthesized using CPDT as the RAFT agent. Based on the trithiocarbonate unit's UV absorbance at 310 nm (ε = 11000 L/mol/cm), the average molecular weight of PBMA was calculated to be 2600 g/mol [29]. DMAPAAm was subsequently propagated from PBMA to produce PBMA-*b*-PDMAPAAm-DTC. Using ^{1}H-NMR spectra, the DMAPAAm unit in the block copolymer was verified by contrasting the proton intensities of the methylene protons of BMA (–OCH_2–, 2H, 3.84–4.05 ppm) and DMAPAAm (–N–CH_2–, 2H, 2.94–3.42 ppm). The units of BMA and DMAPAAm monomers in the block copolymer were determined to be 14 and 74, respectively. Additionally, the GPC chart showed a monomodal peak derived from the block copolymer, indicating the formation of the PBMA-*b*-PDMAPAAm-DTC diblock polymer.

The DTC group on the terminus of the diblock copolymer was converted into the PBA unit by its aminolysis, followed by Michael's addition of APBA. The terminal conversion was determined to be greater than 95% by comparing the aromatic protons of PBA at 6.98 ppm and the methylene protons of BMA at 3.84–4.05 ppm in the ^{1}H-NMR spectrum. The aromatic protons of PBA in PBMA-*b*-PDMAPAAm-PBA were confirmed at 6.98 and 7.51 ppm (Figure 2). A monomodal peak similar to that of PBMA-*b*-PDMAPAAm-DTC was visible on the GPC chart of PBMA-*b*-PDMAPAAm-PBA (Figure 3). Additionally, the terminal conversion of the PBA was confirmed by UV absorbance (Figure 4). The PBA-free diblock copolymer, which was synthesized without the use of APBA in the terminal conversion reaction, had a low UV absorbance in the 280–330 nm range, which matched the absorbance of PBA. Thus, the successful conversion of the PBA substitution at the block copolymer was confirmed.

Nonionic PBMA-*b*-PACMO-PBA was synthesized similarly to PBMA-*b*-PDMAPAAm-PBA. The units of BMA and ACMO monomers in the block copolymer were 14 and 89, respectively, and the block copolymer showed a monomodal peak in the GPC profile (Figure 3).

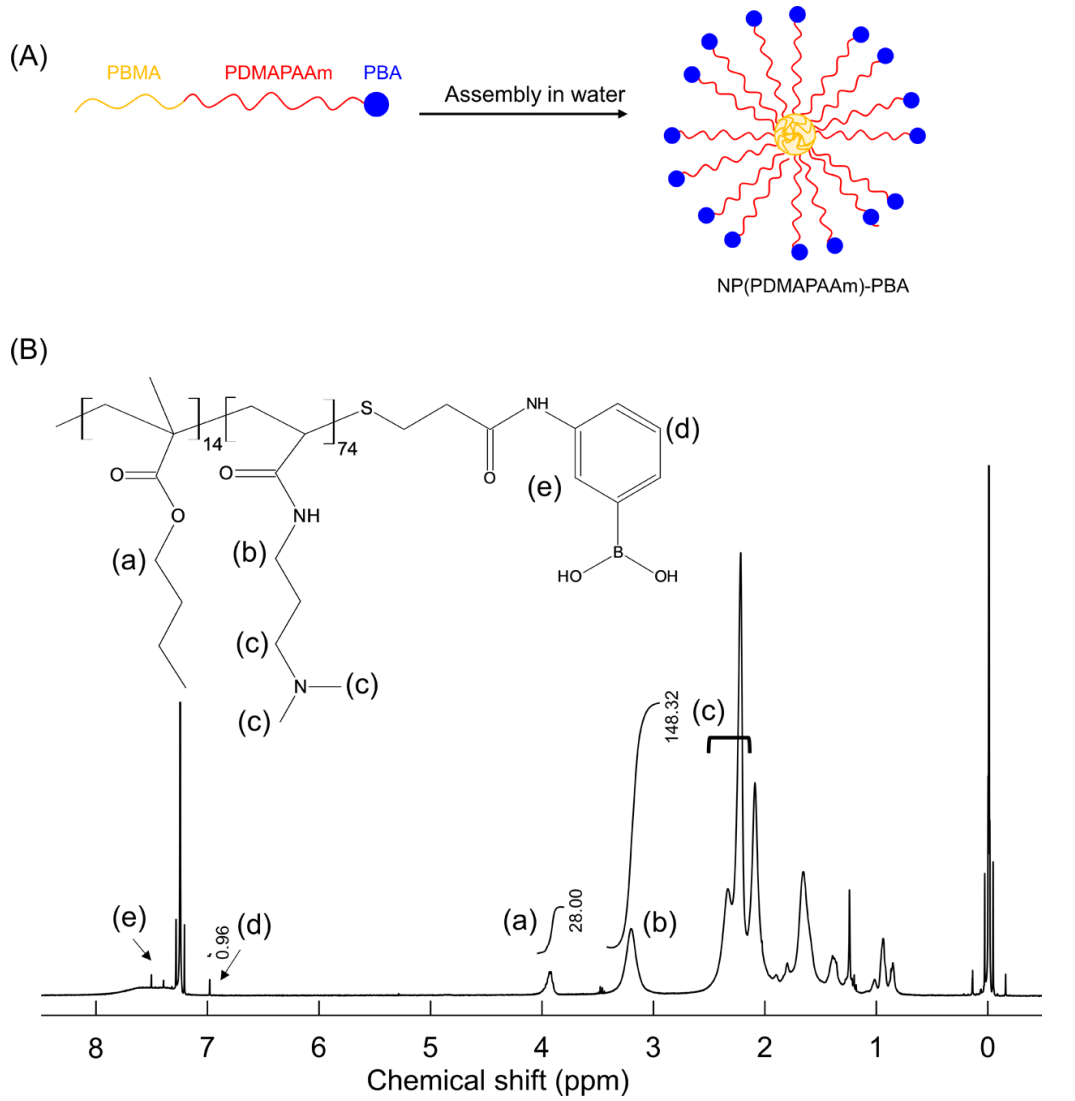

Figure 2. (A) Preparation of NP(PDMAPAAm)-PBA and (B) the ^{1}H-NMR spectrum of PBMA-*b*-PDMAPAAm-PBA (solvent: $CDCl_3$).

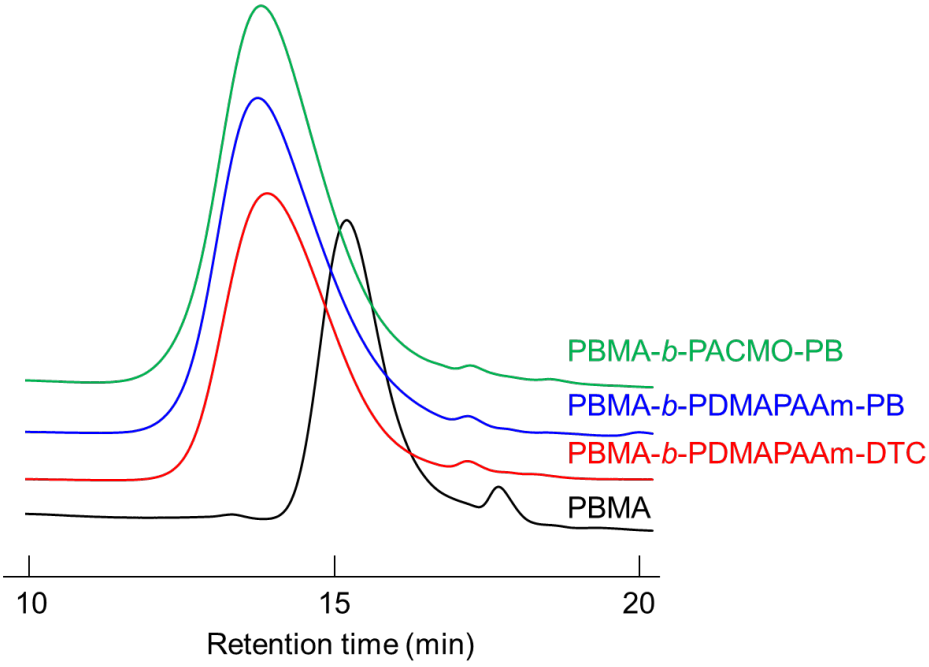

Figure 3. GPC charts of polymers. Eluent: N,N-dimethylformamide continuing 10 mmol/L lithium bromide, flow rate: 1 mL/min.

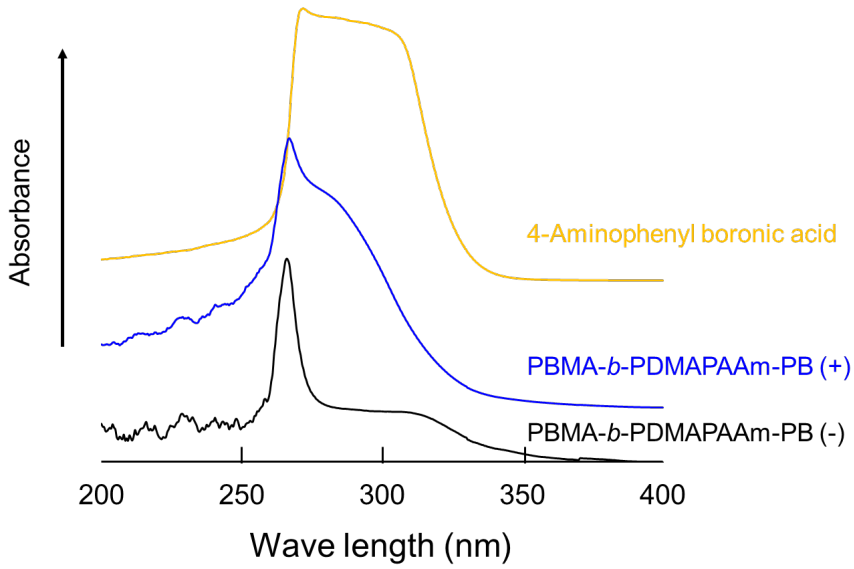

Figure 4. UV spectra of block copolymers and 4-aminophenyl boronic acid in water.

3.2. Preparation and characterization of synthesized nanoparticles

Nanoparticles with a PBA surface, hydrophobic core, and hydrophilic corona [NP(PDMAPAAm)-PBA] were prepared by the assembly of PBMA-b-PDMAPAAm-PBA in water (Figure 2). Although PBMA-*b*-PDMAPAAm-PBA was soluble in water, a higher concentration (5 wt.%) prevented it from dissolving easily. As a result, acetone was used to completely dissolve the PBMA-*b*-PDMAPAAm-PBA compound before water was added. After preparing the polymer solution, the acetone was removed from the mixture under reduced pressure.

DLS analysis showed that NP(PDMAPAAm)-PBA exhibited a unimodal peak, with a volume-average diameter of 54 ± 0.16 nm (Figure 5A). The morphology of the nanoparticles was confirmed by TEM, which revealed uniformly dispersed ~30-nm-sized spherical dots (Figure 5B).

To determine the ideal pH range for the ionization of PBA and PDMAPAAm in the formation of the boronic ester, the effect of pH on the ζ-potential of NP(PDMAPAAm)-PBA was examined (Figure 6). The ζ-potential of NP(PDMAPAAm)-PBA at pH 7.4 (39.5 ± 1.1 mV) decreased as pH increased and turned negative at pH > 11.5. PBA and DMAPAAm are two pH-dependent molecules found in NP(PDMAPAAm)-PBA. The dissociation constant (p*K*a) of PBA is 8.6, and boron atoms form tetrahedral negative ions at higher pH levels [30]. However, DMAPAAm has a p*K*a of 10.35, and deprotonation proceeds above this pH. Because NP(PDMAPAAm)-PBA has a PDMAPAAm chain, protonation of DMAPAAm is suppressed because of the adjunct protonated DMAPAAm unit, and the p*K*a of PDMAPAAm decreases by ~1 compared to that of the DMAPAAm monomer (10.35) [31]. When the pH was 8.6 or higher, PBA on the particle surface was ionized and PDMAPAAm was deprotonated simultaneously, which led to a decreased ζ-potential. The effect of protonated PDMAPAAm was hardly observed as the pH rose above 11, and the influence of boronate ions on the surface increased, causing a negative shift in the ζ-potential.

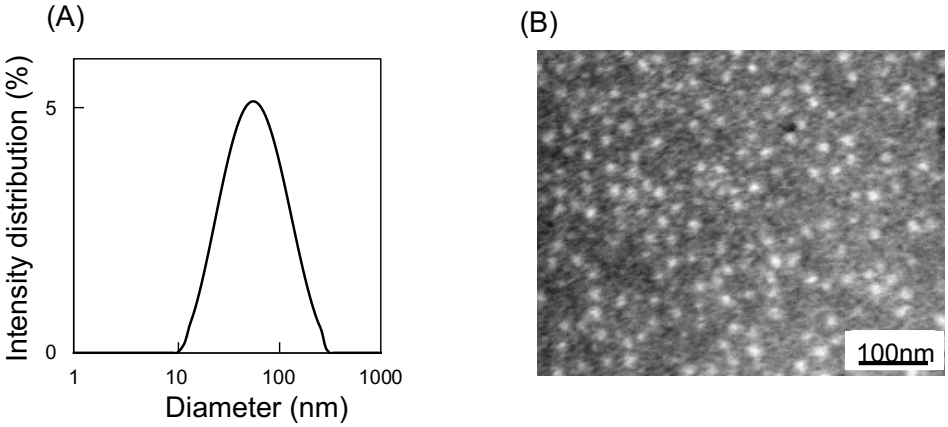

Figure 5. (A) DLS chart and (B) TEM image of NP(PDMAPAAm)-PBA.

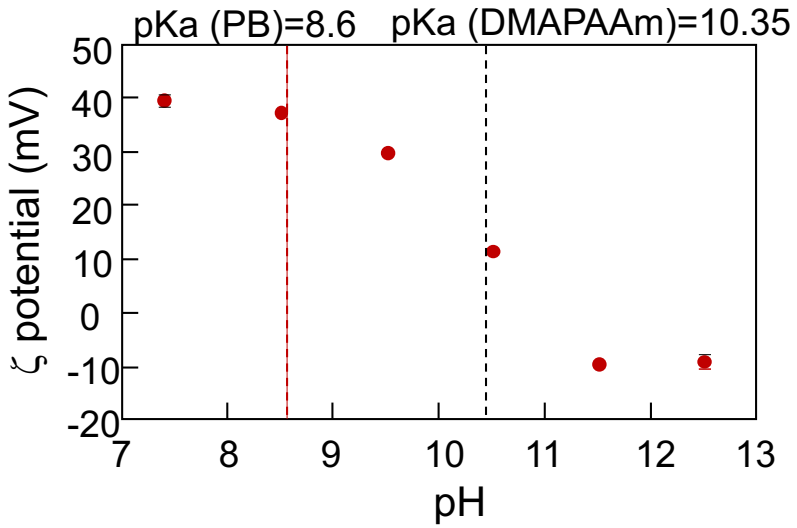

Figure 6. ζ-potentials of NP(PDMAPAAm)-PBA at different pH values (n = 3).

3.3. Thermal properties of boronic ester

PBA is used to prepare a variety of biomedical materials by forming boronic esters with diols. Except for the temperature-response behavior of thermoresponsive polymers for glucose sensing that contains PBA, the temperature responses of these boronic esters have not yet undergone a thorough analysis. As a result, the thermal properties of the boronic ester under investigation in this study were assessed using the fluorescent molecule ARS which has been catechol-functionalized and has a high affinity for PBA. When ARS binds to a PBA, it turns fluorescent, acting as a fluorescent reporter that makes it possible to figure out binding constants [28, 32].

From 20 to 50 °C, temperature-dependent fluorescence changes were seen in ARS and NP(PDMAPAAm)-PBA (Figure 7). The PBA-conjugated ARS displayed strong fluorescence at 20 °C. With the rising of temperature, the fluorescence intensity decreased and was hardly ever seen above 40 °C. According to these findings, the boronic ester gradually dissociated in a mild environment as it went from room temperature to body temperature.

DSC measurements were carried out using PBA-modified nanoparticles and PVA at various pH values to examine the thermal sensitivity of the DCBs made by NP(PDMAPAAm)-PBA and PVA diols (Figure 8) because the p*K*a of the boronic ester was affected by pH (Figure 9A). The NP(PDMAPAAm)-PBA and PVA solution displayed a small exothermal peak at pH 7.4 that began at 25–30 °C and peaked at 46 °C. However, at pH 9.5 and 11.5 the heat capacities of the NP(PDMAPAAm)-PBA and PVA solution were six times greater than at pH 7.4. Furthermore, the peaks terminated between 65 and 70 °C. However, the DSC curves were almost identical except for the value regardless of pH. Additional DSC measurements were performed using the nonionic NP(PACMO)-PBA/PVA system at pH 9.5 to confirm the influence of PDMAPAAm on PBA.

Interestingly, the resulting exothermic peak was nearly identical to the NP(PDMAPAAm)-PBA/PVA exothermic peak at pH 7.4. Additionally, the DSC analysis showed that the boronic ester could be thermally dissociated and that the DCB dissociation was triggered from 25 to 30 °C, regardless of the pH change. In particular, the fact that almost identical peak temperatures appear regardless of pH and whether cationic segments are present or not suggests that the boronic ester is generally easily dissociated by heating.

However, the stability of the bonds was found to be highly dependent on pH; DSC analysis revealed the higher diol binding strength of PBA ionized at a high pH and the high thermodynamic stability in the high-pH region.

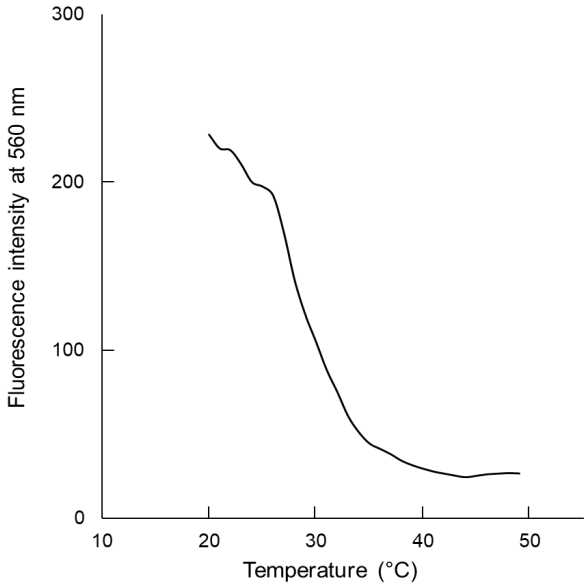

Figure 7. Fluorescence intensity changes of ARS and NP(PDMAPAAm)-PBA.

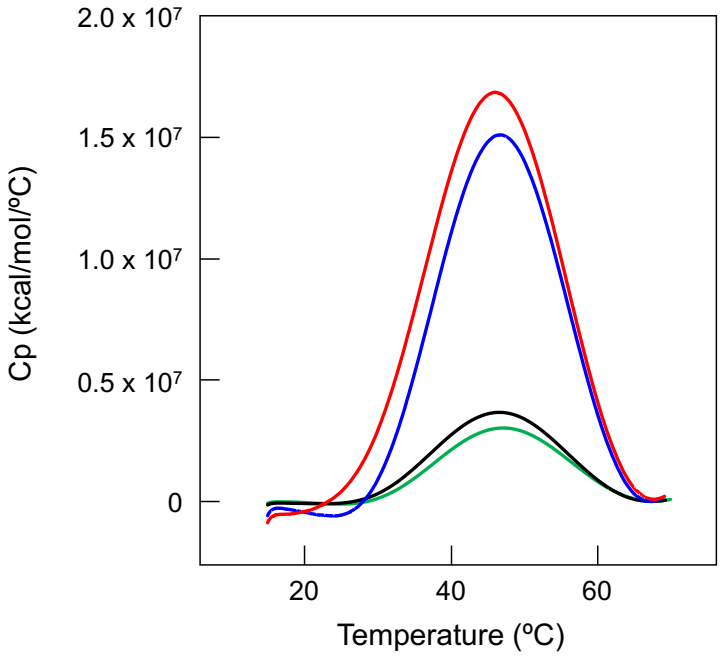

Figure 8. DSC thermograms of NP(PDMAPAAm)-PBA/PVA and NP(ACMO)-PBA/PVA at different pH values. Green, red, and blue profiles represent data of NP(PDMAPAAm)-PBA/PVA at pH 7.4, 9.5, and 11.5, respectively. The black profile represents NP(ACMO)-PBA/PVA data at pH 9.5. A nanoparticle/PVA system concentration of 0.5 wt.% was used.

Amines cause PBA to become strongly ionized, which stabilizes the ionic state of boron (Figure 9). The coordination of the nitrogen center and boron to form a tetrahedral boronate is a distinctive property of the family of boronic acids that contain an adjacent coordinating amine center [33]. Additionally, the presence of an amino group makes the polymer more soluble in water and makes it easier to form complexes with PVA. In addition, the amino group works with boronate to stabilize it in its ionized form, resulting in a powerful boronate-diol complexation [34]. The presence of NP(PDMAPAAm)-PBA involving a PBA unit on the nanoparticle surface decreased the density of the polymer chains at the outermost layer. However, PBA was connected to the PDMAPAAm chain, and numerous DMAPAAm units surrounded the PBA unit. As a result, coordination bonds between the boron and nitrogen atoms were successfully formed by the PBA and DMAPAAm units.

The optimal pH of boronic esters is between the pK_a values of PBA and diols [$pH_{optimal} = (pK_{a\text{-}acid} + pK_{a\text{-}diol})/2$] [35–37]; therefore, the optimal pH was assumed to be 12.6 in the present study. Therefore, the ionic boron was stabilized in NP(PDMAPAAm)-PBA and at the high-pH region, the boronic ester showed higher thermochemical stability.

In contrast, at pH 9.0, which was slightly higher than the p*K*a of PBA, PBA did not sufficiently form the boronic ester in the absence of the cationic segment on the particles. As a result, changes in boron's ionization state may have had a significant impact on bond stability.

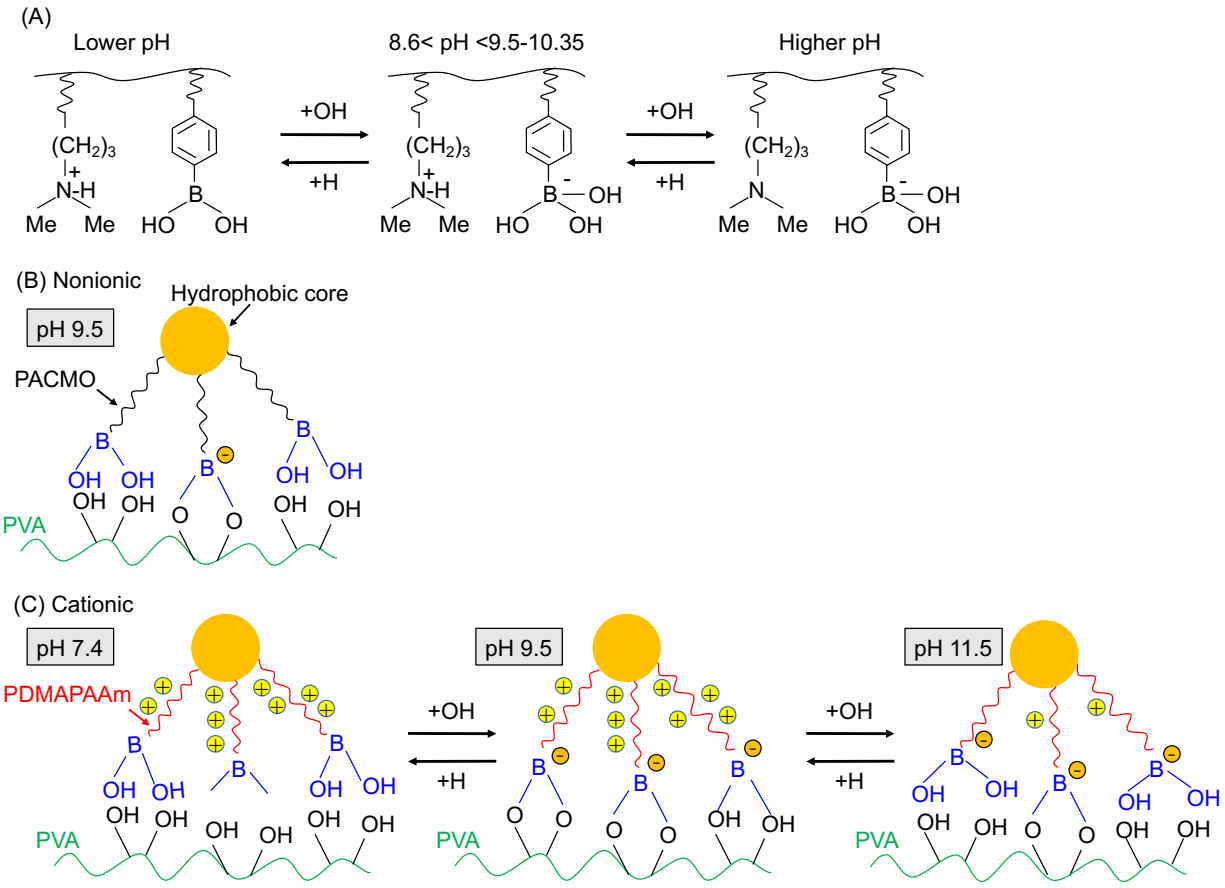

Figure 9. (A) Influence of pH on the charge of DMAPAAm and PBA. Illustration of possible changes in interactions of PVA with (B) nonionic NP(PACMO)-PBA and (C) cationic NP(PDMAPAAm)-PBA at different pH values.

3.4. Preparation and characterization of PBA-nanoparticle/PVA hydrogel

The DCBs of the boronic ester initiated temperature-responsive binding and dissociation under mild conditions from room temperature to close to body temperature, according to the fluorescence and DSC results. Following that, the circumstances for hydrogel formation using NP(PDMAPAAm)-PBA and PVA were investigated. To ionize the PBA, 1–5 wt.% of NP(PDMAPAAm)-PBA and PVA were combined at a pH of 9.5, and the viscosity of the resulting solution was measured. As a control, NP(PDMAPAAm)-DTC and PVA were prepared and mixed; regardless of the solution concentration or the NP(PDMAPAAm)-DTC/PVA mixing ratio, the viscosity of this solution did not rise.

Contrarily, when NP(PDMAPAAm)-PBA and PVA were added, the viscosity of the resulting solution increased and gelation started to take place at a solution concentration of 5 wt.% (Table 1). Due to the PBA unit only existing at the terminus of the block copolymer, which reduced the molar concentration of PBA in comparison to other PBA and PVA hydrogels [25], the concentration of NP(PDMAPAAm)-PBA was higher than that of conventional PBA and PVA hydrogels.

Table 1. Viscoelastic properties of synthesized nanoparticle/PVA mixtures at 25 °C (pH 9.5)

NP	[NP] (wt.%)	[PVA] (wt.%)	G′ (Pa)	G″ (Pa)
NP(PDMAPAAm)-PBA	5	1	4.75	5.89
	5	2.5	14.4	19.3
	5	5	68.4	50.4
	2.5	5	30.0	21.1
NP(PACMO)-PBA	5	5	0.114	1.20
NP(PDMAPAAm)-DTC	5	5	5.48	8.17

A glucose solution (1 mol/L) was used to demonstrate the bonding between the PBA on the nanoparticles and the PVA diols in the hydrogel, which was made possible by the boronic ester. The hydrogel quickly degraded because the boronic ester at the PVA diols was replaced with glucose after the addition of the glucose solution [38]. The crosslinking points of the boronic ester between PBA on the nanoparticles and PVA were therefore dissociated, indicating hydrogel formation by the DCBs of the boronic ester (Figure 10).

The viscoelasticity of the hydrogel was then studied concerning pH (Figure 11). The mixture remained in sol form at a pH of 7.4. When the pH was raised, the viscoelasticity

increased, resulting in the formation of hydrogel, and peaked at pH 9.5. Nonetheless, starting at pH 9.5, the viscoelasticity gradually decreased, producing a sol at a pH greater than 11. These findings suggest that if the pH of the solution is higher than the p*K*a of PBA and lower than the p*K*a of PDMAPAAm, a stable hydrogel can be prepared using PVA and the PDMAPAAm nanoparticles, with PBA being ionized and further stabilized by protonated DMAPAAm.

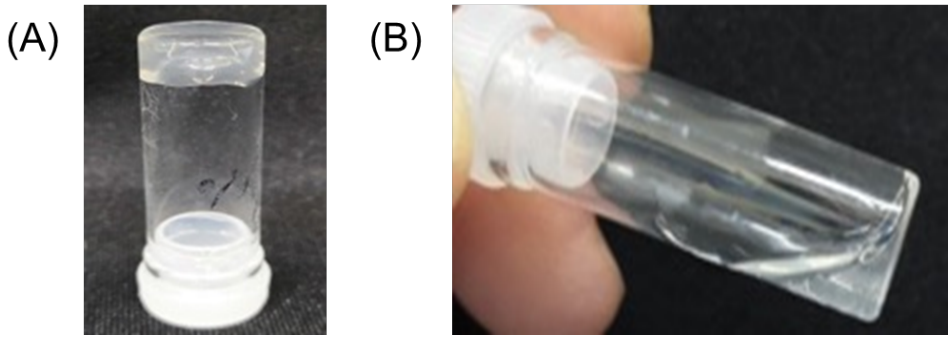

Figure 10. Photos of NP(PDMAPPAm)-PBA/PVA (A) before and (B) 30 s after adding 1 mg/mL glucose solution.

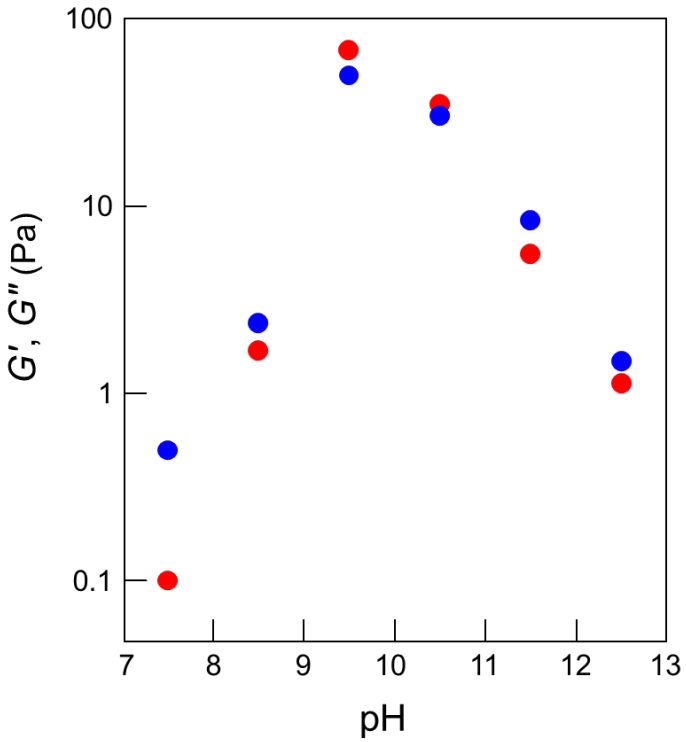

Figure 11. Effect of pH on the viscoelasticity of NP(PDMAPAAm)-PBA/PVA hydrogel. Red and blue circles indicate G′ and G″, respectively.

The addition of PBA to the nanoparticle surface produced multivalent binding between the PVA diols and PBA on the nanoparticles. By preparing linear P(DMAPAAm-*co*-PBA) (DMAPAAm/PBA = 475/25 (unit) as determined by ^{1}H-NMR spectroscopy) and mixing it with PVA, this multivalent binding effect was assessed. Similar to the mixture of NP(PDMAPAAm)-PBA and PVA, linear P(DMAPAAm-*co*-PBA) and PVA showed the highest value in a region with values higher than the p*K*a of PBA, though it failed to form a hydrogel (Table 2). These results suggest that the introduction of PBA to the nanoparticle surface is critical to the preparation of stable hydrogels because the multivalent-bond-formation characteristic of the boronic ester; furthermore, the formation of the boronic ester on the nanoparticle surface in 3D enables efficient nanoparticle-PVA bonding.

Table 2. Viscoelasticity change of P(DMAPAAm-*co*-APBA)/PVA(5 wt.%/5 wt.%) solution

pH	G′ (Pa)	G″ (Pa)
8.5	1.9	2.7
9.5	2.7	4.2
10.5	2.9	4.6

3.5. Thermally induced formation and dissociation of crosslinking points in hydrogel

The thermal characteristics of NP(PDMAPAAm)-PBA/PVA hydrogel at pH 9.5 were subsequently examined using a rheometer (Figure 12). As the temperature rose above 25 °C, the viscoelasticity of the gel gradually decreased. At 39.7 °C, G″ surpassed G′, indicating a gel-sol phase transition. In contrast, as the solution temperature dropped from 50 °C, the viscoelasticity gradually increased. In addition, at 21.3 °C, G′ overtook G″ and gelation took place, demonstrating the reversibility of the sol-gel transition of the PBA-nanoparticle/PVA mixture. According to the DSC measurements, bond dissociation was almost complete at 65 °C. In order to study the viscoelasticity of the sol phase, the solution temperature was elevated to more than 50 °C. Viscoelasticity gradually decreased as the temperature rose above 50 °C, resulting in G′ and G″ values of less than 1 Pa above 65 °C. These findings show that the crosslinking points formed by the PBA-PVA bonds, gradually dissociated with rising temperature. The structure of the hydrogel containing 5 wt.% NP(PDMAPAAm)-PBA at pH 9.5 collapsed at a temperature below that at which half of the bonds dissociated, turning the hydrogel into a sol, according to DSC analysis. When the temperature was raised to 65 °C or higher, almost all of the PBA-diol bonds broke down, and the PBA particles and PVA

molecules were thought to exist independently. As a result, the PBA-diol bonds dissociated at mild temperatures, and it was simple to control the crosslinking state of the gel by adjusting the temperature. The hydrogel's restoration effectiveness was finally verified by varying the temperature (between 25 and 50 °C). The hydrogel's G′ and G″ values were 145 and 82 Pa, respectively, at 25 °C. Following 10 minutes of heating at 50 °C and 10 minutes of cooling at 25 °C, the sample had G′ values for the hydrogel of 119 and 66 Pa, respectively. The restoration efficiency, which was estimated to be 82%, gradually declined with repeated heating and cooling, becoming only 70% after the fifth cycle.

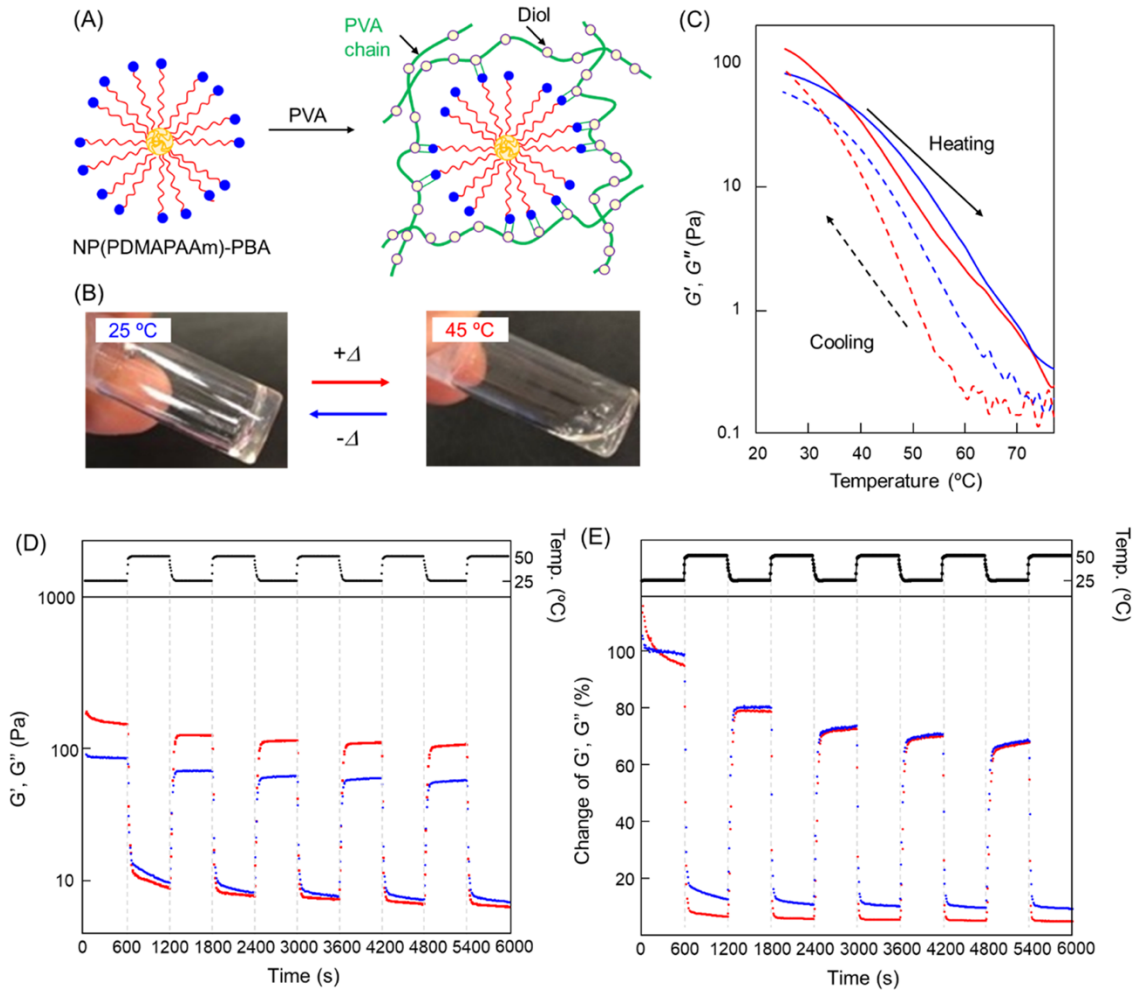

Figure 12. Changes in thermo-viscoelasticity of NP(PDMAPAAm)-PBA/PVA. (A) Preparation of hydrogel using NP(PDMAPAAm)-PBA and PVA. (B) Images of a mixture of NP(PDMAPAAm)-PBA (5 wt.%) and PVA (5 wt.%) at 25 and 45 °C. Sol–gel phase transition occurred reversibly in response to temperature variations. (C) Changes in viscoelasticity of NP(PDMAPAAm)-PBA (5 wt.%) and PVA (5 wt.%) at pH 9.5. Red and blue profiles indicate G′ and G″, respectively. Solid and dashed profiles indicate heating and cooling processes (5 °C/min), respectively. (D) G′ and G″ data and (E) restoration efficiency of NP(PDMAPAAm)-PBA (5 wt.%) and PVA (5 wt.%) at 25 and 50 °C. The temperature was alternated between 25 and 50 °C every 10 min.

By crosslinking the hydrogel with glutaraldehyde, the self-healing capability of the material was examined. The NP(PDMAPAAm)-PBA/PVA hydrogel was crosslinked with glutaraldehyde to maintain its structure at higher temperatures because the hydrogel turned into a sol at temperatures over 39 °C. The hydrogel maintained its structure at 45 °C, as shown in Figure 13. The Young's moduli of the hydrogel were calculated using the following equation before and after thermal cycling:

$$E = 2G'(1+ \nu),$$

where E and ν represent Young's modulus and Poisson's ratio, respectively.

The Young's moduli of the unheated, heat-treated (50 °C), and cooled (25 °C) hydrogel were determined to be 321, 33, and 119 Pa, respectively. As shown in Figure 12D, the stiffness of the hydrogel was not sufficiently restored after 10 min of cooling. However, the boronic ester was gradually formed at a low temperature, which increased the stiffness of the hydrogel.

Using colored hydrogel samples, the hydrogel's capacity to reestablish connections was examined in order to verify its self-healing ability. The hydrogels were prepared, formed into cubes, and tested for adhesion by changing the temperature (Figure 13B). At first, no adhesion was seen when the cut surfaces of the gels were brought into contact with one another at 25 °C. The hydrogel cubes were then heated on a hot plate at 45 °C, which caused them to soften and significantly raise G″; at 25 °C, G′ and G″ values were 128 and 81 Pa, respectively, and changed to 7 and 11 Pa at 50 °C. Furthermore, under heated conditions, no adhesion between the cut surfaces was seen. However, adhesion was observed when these gels were cooled to room temperature with the cut surfaces in contact. The strong connections due to the self-healing ability of the NP(PDMAPAAm)-PBA/PVA hydrogel were confirmed by stretching it to more than two-fold (Figure 13).

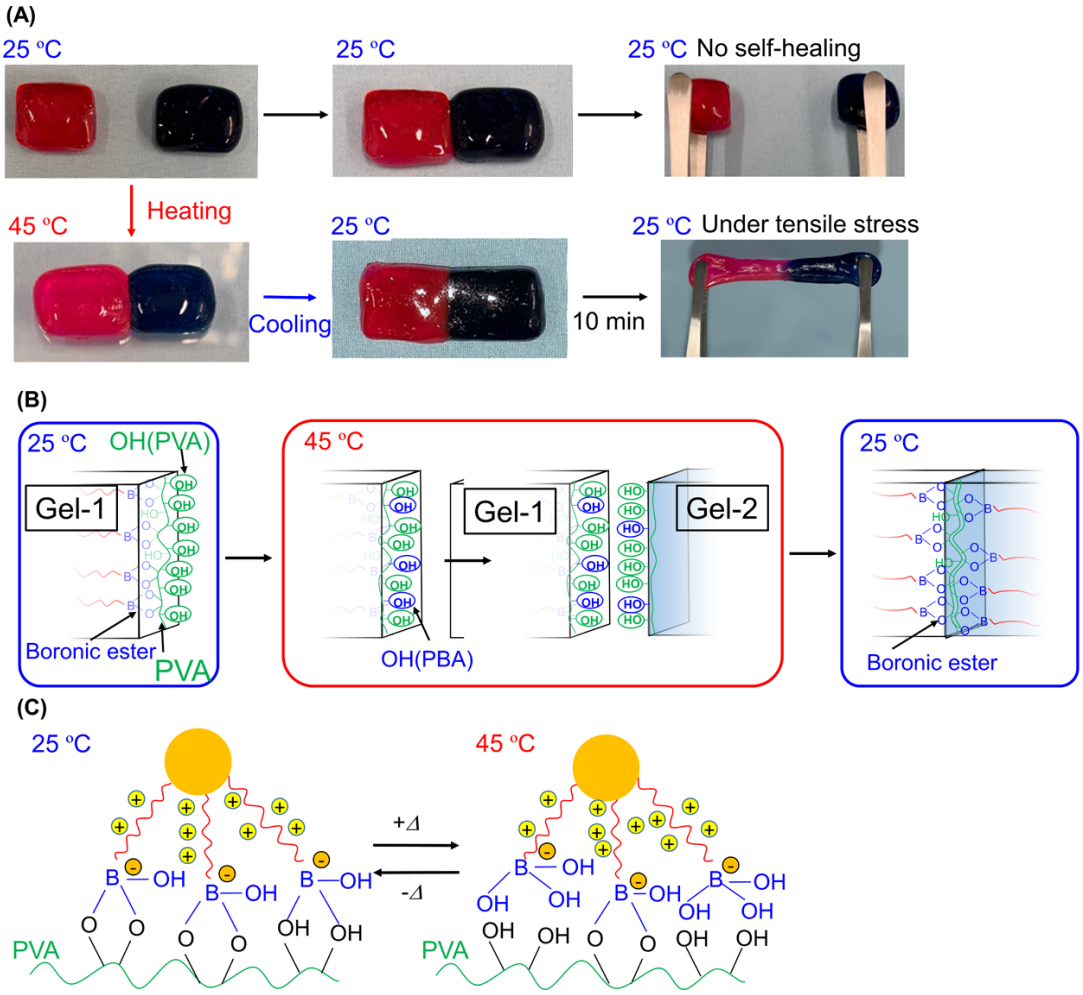

Figure 13. Self-healing properties of NP(PDMAPAAm)-PBA/PVA hydrogel. (A) Photos of hydrogels at each step of the thermal investigation. Red and blue hydrogels were stained with sulforhodamine B and methylene blue, respectively. (B) Possible changes in surface chemistry of the NP(PDMAPAAm)-PBA/PVA hydrogel at each investigated temperature. (C) Illustration of possible changes in interactions between PVA and NP(PDMAPAAm)-PBA at different temperatures.

Overall, by defining the thermochemical characteristics of PBA-diol bonds, a hydrogel capable of undergoing sol-gel transition under incredibly mild conditions was successfully synthesized. It is known that the thermal dissociation of various DCBs causes gels to acquire thermal properties. Schiff bases, which are frequently thermally dissociable DCBs, must still withstand temperatures above 67 °C to undergo thermal dissociation [8]. Through the evaporation of water and drying of the surface, high temperatures have a significant impact on the characteristic of hydrogels. However, in contrast to other DCBs, the PBA-diol bonds can start to break down at 30 °C and completely do so at 60 °C. As a result, using mild temperature treatments, the PBA-diol hydrogel can easily acquire self-healing properties. Furthermore, functional control of this hydrogel made of boronic esters was shown to work at temperatures close to body temperature. Although a high pH is needed for its preparation, this hydrogel is anticipated to have a wide range of applications and be suitable for use as a medical material on skin surfaces. Basically, this boronic-ester-DCB-based hydrogel can be used as a substance that can express its functions in ambient environments, like body surfaces, because it works well in conditions of mild temperature changes.

4. Conclusion

In contrast to other temperature-responsive DCBs, the thermal cleavage of the boronic ester DCBs was found to start at a low temperature of 25–30 °C and dissociate (half of the DCBs) at 46 °C. With rising temperatures, the viscoelasticity of the hydrogel, which uses a boronic ester for crosslinking, changed significantly. In particular, the hydrogel transformed into a sol at temperatures over 39.7 °C because of the dissociation of its boronic- ester-based cross-linking points. The hydrogel recovered after cooling at 25 °C because the boronic ester was rebuilt. By lowering the temperature, the thermally cleaved boronic ester inside the hydrogel or on its surface could be randomly reconjugated. As a result, exchange between the boronic ester on the hydrogel surfaces allowed for their connection, demonstrating its capacity for self-healing. The boronic ester could be controlled under gentle conditions at temperatures slightly higher than body temperature, and the self-healing property was demonstrated without changing the properties of the hydrogel derived via water evaporation, for instance. As a result, the NP(PDMAPAAm)-PBA system, based on boronic esters, has the potential to be a promising hydrogel crosslinker for the creation of intelligent hydrogels for biomedical applications.

5. References

1. Zhang, Y.; Xie, S.; Zhang, D.; Ren, B.; Liu, Y.; Tang, L.; Chen, Q.; Yang, J.; Wu, J.; Tang, J., Thermo-responsive and shape-adaptive hydrogel actuators from fundamentals to applications. Eng. Sci. 2019, 6.
2. Zhang, D.; Ren, B.; Zhang, Y.; Xu, L.; Huang, Q.; He, Y.; Li, X.; Wu, J.; Yang, J.; Chen, Q., From design to applications of stimuli-responsive hydrogel strain sensors. J. Mater. Chem. B 2020, 8 (16), 3171-3191.
3. Mai, W.; Yu, Q.; Han, C.; Kang, F.; Li, B., Self-healing materials for energy-storage devices. Adv. Funct. Mater. 2020, 30 (24), 1909912.
4. Li, S.; Wang, L.; Zheng, W.; Yang, G.; Jiang, X., Rapid fabrication of self-healing, conductive, and injectable gel as dressings for healing wounds in stretchable parts of the body. Adv. Funct. Mater. 2020, 30 (31), 2002370.
5. Chen, Y.; Tan, Z.; Wang, W.; Peng, Y.-Y.; Narain, R., Injectable, self-healing, and multi-responsive hydrogels via dynamic covalent bond formation between benzoxaborole and hydroxyl groups. Biomacromolecules 2018, 20 (2), 1028-1035.
6. Perera, M. M.; Ayres, N., Dynamic covalent bonds in self-healing, shape memory, and controllable stiffness hydrogels. Polym. Chem. 2020, 11 (8), 1410-1423.
7. Habault, D.; Zhang, H.; Zhao, Y., Light-triggered self-healing and shape-memory polymers. Chem. Soc. Rev. 2013, 42 (17), 7244-7256.
8. Miao, J.-T.; Ge, M.; Peng, S.; Zhong, J.; Li, Y.; Weng, Z.; Wu, L.; Zheng, L., Dynamic imine bond-based shape memory polymers with permanent shape reconfigurability for 4D printing. ACS Appl. Mater. Interfaces 2019, 11 (43), 40642-40651.
9. Taylor, D. L.; in het Panhuis, M., Self-healing hydrogels. Adv. Mater. 2016, 28 (41), 9060-9093.
10. Wu, G.; Jin, K.; Liu, L.; Zhang, H., A rapid self-healing hydrogel based on PVA and sodium alginate with conductive and cold-resistant properties. Soft Matter 2020, 16 (13), 3319-3324.
11. Zhang, H.; Wang, D.; Wu, N.; Li, C.; Zhu, C.; Zhao, N.; Xu, J., Recyclable, self-healing, thermadapt triple-shape memory polymers based on dual dynamic bonds. ACS Appl. Mater. Interfaces 2020, 12 (8), 9833-9841.
12. de Hatten, X.; Bell, N.; Yufa, N.; Christmann, G.; Nitschke, J. R., A dynamic covalent, luminescent metallopolymer that undergoes sol-to-gel transition on temperature rise. J. Am. Chem. Soc. 2011, 133 (9), 3158-3164.

13. Folmer-Andersen, J. F.; Lehn, J.-M., Thermoresponsive dynamers: thermally induced, reversible chain elongation of amphiphilic poly(acylhydrazones). J. Am. Chem. Soc. 2011, 133 (28), 10966-10973.
14. Bapat, A. P.; Ray, J. G.; Savin, D. A.; Hoff, E. A.; Patton, D. L.; Sumerlin, B. S., Dynamic-covalent nanostructures prepared by Diels-Alder reactions of styrene-maleic anhydride-derived copolymers obtained by one-step cascade block copolymerization. Polym. Chem. 2012, 3 (11), 3112-3120.
15. Liu, Y.-L.; Chuo, T.-W., Self-healing polymers based on thermally reversible Diels-Alder chemistry. Polym. Chem. 2013, 4 (7), 2194-2205.
16. Tuten, B. T.; Chao, D.; Lyon, C. K.; Berda, E. B., Single-chain polymer nanoparticles via reversible disulfide bridges. Polym. Chem. 2012, 3 (11), 3068-3071.
17. Otsuka, H.; Aotani, K.; Higaki, Y.; Takahara, A., A dynamic (reversible) covalent polymer: radical crossover behaviour of TEMPO–containing poly(alkoxyamine ester)s. Chem. Commun. 2002, (23), 2838-2839.
18. Chen, Q.; Zhu, L.; Chen, H.; Yan, H.; Huang, L.; Yang, J.; Zheng, J., A novel design strategy for fully physically linked double network hydrogels with tough, fatigue resistant, and self-healing properties. Adv. Funct. Mater. 2015, 25 (10), 1598-1607.
19. Cai, Y.; Zou, H.; Zhou, S.; Chen, Y.; Liang, M., Room-temperature self-healing ablative composites via dynamic covalent bonds for high-performance applications. ACS Appl. Polym. Mater. 2020, 2 (9), 3977-3987.
20. Xu, J.; Guo, Z.; Chen, Y.; Luo, Y.; Xie, S.; Zhang, Y.; Tan, H.; Xu, L.; Zheng, J., Tough, adhesive, self-healing, fully physical crosslinked κ-CG-K+/pHEAA double-network ionic conductive hydrogels for wearable sensors. Polymer 2021, 236, 124321.
21. Bapat, A. P.; Sumerlin, B. S.; Sutti, A., Bulk network polymers with dynamic B–O bonds: healable and reprocessable materials. Mater. Horiz. 2020, 7 (3), 694-714.
22. Cho, S.; Hwang, S. Y.; Oh, D. X.; Park, J., Recent progress in self-healing polymers and hydrogels based on reversible dynamic B–O bonds: boronic/boronate esters, borax, and benzoxaborole. J. Mater. Chem. 2021, 9 (26), 14630-14655.
23. Anzai, J.-i., Recent progress in electrochemical biosensors based on phenylboronic acid and derivatives. Mater. Sci. Engi.C 2016, 67, 737-746.
24. Matsumoto, A.; Yoshida, R.; Kataoka, K., Glucose-responsive polymer gel bearing phenylborate derivative as a glucose-sensing moiety operating at the physiological pH. Biomacromolecules 2004, 5 (3), 1038-1045.

25. Konno, T.; Ishihara, K., Temporal and spatially controllable cell encapsulation using a water-soluble phospholipid polymer with phenylboronic acid moiety. Biomaterials 2007, 28 (10), 1770-1777.
26. Kataoka, K.; Miyazaki, H.; Okano, T.; Sakurai, Y., Sensitive glucose-induced change of the lower critical solution temperature of poly[N, N-(dimethylacrylamide)-co-3-(acrylamido)-phenylboronic acid] in physiological saline. Macromolecules 1994, 27 (4), 1061-1062.
27. Hoare, T.; Pelton, R., Charge-switching, amphoteric glucose-responsive microgels with physiological swelling activity. Biomacromolecules 2008, 9 (2), 733-740.
28. Yan, J.; Springsteen, G.; Deeter, S.; Wang, B., The relationship among pKa, pH, and binding constants in the interactions between boronic acids and diols—it is not as simple as it appears. Tetrahedron 2004, 60 (49), 11205-11209.
29. Akimoto, J.; Nakayama, M.; Sakai, K.; Okano, T., Temperature-induced intracellular uptake of thermoresponsive polymeric micelles. Biomacromolecules 2009, 10 (6), 1331-1336.
30. Shno, D.; Kubo, A.; Murata, Y.; Koyama, Y.; Kataoka, K.; Kikuchi, A.; Sakurai, Y.; Okano, T., Amine effect on phenylboronic acid complex with glucose under physiological pH in aqueous solution. J. Biomater. Sci. Polym. Ed. 1996, 7 (8), 697-705.
31. Brilmayer, R.; Hess, C.; Andrieu-Brunsen, A., Influence of chain architecture on nanopore accessibility in polyelectrolyte block-co-oligomer functionalized mesopores. Small 2019, 15 (41), 1902710.
32. Mulla, H. R.; Agard, N. J.; Basu, A., 3-Methoxycarbonyl-5-nitrophenyl boronic acid: high affinity diol recognition at neutral pH. Bioorg. Med. Chem Lett. 2004, 14 (1), 25-27.
33. Wulff, G.; Lauer, M.; Böhnke, H., Rapid proton transfer as cause of an unusually large neighboring group effect. Angew. Chem. Int. Ed. 1984, 23 (9), 741-742.
34. Kitano, S.; Hisamitsu, I.; Koyama, Y.; Kataoka, K.; Okano, T.; Sakurai, Y., Effect of the incorporation of amino groups in a glucose-responsive polymer complex having phenylboronic ac moieties. Polyme. Adv. Technol. 1991, 2 (5), 261-264.
35. Sienkiewicz, P. A.; Roberts, D. C., Chemical affinity systems-I: pH dependence of boronic acid-diol affinity in aqueous solution. J. Inorg. Nucl. Chem. 1980, 42 (11), 1559-1575.
36. Liu, X.-C.; Scouten, W. H., New ligands for boronate affinity chromatography. J. Chromatogr. A 1994, 687 (1), 61-69.

37. Van Duin, M.; Peters, J.; Kieboom, A.; Van Bekkum, H., Studies on borate esters 1: The ph dependence of the stability of esters of boric acid and borate in aqueous medium as studied by 11B NMR. Tetrahedron 1984, 40 (15), 2901-2911.
38. Nakahata, M.; Mori, S.; Takashima, Y.; Hashidzume, A.; Yamaguchi, H.; Harada, A., pH- and sugar-responsive gel assemblies based on boronate–catechol interactions. ACS Macro Lett. 2014, 3 (4), 337-340.

CHAPTER III

STRONG AND EFFICIENT SELF-HEALING HYDROGEL BY TEMPLATE POLYMERIZATION AROUND 3D NANOPARTICLE COMPOSED OF DYNAMIC COVALENT BOND

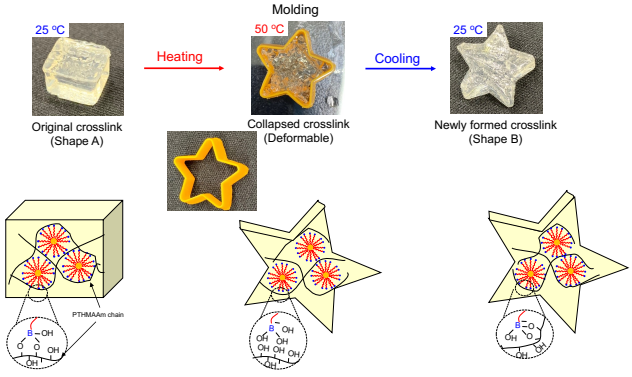

1. Introduction

As described in chapter II, self-healing and thermoplastic hydrogels were prepared using DCB, which exhibits reversible dissociation and bonding through stimuli as the crosslinking points in the hydrogels [1–3]. By controlling the bonding and dissociation of the DCBs, the DCB-derived functional groups can be reconnected with their counterparts to recover the crosslinking points in the hydrogel, allowing the hydrogel to exhibit self-healing characteristics [4,5]. In addition, the dissociation of DCBs can drastically affect the structural stability of the hydrogel, thus imparting thermoplastic properties to the hydrogel [6,7]. Because the DCBs between the functional groups that form the crosslinking points are in equilibrium, they are temporally dissociated at the cracking or fracture point of the hydrogel.

In contrast, such broken gel surfaces are gradually restored through contact under appropriate conditions because the DCBs reach equilibrium to form new connections to re-adhere and strengthen the hydrogel [8,9]. The recovery of the crosslinked structure occurs when the functional groups on the polymer come into contact with each other; thus, the diffusion of molecules is the most important factor in determining the re-adhesion performance of the hydrogel [10,11]. Because recombination between functional groups is time- and temperature-dependent, functional groups can recombine when their density becomes high. Thus, polymer diffusion and mobility highly depend on the improvement of the gel-to-gel re-connection [12,13].

Generally, DCB-based hydrogels are prepared by mixing polymers to connect them via chemical or physical interactions. After mixing the polymers, DCB-derived functional groups form DCBs to crosslink the polymers [1]. The crosslinking formation is highly dependent on the diffusion of molecules [10,13]. However, the diffusivity of a polymer is significantly lower than that of small molecules owing to its high molecular weight, limiting its contact with DCB-derived functional groups [14,15]. In addition, the steric hindrance of a polymer also limits DCB formation [1,15]. Thus, some of the DCB-derived functional groups remain free in the gel, and the reaction rate is low. Moreover, the structure of the hydrogel becomes non-uniform because of the free functional groups, delaying the recombination of the hydrogel in the self-healing reaction [16]. Indeed, some self-healing hydrogels exhibit instantaneous reattachments. When a large number of functional groups exist on the surface of a hydrogel, the formation of new crosslinking points on surfaces of hydrogel causes fast adhesion between the gels; however, not all functional groups are reconnected to completely recover the physical properties of the hydrogel. Thus, the diffusion, mobility, and exclusion volume effects of a polymer must be

reduced to promote the recombination of crosslinking points to completely recover the hydrogel properties [16–18].

In this study, DCB bonds, which become the crosslinking points of a hydrogel, were formed in advance between nanoparticles (NPs) and small molecules, and the NPs were polymerized through “template polymerization” to enhance the recombination ability of the DCBs.

2. Materials and Methods

2.1. Materials

PBA-NPs were prepared as the previously reported method [1]. N-[Tris(hydroxymethyl)methyl]acrylamide (THMAAm) was purchased from Thermo Fisher Scientific (Horsham, UK). N,N-dimethylaminopropyl acrylamide (DMAPAAm) was purchased from FUJIFILM Wako Pure Chemicals (Tokyo, Japan) and was purified by distillation under reduced pressure. N,N,N′,N′-tetramethyl ethylenediamine (TEMED), Ammonium persulfate (APS), 2-ethanolamine, 2,2′-azobisisobutyronitrile (AIBN), hexane, and 1,4-dioxane, were also bought from FUJIFILM Wako Pure Chemicals. 3- (acrylamido) phenylboronic acid (APBA; Combi-Blocks, San Diego, CA), tris(2-carboxyethyl) phosphine hydrochloride (TCEP; Tokyo Chemical Industry, Tokyo, Japan). 2-cyano-2-propyl dodecyl trithiocarbonate (CPDT; Sigma-Aldrich, St. Louis, MO) was used as received.

2.2. Preparation of TempGel(NP)

The PBA-NPs were prepared as previously described [1]. PBA-NP and THMAAm were dissolved in water and the resulting solution was bubbled with N_2 gas for 10 min. Ammonium persulfate (APS) and N,N,N′,N′-tetramethyl ethylenediamine (TEMED) were then added to the solution in an ice bath. After 10 min, the hydrogel was collected from a vial and put into a mold at 50 °C. For visual observation, the hydrogel was stained with methylene blue.

2.3. Preparation of TempGel(LN)

P(APBA-*co*-DMAPAAm) diblock copolymer (LN) was prepared by sequential RAFT polymerization. Briefly, DMAPAAm, CPDT, and AIBN were dissolved in 1,4-dioxane and then bubbled with N_2 for 20 min at 25 °C. The solution was reacted at 80 °C for 24 h. Subsequently, APBA and TCEP were added. Then, 2-aminoethanol was slowly added to the preceding solution to convert the dodecyl trithiocarbonate (DTC) group into APBA on the terminus of the block copolymer. The solution was stirred at 25 °C for 12 h. After the reaction, the reactant solution was dialyzed against water for 72 h using a dialysis membrane (MWCO

3500), yielding polymers upon freeze-drying. TempGel(LN) was prepared as the above protocol of TempGel(NP).

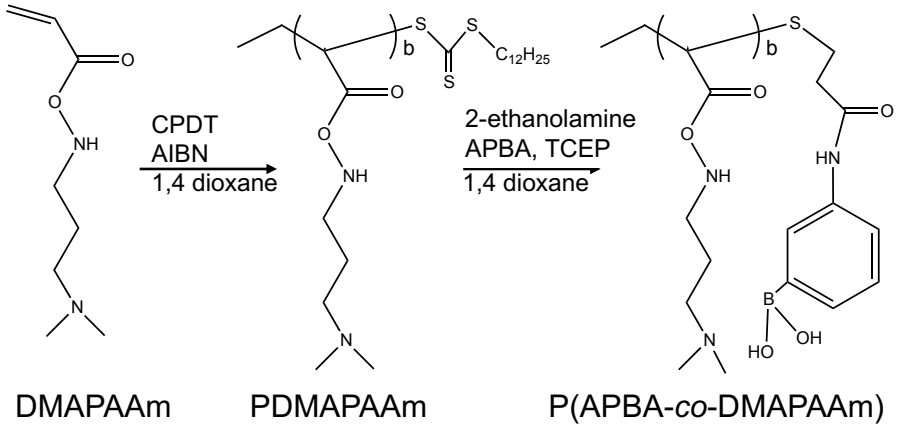

Scheme 1. Preparation of linear P(APBA-co-DMAPAAm) diblock copolymers

2.4. Viscoelasticity measurements

The hydrogel was then placed on a rheometer plate (AR-G2, TA Instruments, New Castle, DE, USA). The solution was covered with silicon oil to avoid water evaporation, and time sweep measurements were performed at a fixed frequency (ω = 1 Hz) and strain (γ = 1 and 1000%). The measurements were taken in a temperature range of 20–80 °C.

To confirm the self-healing property of the hydrogel, colored and non-colored cubic hydrogels were brought together at 50 °C using a hot plate. Subsequently, the heated hydrogels were cooled to room temperature, and the hydrogel connection was visually confirmed for each process.

In addition, the thermoplastic properties of the hydrogels were confirmed. First, the cubic hydrogel was maintained at room temperature. Then, the hydrogel was heated to 50 °C to soften and sealed in a star-shaped mold. After cooling to 25 °C, the hydrogel was recovered from the mold and the shape of the hydrogel was observed.

3. Results and discussion

3.1. Preparation of THMAAm hydrogel

PB surface NPs (PBA-NPs) were prepared by the assembly of ω-PBA-poly(butyl methacrylate)$_{14}$-*b*-poly(N,N-dimethylaminopropylacylamide)$_{74}$ (PBMA-*b*-PDMAPPAm-PBA), as previously reported [1]. PBA-NPs and N-[Tris(hydroxymethyl)methyl] acrylamide (THMAAm) were mixed in water to form a boronic ester bonding between PBA on the surface of the NPs and the hydroxyl groups on THMAAm in advance. Subsequently, THMAAm was polymerized using ammonium persulfate (APS) and N,N,N′,N′-tetramethyl ethylenediamine (TEMED) to obtain a hydrogel (Figure 1), which is denoted as TempGel(NP). Furthermore, a hydrogel prepared using the conventional method of mixing PBA-NPs and poly (N-[Tris(hydroxymethyl)methyl] acrylamide) (PTHMAAm) is denoted as MixGel(NP)) (Figure 1).

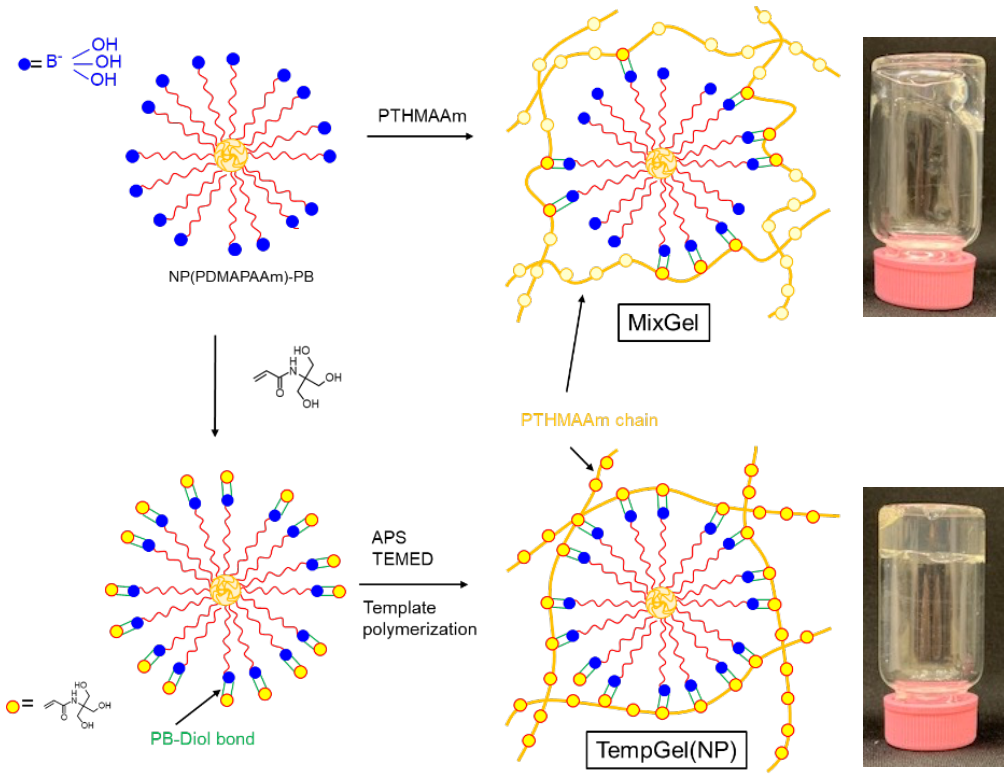

Figure 1. Schematic illustration of hydrogel preparation by mixing a PTHMAAm chain and PBA-NP (MixGel(NP)) and the template polymerization of THMAAm using PBA-NP as the crosslinker (TempGel(NP)).

3.2. Optimization of hydrogel preparation

3.2.1. The effect of preparation methods

Changes in the thermal viscoelasticity of the hydrogels were investigated using a rheometer. In the case of MixGel(NP), the elasticity modulus (G′) gradually decreased with increasing temperature above 25 °C. Furthermore, the fluidity modulus (G″) of the hydrogel slightly increased up to 60 °C and then decreased from 60 °C (Figure 2A). The temperature was decreased from 80 °C, and the G′ and G″ of the hydrogel recovered with decreasing temperature, confirming the hysteresis. However, the values of G′ and G″ were not the same as those of the original hydrogel at 25 °C, and the value of G′ of MixGel(NP) after four thermal cycles was 90% of the original hydrogel.

In contrast, the G′ of TempGel(NP) was nearly constant with increasing temperature up to 60 °C and then gradually decreased over 60 °C. Interestingly, the G″ of TempGel(NP) increased with increasing temperature up to 60 °C (Figure 2B). A high hysteresis was observed during the cooling of the hydrogel. To confirm the thermoresponsive behavior, changes in viscoelasticity of the hydrogels at the temperature cycles of 25 and 50 °C were observed concerning time (Figure 2C-D). While TempGel(NP) exhibited a significant change in thermal viscoelasticity, MixGel(NP) did not recover its original G′ value by leaving a low temperature for 10 min after high-temperature treatment. In chapter I, a hydrogel was prepared by mixing PBA-NPs and poly(vinyl alcohol) instead of PTHMAAm. In the mixing method, regardless of the polymer composition, once the crosslinking point is dissociated by high temperatures, hydrogels cannot reorganize the crosslinking points as the temperature decreases [1]. The results indicated that the properties of a hydrogel had significant effects on the hydrogel preparation method, and TempGel(NP) exhibited high hysteresis and structural stability.

As mentioned earlier, MixGel(NP) was prepared using a conventional method of mixing two macromolecules, PBA-NPs and PTHMAAm, to form a boronic ester as the crosslinking point. To form this boronic ester, PBA on the surface of NPs and diol molecules on the PTHMAAm must be diffused in the resulting solution. The low diffusion, motility, and steric hindrance of the PTHMAAm molecules reduce the formation efficiency of the boronic ester, resulting in the low viscoelasticity of the hydrogel.

In chapter I, the thermoresponsive behavior of a boronic ester between PBA-NPs and poly(vinyl alcohol) (PVA) was investigated. The boronic ester was found to be dissociated at 25–30 °C and almost completely dissociated at temperatures above 60 °C (half dissociated temperature was 46 °C) [1]. Therefore, the crosslinking point of the boronic ester in

MixGel(NP) gradually collapsed with increasing temperature. In addition, the motility of PTHMAAm, which forms the skeleton of the gel, increased, and the hydroxyl groups on PTHMAAm shifted away from PBA on the surface of NPs. As a result, NPs and PTHMAAm chains independently existed as a solution when all the boronic acid esters were dissociated at above 60 °C. Once the PTHMAAm chains are separated from the NPs, each functional group on the diffused molecule must contact again to reform the boronic ester. PBA on the NPs and hydroxyl groups on PTHMAAm were randomly conjugated during this recombination. Thus, the reformation of the boronic ester was suppressed and incomplete, owing to the excluded volume effect of PTHMAAm. In addition, not all the PBA on the NPs formed boronic esters with PTHMAAm, resulting in low viscoelasticity of the MixGel(NP).

TempGel(NP) was prepared via template polymerization using PBA-NPs and THMAAm. The THMAAm molecule has a low molecular weight and is mixed with PBA-NPs before polymerization; therefore, all the PBAs on the surface of NPs formed boronic ester. After polymerization, the PTHMAAm chains densely surrounded the NPs with a multivalent boronic ester, which gradually dissociated with increasing temperature. Although the number of boronic esters between PTHMAAm and the NPs decreased, the PTHMAAm chains did not diffuse from the NPs because the boronic ester partially remained between the NPs and PTHMAAm. As shown in Figure 2B, the G″ of TempGel(NP) increased with increasing temperature without changing its G′, indicating that TempGel(NP) can modify the fluidity parameter G″ with a temperature change without changing the elastic parameter G′. That is, the number of crosslinking points in the hydrogel, which was determined by the number of NPs, remained unchanged at temperatures up to 60 °C. Moreover, the number of boronic esters on the NPs decreased concerning temperature to increase the mobility of the NPs inside the gel. In the case of TempGel(NP), above 60 °C, G″ remained constant, and G′ gradually decreased with increasing temperature. Because almost all the boronic esters in hydrogel dissociated over 60 °C, the mobility of NPs was saturated. In addition, the PTHMAAm chain of MixGel(NP) can diffuse from the NP due to the loss of the boronic ester.

Interestingly, TempGel(NP) exhibited considerably high hysteresis under the temperature cycles of 25–50 °C. At 60 °C, TempGel(NP) lost the boronic ester on the surface of NPs. However, at 50 °C, approximately 50% of the boronic ester remained to connect NPs and PTHMAAm, as discussed in the previous differential scanning calorimetry (DSC) analysis (Figure 3) [1]. Thus, the dissociated boronic ester quickly reconnected to form a boronic ester. This behavior is almost the same as the “zipper mechanism” of reactions between

macromolecules. Therefore, after the temperature-induced dissociation of the boronic ester, numerous hydroxyl groups closely surrounded PBA to reform rapidly and efficiently the boronic ester in the hydrogel.

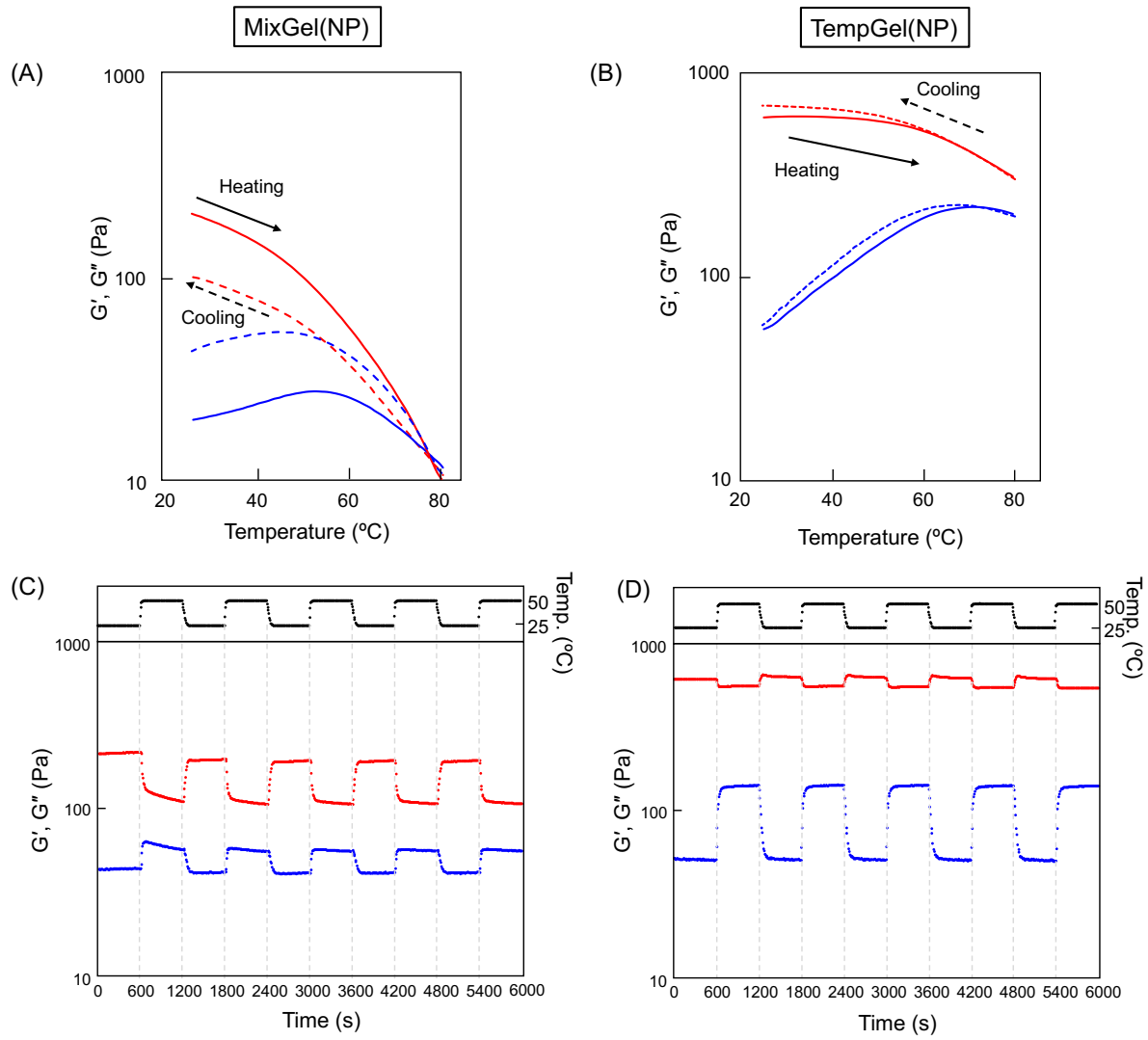

Figure 2. Changes in thermal viscoelasticity of (A) MixGel(NP) and (B) TempGel(NP). Red and blue lines represent changes in G′ and G″, respectively, concerning temperature. Solid and dashed lines indicate heating and cooling processes (5 °C/min), respectively. Changes in G′ and G″ of (C) MixGel(NP) and (D) TempGel(NP) at 25 and 50 °C concerning time. The temperature was alternated between 25 and 50 °C every 10 min. Red and blue dots indicate G′ and G″, respectively.

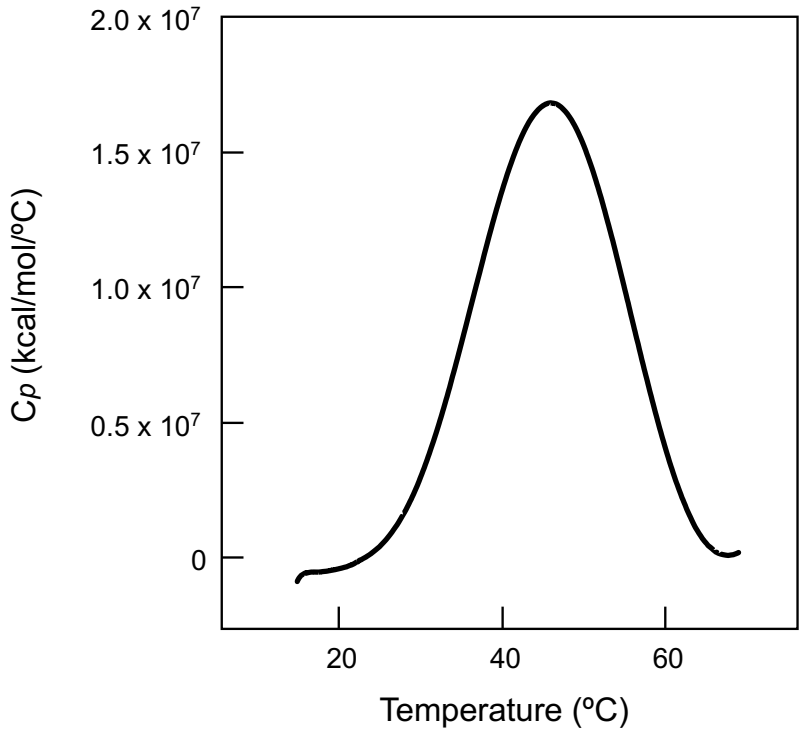

Figure 3. DSC thermograms of NP(PDMAPAAm)-PBA/PVA. A nanoparticle/PVA system concentration of 0.5 wt. % was used.

3.2.2. The effect of nanoparticles as crosslinker

To investigate the possible mechanism of the high hysteresis of TempGel(NP), the influence of hydrogel density, the diffusion effect of molecules, and the multivalency effect were further analyzed.

First, the density of the hydrogel was confirmed through scanning electron microscopy (SEM) imaging. As shown in Figure 4, MixGel(NP) had a dense porous structure similar to that of conventional hydrogels prepared via a polymer reaction [19]. In contrast, TempGel(NP) exhibited a packed structure; the NPs were dense and completely covered by PTHMAAm. These results indicate that numerous hydroxyl groups derived from the PTHMAAm chain existed on the surface of the NPs; therefore, the PBA groups nearby permitted rapid reconjugation of the boronic ester by decreasing the temperature. The viscoelasticity of TempGel(NP) was recovered rapidly when heated at 80 °C to completely dissociate the boronic ester. Furthermore, the NPs and PTHMAAm chains were supposed to be completely isolated owing to the dissociation of the boronic ester. However, quick recovery was confirmed by decreasing the temperature from 80 °C. Thus, the dense packing structure of TempGel(NP) facilitates the reformation of the boronic ester to completely recover its viscoelastic property after a short-term temperature treatment.

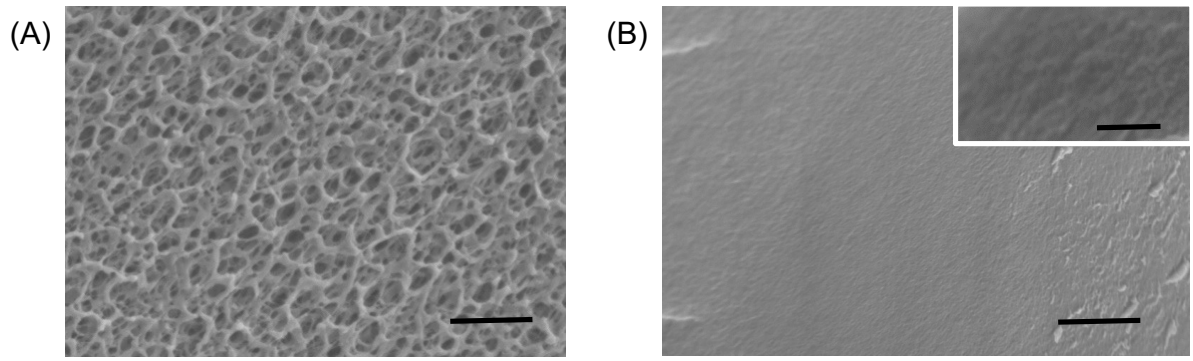

Figure. 4: SEM images of (A) MixGel(NP) and (B) TempGel(NP). Scale bar: 1 μm. The scale bar in the inset of (B) is 200 nm.

The internal mobility of TempGel(NP) was investigated. Because TempGel(NP) uses NPs as the crosslinker of PTHMAAm, the diffusion of NPs was smaller than that of small molecules. TempGel was also prepared using linear polymer, P(APBA-*co*-DMAPAAm) (APBA/DMAPAAm=475/25 (units) figure 5) which is denoted as (TempGel(LN). TempGel(NP) and TempGel(LN) were left in the water at 25, 50, and 80 °C (Figure 6). In the

case of TempGel(LN), the hydrogel was completely dissociated after one day of incubation, regardless of the temperature change. In contrast, TempGel(NP) maintained its structure for more than 60 days at 25 °C. At 50 °C, TempGel(NP) partially maintained its structure for the long term. However, it gradually swelled, and a long-term disintegration process was observed. At 80°C, the swelling of TempGel(NP) was faster than that at 50 °C, and it completely decomposed after 3 days.

TempGel(LN) was crosslinked using a linear polymer of P(APBA-*co*-DMAPAAm) and PTHMAAm. Thus, the linear polymers were considered to gradually diffuse from the hydrogel. Generally, because the boronic ester is in equilibrium, a part of the boronic ester is dissociated even at 25 °C. Once the boronic ester was dissociated, the distance between PBA and hydroxyl groups became significantly large to reconnect with the same functional group. In addition, the mobility of the linear polymers inside the hydrogel increased (Figure 6). As a result, the linear polymers diffused outside the hydrogel, which was insufficient to maintain the hydrogel structure. In contrast, TempGel(NP) was crosslinked using NPs, and the crosslinking points became a three-dimensional structure. Therefore, the diffusion of the NP crosslinker was smaller than that of the linear polymer. At 50 °C, half of the boronic esters were dissociated, and the other half remained to maintain the cross-linking structure. Thus, the NPs hardly diffused from the hydrogel at low temperatures. In contrast, the recombination of boronic esters gradually occurred under a low dissociation constant at high temperatures, thereby disassembling the hydrogel.

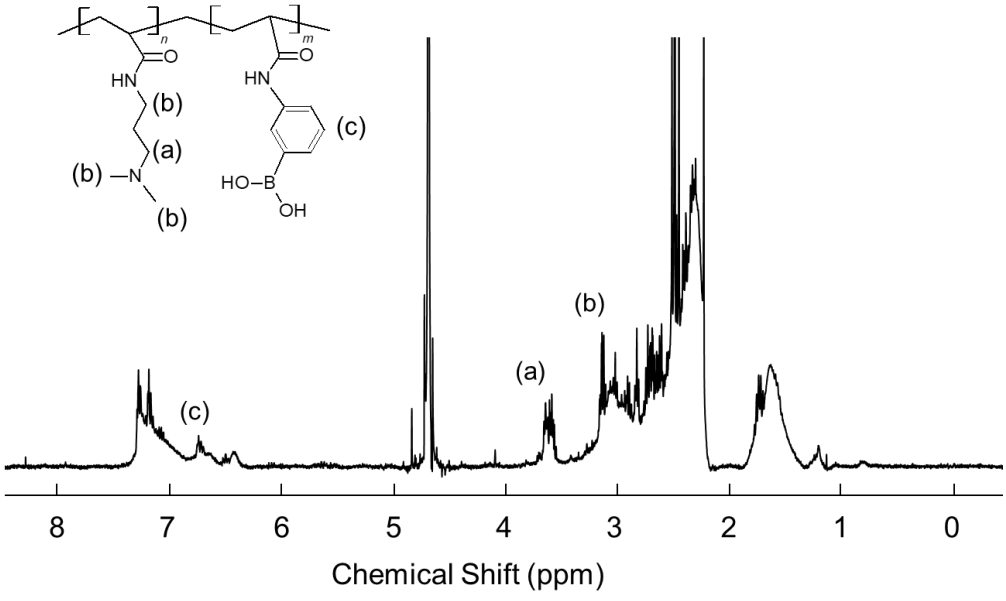

Figure 5. ^{1}H-NMR spectra of P(APBA-*co*-DMAAm) (LN) (solvent: D_2O).

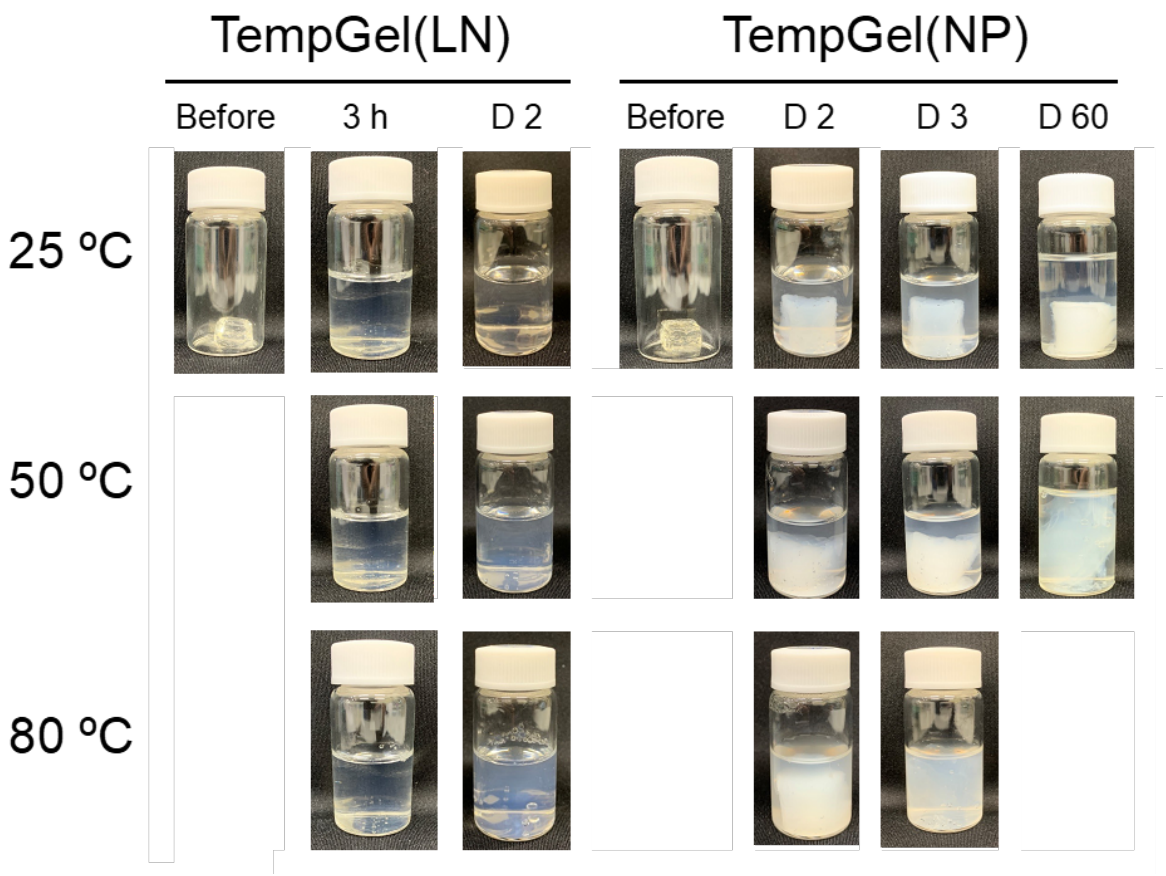

Figure 6. Photos of TempGel(LN) and TempGel(NP) in water at 25, 50, and 80 °C.

3.2.3. The effect of multivalency

The effect of multivalent boronic ester formation between the NPs and PTHMAAm on the stability of the TempGel(NP) was investigated (Figure 7). Because PBA-NPs contained various PBA units on the surface, they connect to PTHMAAm chains in a multivalent manner. To control the amount of PBA units on the surface of PBA-NPs, PBMA-*b*-PDMAPAAm-PBA, and PBMA-*b*-PDMAPAAm-DMAPAAm, which do not contain a PBA unit at its ω-terminus (Figure 8), were assembled to prepare the NPs.

As shown in Figure 7, the G′ and G″ values of the TempGel(NP) decreased with decreasing amounts of PBA on PBA-NPs. In particular, gel–sol phase transition was observed when the amount of PBA on the surface of the NPs was less than 50%. In this experiment, the amount of PBA on the surface of the NPs was reduced. Thus, the number of NP crosslinkers in the hydrogel remained unchanged, regardless of the amount of PBA on the PBA-NPs. As shown in Figure 2, G′ of the hydrogel remained unchanged while G″ increased with increasing temperature. Thus, when approximately half of the boronic ester was dissociated, the G′ of

TempGel(NP) did not change. However, the G′ and G″ values of TempGel(NP) decreased when the number of PBA on the PBA-NPs was reduced, suggesting that the density of boronic acid on the NP surface significantly affected the viscoelasticity of the hydrogel. Considering the equilibrium state of boronic esters, when the boronic acid density on the NP surface was high, the diols on PTHMAAm could rebind to surrounding PBA. However, as the density of PBA on the surface of NPs decreased, the formation of boronic esters was suppressed because of the decrease in the concentration of PBA on the surface of NPs. Thus, the viscoelasticity of the gel decreased owing to the destabilization of the crosslinking points caused by a decrease in the local boronic acid density. These results suggest that the multivalency effect is influenced by the number of boronic acid ester bonds on the particle surface and the density of functional groups on the surface of the NPs.

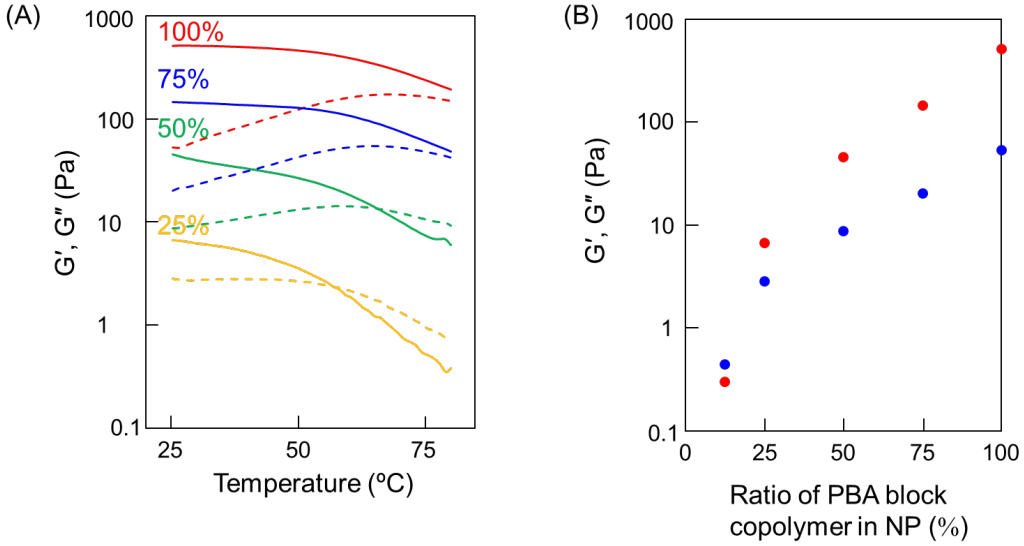

Figure 7. (A) Changes in thermal viscoelasticity of TempGel(NP) containing 100% (red), 75% (blue), 50% (green), and 25% (yellow) PBA on the surface of PBA-NPs. Solid and dotted lines indicate the G′ and G″, respectively. (B) G′ (red dots) and G″ (blue dots) of TempGel(NP) with different PBA densities on the surface of PBA-NPs at 25 °C.

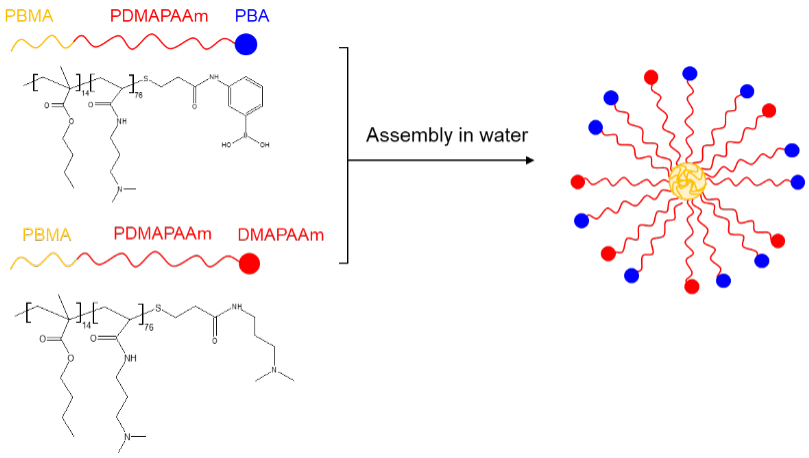

Figure 8. Preparation NP-PBA prepared by mixing PBA-b-PDMAPAAm-PBA and PBA-b-PDMAPAAm-DMAPAAm.

3.3. Reformation effect

Finally, the reformation efficiency of a boronic ester was investigated by adding physical distortions to the hydrogels. The hydrogels were set on a rheometer plate, and then the strain was periodically alternated between 1% and 1000% at 25 °C. By changing the strain from 1% to 1000%, the G′ and G″ values were reversed, confirming the structural collapse of the hydrogels (Figure 9). In the case of MixGel(NP), both G′ and G″ values were restored after approximately 100 s when the gel returned to a low-strain state. However, the recovery rate, which is the change in the G′ and G″ values from that of the original hydrogel, decreased with an increase in the number of strain cycles and was approximately 72% after four cycles. In contrast, TempGel(NP) exhibited a high and rapid recovery against physical stress. The recovery rate after four cycles was approximately 90% and the restoration of G′ and G″ occurred within 60 s.

When the hydrogel physically disintegrated, a part of the boronic ester was forcibly dissociated. Once physical stress was removed, the exposed PBA and hydroxyl groups nearby reformed boronic ester, and the hydrogel can be restored its mechanical properties. TempGel(NP) had numerous hydroxyl groups surrounding PBA on the NPs, allowing the reformation of the boronic ester in the static state. However, PBA and hydroxyl groups in the hydrogel did not return to their original state in response to physical stress. Therefore, TempGel(NP) also gradually decreased its recovery rate against repeated physical brakes, although TempGel(NP) recovered more than MixGel(NP).

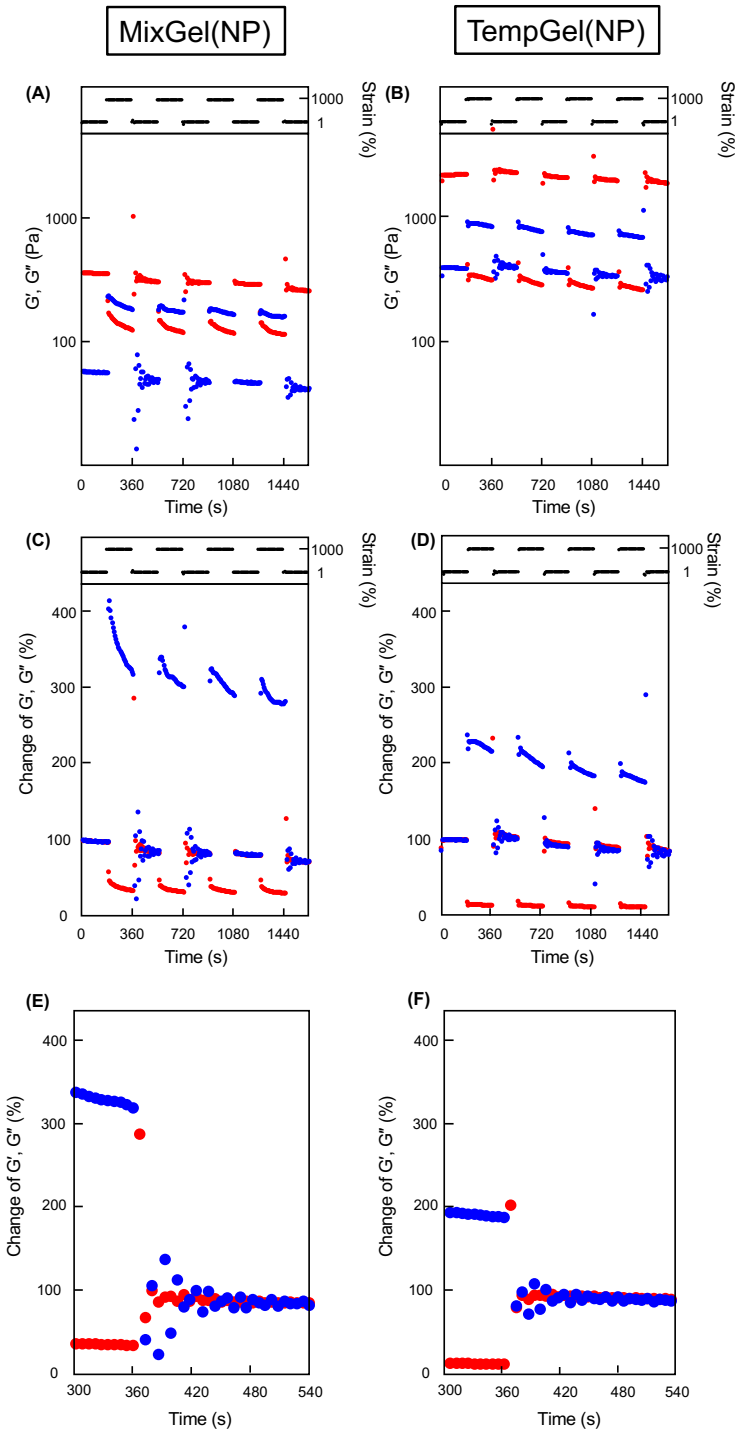

Figure 9. (A, B) G′ and G″ data and (C-F) the change of G′ and G″ against original hydrogel of (A, C, E) MixGel(NP) and (B, D, F) TempGel(NP). The strain was alternated between 1 and 1000% every 3 min. Red and blue dots indicate G′ and G″, respectively.

3.4. Application of THMAAm hydrogel for shape re-modeling

TempGel(NP) exhibited high thermal hysteresis of viscoelasticity and could change the formation of boronic ester on the NP crosslinker without affecting the elasticity of the hydrogel by temperature change. To confirm the thermal recombination of the crosslinking points, the self-healing ability of TempGel(NP) was confirmed by connecting the hydrogels. The gels were formed into cubes, and an adhesion test of the gels was conducted by changing the temperature. Initially, the surfaces of the gels were brought into contact with each other at 25 °C; however, no adhesion was observed between the gels. Subsequently, the hydrogel was heated on a hot plate at 50 °C (Figure 10A). The hydrogel softened upon heating, and the loss modulus values increased significantly as the G′ and G″ values changed from 483 and 60 Pa at 25 °C to 390 and 124 Pa at 50 °C. No adhesion of the surfaces was observed under the heating conditions. Immediately after sufficient cooling of the hydrogel at 25 °C, the connection was confirmed, indicating the recombination of the crosslinking point of the hydrogel on the surface. Thus, TempGel(NP) exhibited a high thermal self-healing ability.

Subsequently, the thermoplasticity of TempGel(NP) was confirmed from the recombination of the crosslinking point of the hydrogel with changing temperature. The cubic hydrogel was heated to 50 °C to soften and then sealed in a star-shaped mold. After cooling to 25 °C, the hydrogel was removed from the mold, and the shape of the star was maintained. The new structure was quickly stabilized once the hydrogel was cooled. Thus, TempGel(NP) can easily change the original structure of the hydrogel through thermal treatments (Figure 10B). In addition, the thermoplasticity of TempGel(NP) can be induced at ambient temperatures. Thus, TempGel(NP) was effective in reforming the crosslinking point and changing the shape of the hydrogel.

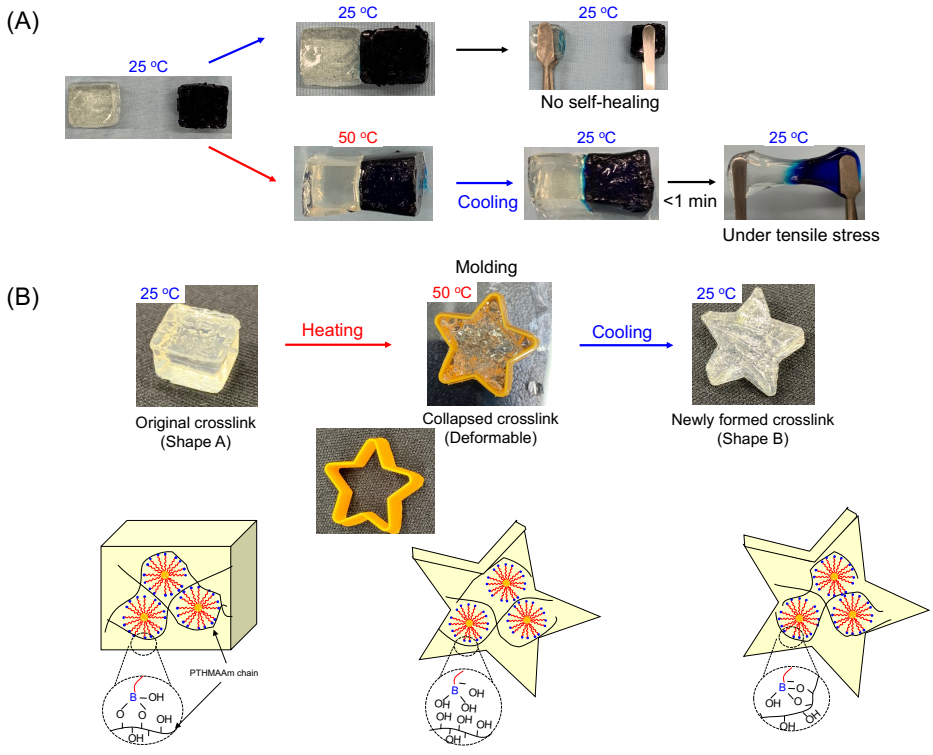

Figure 10. Photographs of TempGel(NP) at different temperatures. (A) Photographs of TempGel(NP) illustrating its self-healing properties. The blue hydrogel was stained with methylene blue dye. (B) Illustration of the thermoplastic property of TempGel(NP) and possible mechanism of shape-change of the hydrogel. Increasing the temperature collapsed the crosslinking point formed by the boronic ester, and it was reformed by decreasing the temperature to form a new permanent shape.

As mentioned, some studies have already reported self-healing hydrogels that can be connected to different hydrogels in a few seconds. Although the hydrogel connections occur in a short time, the bonding reformation on the surface of the hydrogel is dominated by the diffusion of functional groups. Thus, full self-healing of a hydrogel with a complete reformation of covalent bonds is difficult because of the limited diffusion of molecules or steric hindrance of polymers to promote coupling reactions on the hydrogel. In the case of TempGel(NP), the diffusion of molecules was highly suppressed, supporting a high thermal hysteresis. Thus, TempGel was supposed to complete the conjugation of the boronic ester immediately after decreasing the temperature to exhibit its self-healing and thermoplastic properties (Figure 11). In this study, no direct evidence of instant thermal reformation of boronic ester on TempGel(NP) has been provided because TempGel(NP) exhibited rapid and complete recovery. However, the study, in particular, the high hysteresis of TempGel(NP) strongly supports the quick and complete reformation of boronic esters by temperature treatment.

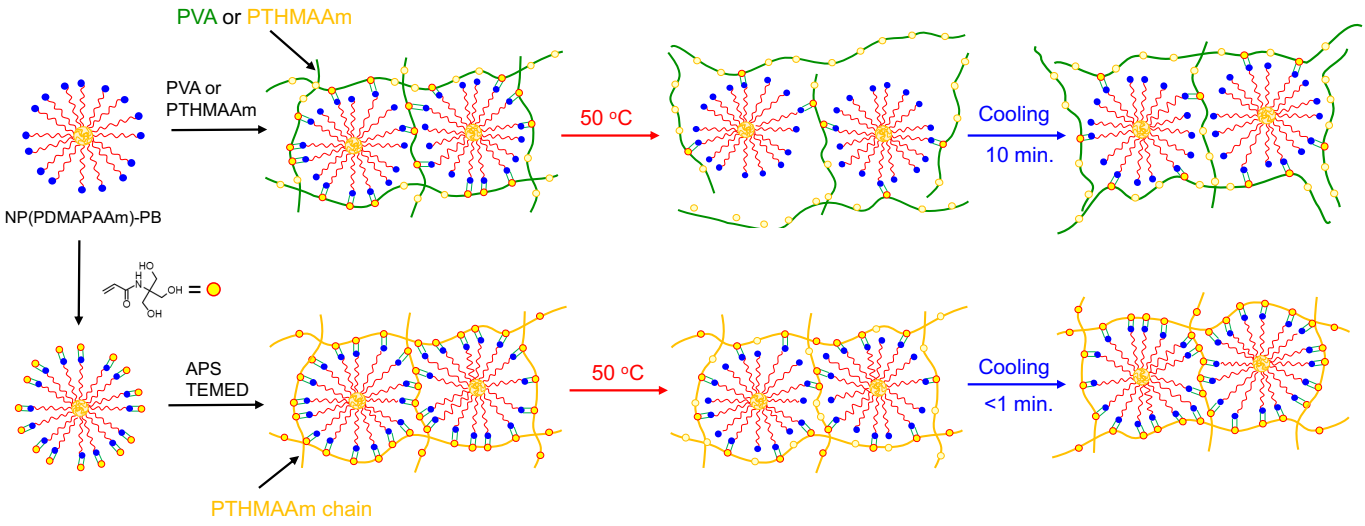

Figure 11. Differences between the MixGel(NP) hydrogel and TempGel(NP) regarding the temperature effect. The PB-Diol bonds can be collapsed by the temperature increase and re-connected by cooling to form new crosslinking points. In the MixGel(NP), the polymer chains are diffused outward of PB with temperature elevation. After cooling, the newly formed crosslinking points were slowly and partially re-connected. In the TempGel(NP), only around half of the crosslinking points are dissociated by temperature and display rapid, complete re-connection by cooling.

In this study, a hydrogel was prepared via template polymerization using boronic ester-coated NPs. Because template polymerization is a general method, other DCBs can also be used to prepare high-hysteresis hydrogels. In addition, this study is focused on controlling the equilibrium of the DCBs through temperature. The equilibrium of other DCBs can be controlled by other stimuli such as pH and light. Thus, the method proposed in this study can be widely applied to prepare stimuli-responsive smart hydrogels. The factors that are necessary to induce high hysteresis in a hydrogel are the equilibrium of DCBs, three-dimensional crosslinker with multivalent conjugation, and densely packed structure with template polymerization.

4. Conclusion

In this study, a highly thermally sensitive smart hydrogel was successfully prepared through template polymerization using DCB-introduced NPs as the crosslinker. The bonding state of the boronic ester on the crosslinking points of the hydrogel was changed by changing the temperature. Moreover, temperature changes markedly reduced the G″ of the hydrogel without changing the G′. Consequently, the mobility of crosslinking points can be freely controlled by changing the temperature, allowing the hydrogel to exhibit high hysteresis, efficient thermoplasticity, and self-healing properties. Particle-type crosslinkers are expected to connect polymers in multivalent three-dimensional structures. However, high hysteresis was never achieved by crosslinking them with the polymer, owing to the incomplete formation of DCBs. Thus, template polymerization improves the formation of DCBs on the surface of NPs. As a result, NPs can be fixed inside the hydrogel, increasing the strength of the hydrogel and changing its viscoelasticity by changing its temperature. The NP-type crosslinker with highly efficient conjugation with the backbone polymer via template polymerization is a useful approach for the recombination of crosslinking points of self-healing and thermoplastic smart hydrogels.

5. References

1. Othman, M.H.; Ito, Y.; Akimoto, J. Mild-Temperature-Induced Recombination of Crosslinking Structures in Hydrogels Using Phenylboronic-Acid-Functionalized 3D Nanoparticle Crosslinkers. ACS Appl. Polym. Mater. 2022, 4, 5047–5055.
2. Chen, Y.; Tan, Z.; Wang, W.; Peng, Y.-Y.; Narain, R. Injectable, Self-Healing, and Multi-Responsive Hydrogels via Dynamic Covalent Bond Formation between Benzoxaborole and Hydroxyl Groups. Biomacromolecules 2018, 20, 1028–1035.
3. Perera, M.M.; Ayres, N. Dynamic Covalent Bonds in Self-Healing, Shape Memory, and Controllable Stiffness Hydrogels. Polym. Chem. 2020, 11, 1410–1423.
4. Taylor, D.L.; in het Panhuis, M. Self‐healing Hydrogels. Adv. Mater. 2016, 28, 9060–9093.
5. Wu, G.; Jin, K.; Liu, L.; Zhang, H. A Rapid Self-Healing Hydrogel Based on PVA and Sodium Alginate with Conductive and Cold-Resistant Properties. Soft Matter 2020, 16, 3319–3324.
6. Liu, Y.; Liu, Y.; Wang, Q.; Han, Y.; Chen, H.; Tan, Y. Doubly Dynamic Hydrogel Formed by Combining Boronate Ester and Acylhydrazone Bonds. Polymers (Basel). 2020, 12, 487.
7. Chen, Y.; Wang, W.; Wu, D.; Zeng, H.; Hall, D.G.; Narain, R. Multiresponsive and Self-Healing Hydrogel via Formation of Polymer–Nanogel Interfacial Dynamic Benzoxaborole Esters at Physiological PH. ACS Appl. Mater. Interfaces 2019, 11, 44742–44750.
8. Cai, Y.; Zou, H.; Zhou, S.; Chen, Y.; Liang, M. Room-Temperature Self-Healing Ablative Composites via Dynamic Covalent Bonds for High-Performance Applications. ACS Appl. Polym. Mater. 2020, 2, 3977–3987.
9. Xu, J.; Guo, Z.; Chen, Y.; Luo, Y.; Xie, S.; Zhang, Y.; Tan, H.; Xu, L.; Zheng, J. Tough, Adhesive, Self-Healing, Fully Physical Crosslinked κ-CG-K+/PHEAA Double-Network Ionic Conductive Hydrogels for Wearable Sensors. Polymer (Guildf). 2021, 236, 124321.
10. Barbucci, R.; Pasqui, D.; Giani, G.; De Cagna, M.; Fini, M.; Giardino, R.; Atrei, A. A Novel Strategy for Engineering Hydrogels with Ferromagnetic Nanoparticles as Crosslinkers of the Polymer Chains. Potential Applications as a Targeted Drug Delivery System. Soft Matter 2011, 7, 5558–5565.
11. Gu, L.; Liu, X.; Dong, S.; Chen, Z.; Han, R.; He, C.; Wang, D.; Zheng, Y. Natural Lignin

Nanoparticles: A Promising Nano-Crosslinker for Constructing Fluorescent Photoswitchable Supramolecular Hydrogels. Polym. Chem. 2020, 11, 1871–1876.

12. Baldock, C.; De Deene, Y.; Doran, S.; Ibbott, G.; Jirasek, A.; Lepage, M.; McAuley, K.B.; Oldham, M.; Schreiner, L. Polymer Gel Dosimetry. Phys. Med. Biol. 2010, 55, R1.
13. Wang, S.; Urban, M.W. Self-Healing Polymers. Nat. Rev. Mater. 2020, 5, 562–583.
14. Desroches, G.; Wang, Y.; Kubiak, J.; Macfarlane, R. Crosslinking of Pressure-Sensitive Adhesives with Polymer-Grafted Nanoparticles. ACS Appl. Mater. Interfaces 2022, 14, 9579–9586.
15. Liu, A.Y.; Emamy, H.; Douglas, J.F.; Starr, F.W. Effects of Chain Length on the Structure and Dynamics of Semidilute Nanoparticle–Polymer Composites. Macromolecules 2021, 54, 3041–3051.
16. Ofridam, F.; Tarhini, M.; Lebaz, N.; Gagniere, E.; Mangin, D.; Elaïssari, A. PH‐sensitive Polymers: Classification and Some Fine Potential Applications. Polym. Adv. Technol. 2021, 32, 1455−1484.
17. Lan, Y.-T.; Cheng, Q.-P.; Xu, J.; Lin, S.-H.; Lin, J.-M.; Hsu, S. Gelation and the Self-Healing Behavior of the Chitosan–Catechol Hydrogel. Polymers (Basel). 2022, 14, 4614.
18. Yang, J.; Bai, R.; Chen, B.; Suo, Z. Hydrogel Adhesion: A Supramolecular Synergy of Chemistry, Topology, and Mechanics. Adv. Funct. Mater. 2020, 30, 1901693.
19. Ranganathan, N.; Bensingh, R.J.; Kader, M.A.; Nayak, S.K. Synthesis and Properties of Hydrogels Prepared by Various Polymerization Reaction Systems. Publ. online 2019, 487–511.

CHAPTER IV

SYNTHESIS AND CHARACTERIZATION OF POLYETHYLENE GLYCOL-GRAFTED PHOTOREACTIVE POLYETHYLENE GLYCOLS FOR ANTIBIOFOULING APPLICATIONS

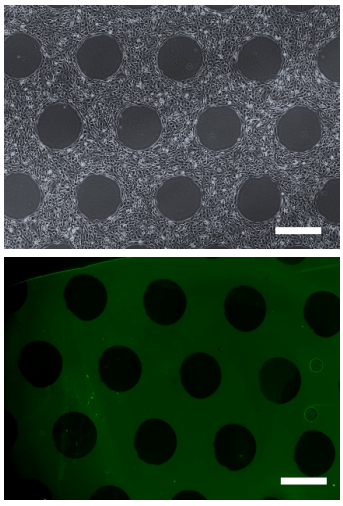

1. Introduction

Surface functionalization can command the interactions between target materials while simultaneously inhibiting nonspecific interactions with the surfaces. Non-biofouling surfaces, in particular, thwart the adsorption of proteins and/or cell adhesion. This is because proteins generally have a strong propensity to adsorb on almost all surfaces, which causes cell adhesion. Surfaces that deter protein adsorption also deter cell adhesion [1,2].

To date, a variety of polymers, such as polyethylene glycol (PEG) [3–7], zwitterionic species [8–11], peptides [12], polypeptides [13], and glycocalyx [14], have been used to suppress nonspecific interactions in cells. These polymers have a high degree of flexibility and hydrophilicity, and they impart antifouling and nonadherent characteristics. Additionally, these polymers have been immobilized on antibiofouling surfaces using a variety of techniques, such as self-assembly [15], electro-grafting [16], and polymerization. More recently, atom transfer radical polymerization [17] and reversible addition-fragment chain transfer polymerization have also been used in this context [18]. The covalent immobilization of the antibiofouling layer is made possible by various methods, including photoimmobilization, which is intriguing [19]. In order to create antibiofouling surfaces, a variety of photoimmobilizable (reactive) polymers have been used, including those containing PEG [20,21], zwitterions (such as phosphorylcholine) [22–24], sulfobetaine [25], carbobetaine [26], pullulan [27], sulfated hyaluronic acid [28], polyvinyl alcohol [29], and polyacrylate derivatives [30].

Regarding photoreactive polymers, photoreactive antifouling acrylic polymers grafted with PEG have been used as microarray matrixes [31–37] and are currently being used commercially in allergy diagnosis (DropScreen^{R}) [38,39]. In a previous study, methacrylate-PEG and acryloyl 4-azidobenzene were copolymerized to create photoreactive PEG. For surface modification to prevent biofouling, the photoreactive polymer was photoimmobilized on titanium, glass, and plastic surfaces [20]. Due to its convenience, this immobilization method is actually very helpful for surface antibiofouling modification. The modified surface can be used to immobilize proteins via photo-induced crosslinking and significantly reduces the interaction with proteins [20].

However, the water solubility of these polymers is relatively low due to the low hydrophilicity of the polymethacrylate backbone and declines further with an increase in the number of azidophenyl groups [7,21]. A PEG-based photoreactive polymer made of ethylene oxide and azidophenyl-coupled ethylene oxide was prepared to increase the water solubility. Nevertheless, its water solubility was still only moderate. In order to increase the water

solubility and photoreactivity, coimmobilization with PEG-carrying ethylene oxide was done in this study. The resulting antibiofouling properties were then investigated.

2. Materials and Methods

2.1. Materials

4-(Glycidyloxymethyl)azidobenzene (AzPheEO) was synthesized in accordance with the prior report [21]. From Biochempeg Scientific (Boston, MA, USA), methyl-PEG epoxide (mPEG-EPO, Mn = 350 and 750) was purchased. Ethanol, methanol, hexane, tetrabutylammonium bromide (TBAB), and dimethylformamide were bought from FUJIFILM Wako Pure Chemical (Osaka, Japan). Triisobutyl aluminum (i-Bu_3Al, 1.0 mol/L toluene solution), lithium bromide, 4-azidobenzoic acid, and ethylene oxide (EO, 1.0 mmol/L toluene solution) were bought from Tokyo Chemical Industry (Tokyo, Japan). Iwaki (Tokyo, Japan) provided polystyrene dishes for tissue culture. Fetal bovine serum (FBS), trypsin, and Alexa488-conjugated immunoglobulin G (Alexa488-IgG) were purchased from Thermo Fisher Scientific (Waltham, MA, USA). Penicillin-streptomycin solution was purchased from Nacalai Tesque (Kyoto, Japan).

2.2. Copolymerization of EO, AzPheEO, and mPEG-EPO

EO was first copolymerized with mPEG-EPO and AzPheEO (Scheme 1). To achieve this, TBAB, AzPheEO, and mPEG-EPO were vacuum-dried for two hours before being exposed to dry nitrogen. The toluene was added to the flask to dissolve the mPEG-EPO. The EO solution, AzPheEO, and i-Bu_3Al were then added to the flask while it was submerged in an ice bath. The mixture was stirred for 18 hours at 25 °C in the dark in order to copolymerize. Methanol was added, and then under reduced pressure, it was taken out of the mixture. The unrefined substance was dissolved in acetone, and the resulting mixture was dialyzed for three days against water. After being freeze-dried, the resulting polymer is known as AzPEGx[y], where x and y stand for the Mn and feed ratio of mPEG-EO, respectively. The obtained polymer AzPEGx[y] was characterized using ^{1}H-nuclear magnetic resonance (NMR) spectroscopy (JNM-ECZ400R, 400 MHz, JEOL, Tokyo, Japan) in chloroform. Additionally, gel permeation chromatography (GPC; JASCO, Tokyo, Japan) was performed. The apparatus included two columns in dimethylformamide (DMF) containing 10 mM lithium bromide (SB-803 HQ and SB804 HQ; Showa Denko, Tokyo, Japan) and a refractive index detector (RI-2032, JASCO).

Further, the ultraviolet (UV) absorbance spectra of the polymers and 4-azidobenzoic acid were measured. The polymer and 4-azidobenzoic acid were dissolved in a mixture of

ethanol/water (0.1 wt.%.). The UV absorbance of each solution was measured between 200 and 400 nm.

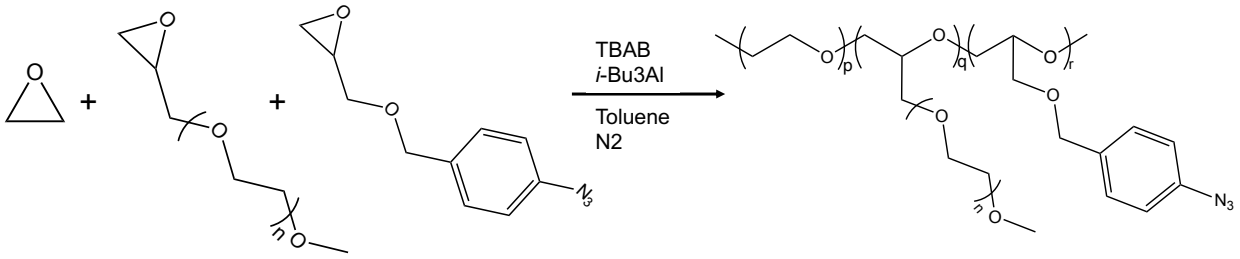

Scheme 1. Preparation of photoreactive polyethylene glycol-grafted polyethylene glycol.

2.3. Contact angle measurements

A drop of water (0.1 µL) was applied to the sample surface of an unpatterned AzPEGx[y]-coated plate that had been set up on the stage of CA-W Automatic Contact Angle Meter (Kyowa Interface Science, Co. Ltd, Saitama, Japan). At room temperature, the contact angle of the drop with the surface was measured. At least ten angles were measured in various locations, and the results were expressed as the average values with the standard deviation.

2.4. Photoimmobilization of AzPEGx[y]

In Scheme 2a, the photoimmobilization process is depicted. On polystyrene dishes (for tissue culture, Iwaki, Tokyo, Japan), the prepared polymer AzPEGx[y] (0.25 wt.% in water, 100 L) was placed. These dishes were then vacuum-dried at 40 °C. As a photomask, a stainless steel punch sheet with 500 m holes from Yasutoyo Trading in Tokyo, Japan, was placed on the substrate. A photoirradiator (45 mW/cm^2 at 270 nm, L5662 UV spotlight source from Hamamatsu photonics in Hamamatsu, Japan) was then used to expose the surface to UV light for 20 seconds. After that, the surface was washed with water and submerged in water for a day. The plates were vacuum-dried and kept in a dark desiccator until use.

To confirm the photoimmobilization of the polymer on a polystyrene substrate, the AzPEGx[y] (0.25 wt.%, 90 µL) solution was mixed with Alexa488-IgG (0.25 wt.%, 10 µL) and coimmobilized on the plate (Scheme 2b). Further, fluorescence images were obtained using a fluorescence microscope (Olympus, Tokyo, Japan).

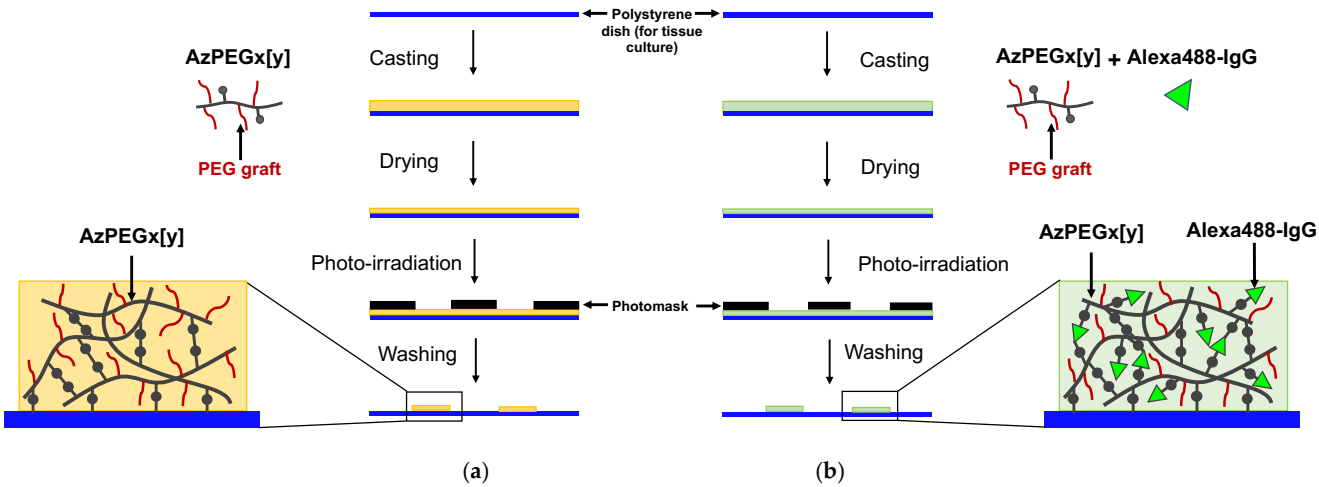

Scheme 2. Micropatterning of the prepared polymer AzPEGx[y] (a) without and (b) with fluorescent-labeled IgG. The circular micropattern was identical to the diameter of the photomask holes.

2.5. Protein adsorption

The AzPEGx[y]-coated surfaces were treated with a solution of Alexa488-IgG (0.25 wt.%, 100 L) and left to stand for 2 hours at 25 °C. Following a water wash, the substrates were submerged in water for the entire night. Following vacuum-drying of the substrates, fluorescence images were captured using a fluorescence microscope (Olympus).

2.6. Cell adhesion

Mouse fibroblast (3T3) cells (Japanese Collection of Research Bioresources, Osaka, Japan) were grown in Dulbecco's modified Eagle's medium (Sigma-Aldrich, St. Louis, MO, USA) supplemented with 10 % FBS and antibiotics (penicillin (100 units/mL) and streptomycin (100 µg/mL)) (Nacalai Tesque). A 0.25% trypsin-ethylenediaminetetraacetic acid solution (Nacalai Tesque) was used to harvest the cells. After being seeded onto the AzPEGx[y]-coated dishes, the cells (1.0×10^6 cells) were incubated for 24 hours at 37 °C in a humid environment with 5% CO_2. After incubation, the dishes were rinsed three times with phosphate-buffered saline, and a phase-contrast microscope was used to view the cells (Olympus, Tokyo, Japan).

3. Results and discussion

3.1. Synthesis of photoreactive PEG (AzPEGx[y])

EO was copolymerized with AzPheEO and mPEG-EPO via activated ring-opening polymerization. TBAB was used as an initiator and i-Bu_3Al as the monomer activator to generate polymers with various PEG chain lengths and azidophenyl group contents.

The AzPEGx[y] polymers synthesized through the copolymerization of AzPheEO with EO and two different molecular weights of mPEG-EPO are summarized in Table 1. The presence of azidophenyl groups was confirmed using UV absorbance spectroscopy. The molecular weights and polydispersity indices (PDIs) of the polymers were investigated using GPC. AzPheEO and mPEG-EPO contents of the copolymers were found to be lower than those of the feed. The decline in the ratio of mPEG-EPO was greater than that of AzPheEO. This is caused by the high steric hindrance of the PEG moiety in mPEG-EPO. The PDI increased at a lower proportion of the azidophenyl group due to the steric interference of mPEG-EPO. When mPEG-EPO was not present, the polymer did not dissolve in pure water. Az[10] was not used for further investigation as a result.

Table 1. Characterization of the prepared polymers.

Code	Feed (mol%)				Composition (mol%) [a]			Mw [b]	PDI [b]
	AzPheEO	EO	mPEG-EPO	mPEG-EPO MW	AzPheEO	EO	mPEG-EPO		
Az[10] [c]	10	90	0	-	9.6	90.4	0	8700	1.6
$AzEG_{350}$[10]	10	80	10	350	8.4	85.8	5.8	7800	1.7
$AzPEG_{750}$[5]	10	85	5	750	7.4	89.8	2.8	13000	1.9
$AzPEG_{750}$[1]	10	89	1	750	9.9	89.5	0.6	12000	1.7

[a] Determined via ^{1}H-NMR. [b] Determined via GPC. [c] No PEG-grafted polymer

Figure 1 displays the synthesized $AzPEG_{750}$[5] ^{1}H-NMR spectrum. Peaks at 3.6 and 3.35 ppm, respectively, were found to correspond to the protons of the PEG ethylene group units and the methyl protons of the grafted PEG chain. In addition, peaks at 4.54 ppm, 7.37 ppm, and 7.05 ppm, respectively, were found to correspond to benzylic protons, aromatic protons, and azidophenyl units.

Figure 2 shows the UV absorbance spectrum of 4-azidobenzoic acid and $AzPEG_{750}[5]$. The azidophenyl group's peak slightly shifted to a shorter wavelength. It was thought that the azidophenyl group was located in the hydrophobic region of the polymer.

The molecular weight and distribution of AzPEGx[y] were determined via GPC (Figure 3). The prepared AzPEGx[y] polymer appeared as a unimodal trace. This revealed an almost complete polymerization between mPEG-EPO and AzPheEO.

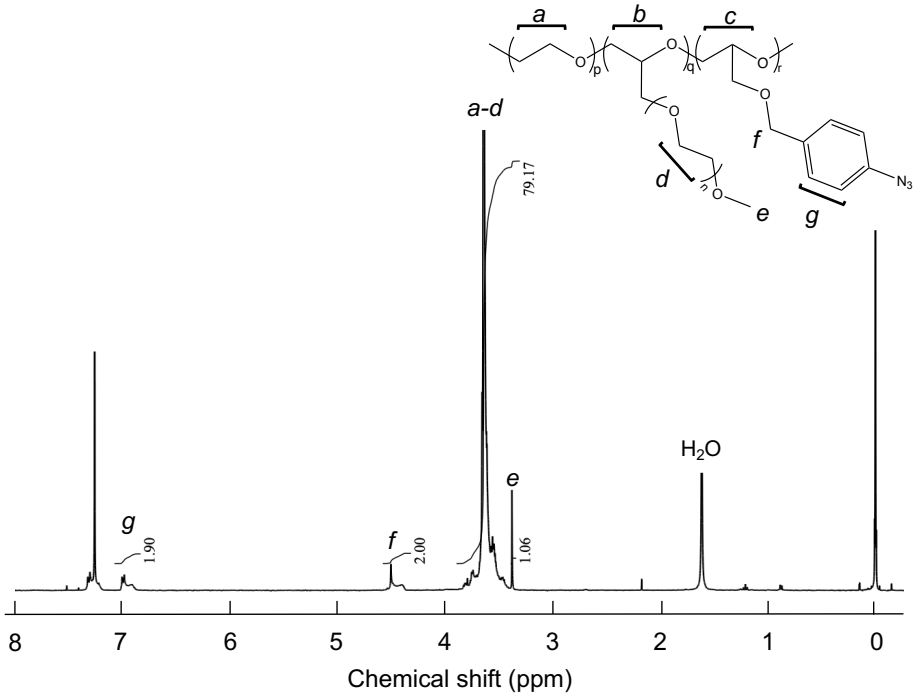

Figure 1. ^{1}H-NMR spectrum of $AzPEG_{750}[5]$ (solvent: chloroform-d).

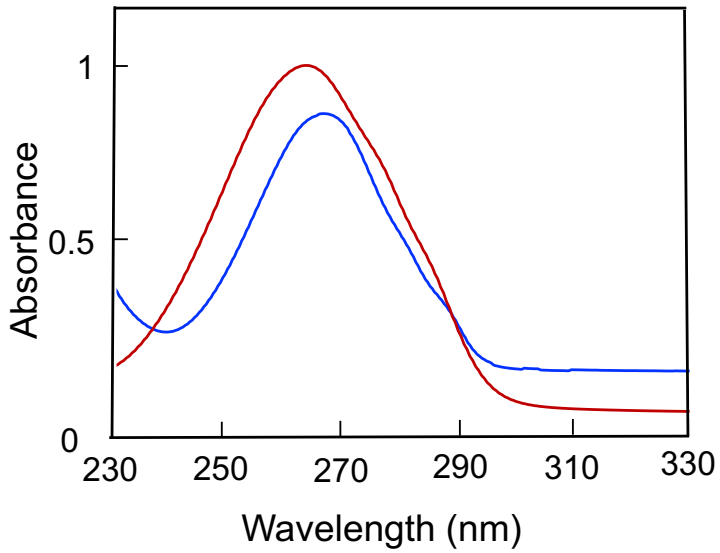

Figure 2. UV absorbance spectra of $AzPEG_{750}[5]$ (red) and 4-azidobenzoic acid (blue) in ethanol/water (0.1 wt.%).

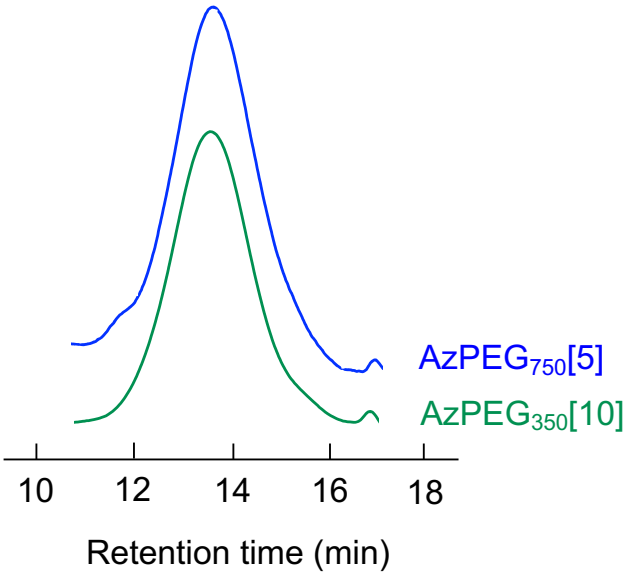

Figure 3. GPC charts of AzPEG$_{350}$[10] (green) and AzPEG$_{750}$[5] (blue), prove that the azidophenyl group was successfully synthesized via the copolymerization of AzPheEO with EO and mPEG-EPO. Eluent: DMF containing 10 mmol/L LiBr. Flow rate 1 mg/mL.

3.2. Contact angle measurements

As mentioned, measurements of the water contact angle were made to examine the surface characteristics of AzPEGx[y] immobilized without a photomask (unpatterned surfaces). Table 2 shows that the photoimmobilized surface had a lower contact angle than the non-immobilized surface. PEG coverage was thought to be the cause of this change in the contact angle. The hydrophilicity of the immobilized surface was almost independent of the copolymer.

Table 2. Contact angles on different surfaces.

Surface	**Contact angle (°) ± standard deviation**
Polystyrene (for tissue culture)	70.7 ± 2.1
Polystyrene with AzPEG$_{350}$[10]	41.1± 1.8
Polystyrene with AzPEG$_{750}$[5]	41.2 ± 1.6

3.3. Formation of micropatterns

AzPEGx[y] was micropatterned on the polystyrene surface in accordance with Scheme 2b. As shown in Figure 4, mixed Alexa488-IgG was coimmobilized with AzPEGx[y], and the immobilized pattern matched the pattern on the photomask. Notably, the highly active nitrenes produced from the azidophenyl moieties randomly attacked the polymer, proteins, and

substrate when exposed to UV irradiation. As a result, polymer-polymer crosslinks of AzPEGx[y]-AzPEGx[y], AzPEGx[y]-Alexa488-IgG, and AzPEGx[y]-Polystyrene substrate were produced (Scheme 2b).

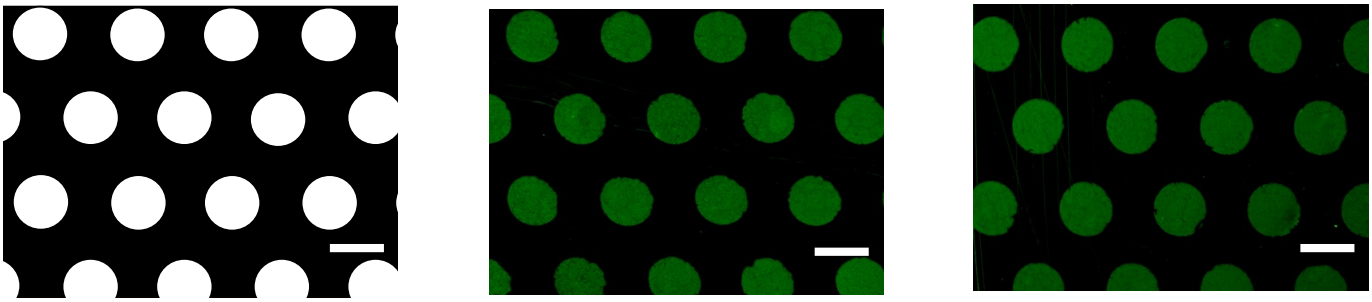

(**a**) (**b**) (**c**)

Figure 4. (a) Phase-contrast image of the photomask. (b) Micropatterning test of $AzPEG_{350}$[10] and (c) micropatterning test of $AzPEG_{750}$[5] performed using a photomask. The micropattern plate had two different regions, indicated by green and dark. In the photomask, the green section allowed UV light to enter the AzPEGx[y]–Alexa488IgG complex, resulting in photoimmobilization, which was not possible in the dark sections.

3.4. Protein adsorption

A fluorescent protein (Alexa488-conjugated IgG) was added to the surface made according to Scheme 2a, and the resulting structure was examined using fluorescence microscopy to gauge the nonspecific adsorption of proteins on immobilized PEG surfaces (Figure 5). The fluorescent-labeled proteins were prevented from adhering by the immobilized AzPEGx[y]. The suppression effect did not depend significantly on the nature of AzPEGx[y]. These findings demonstrated that non-specific protein adsorption is suppressed by the immobilized surface.

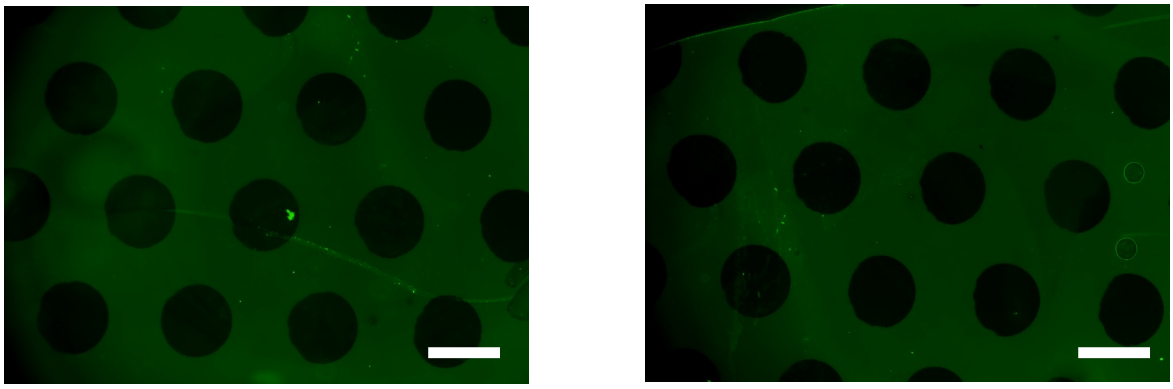

(**a**) (**b**)

Figure 5. Fluorescence microscopy images of (a) $AzPEG_{350}$[10] and (b) $AzPEG_{750}$[5] coated micropatterned polystyrene plates after adsorption of Alexa488-conjugated IgG. Scale bars: 500 μm.

3.5. Cell adhesion

The adhesion of 3T3 mouse fibroblast cells to the AzPEGx[y]-coated polystyrene substrates was assessed (Figure 6). 3T3 cells were cultured for 24 hours on the micropatterned surfaces for this purpose. It was discovered that the hole pattern of the stainless-steel photomask and the non-cell adhered pattern were identical. The cells only adhered to the non-UV exposure regions. Due to the addition of hydrophilic PEG, the prepared AzPEGx[y] polymer almost completely suppressed cell adhesion. The suppressive effect on cell adhesion did not depend on AzPEGx[y].

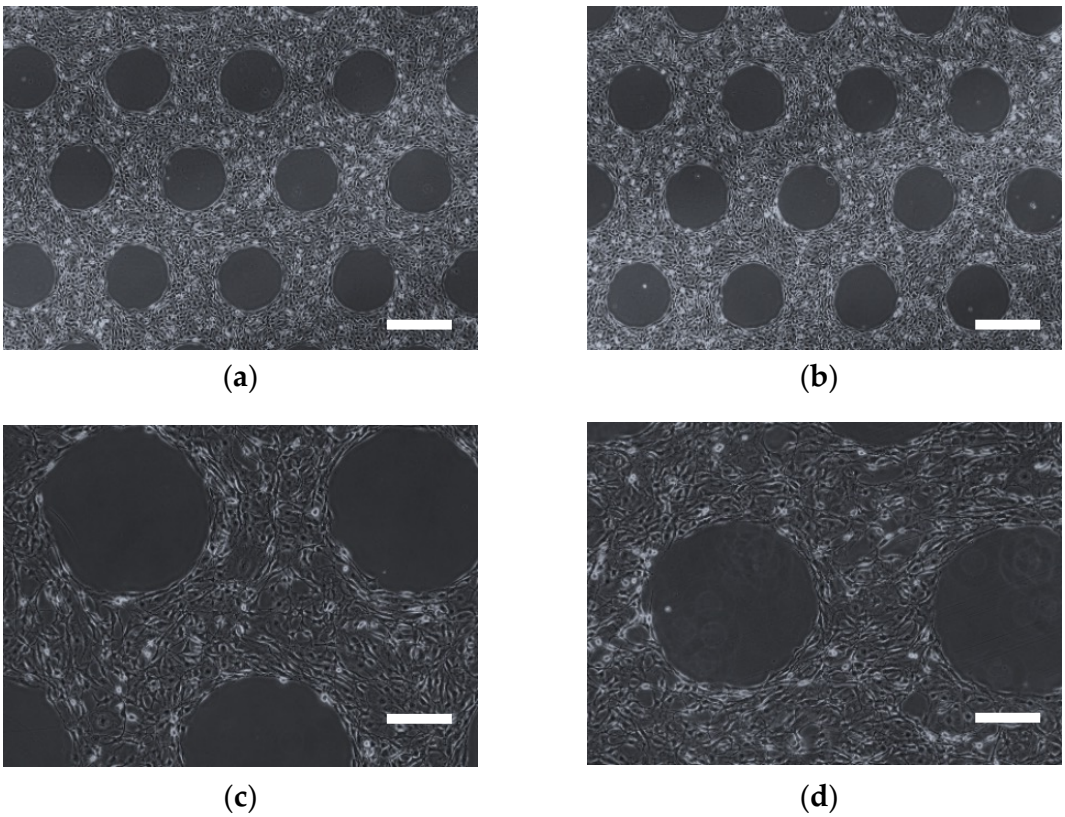

(**a**) (**b**)

(**c**) (**d**)

Figure 6. Phase-contrast images of 3T3 mouse fibroblast cells cultured on the $AzPEG_{350}$[10] (a), (c) and $AzPEG_{750}$[5] (b), (d) coated micropatterned polystyrene plates at 0.25 wt.%. Scale bars: (a), (b) 500 μm, (c), (d) 200 μm.

Notably, PEG is a good example of an antibiofouling polymer. PEG immobilization on biomaterial surfaces is typically done for several reasons. A PEG-based polymer with azidophenyl groups in the side chains had previously been developed [21]. However, pure water did not completely dissolve the polymer. As a result, mPEG-EPO was used for copolymerization, and the resulting copolymer was discovered to be entirely soluble in pure water. It was then combined with a fluorescent protein and immobilized as a mixture on the substrate. The hydrophilicity and repellency of the amphiphilic and flexible grafted polymer chains were thought to be responsible for the antibiofouling effect. A copolymer like this one might be helpful for micropatterning of water-soluble proteins and biomacromolecules with mixing.

4. Conclusion

AzPEGx[y] is a PEG-grafted and azidophenyl-modified PEG that I developed for this study to act as photoreactive polymers for surface antibiofouling modifications. AzPheEO copolymerized with mPEG-EPO and EO allowed for the successful synthesis of photoreactive polymers. The interactions with biological elements, such as proteins and cells, were greatly diminished by AzPEGx[y]. This polymer can be used for surface modification in biomedical applications because it has desirable antibiofouling properties.

5. References

1. Jiang, C.; Wang, G.; Hein, R.; Liu, N.; Luo, X.; Davis, J.J. Antifouling Strategies for Selective in Vitro and in Vivo Sensing. Chem. Rev. 2020, 120, 3852–3889.
2. Zhang, P.; Ratner, B.D.; Hoffman, A.S.; Jiang, S. Nonfouling Surfaces. In Biomaterials Science; Elsevier, 2020; pp. 507–513.
3. Lowe, S.; O'Brien-Simpson, N.M.; Connal, L.A. Antibiofouling Polymer Interfaces: Poly (Ethylene Glycol) and Other Promising Candidates. Polym. Chem. 2015, 6, 198–212.
4. Emilsson, G.; Schoch, R.L.; Feuz, L.; Höök, F.; Lim, R.Y.H.; Dahlin, A.B. Strongly Stretched Protein Resistant Poly (Ethylene Glycol) Brushes Prepared by Grafting-To. ACS Appl. Mater. Interfaces 2015, 7, 7505–7515.
5. Herzberger, J.; Niederer, K.; Pohlit, H.; Seiwert, J.; Worm, M.; Wurm, F.R.; Frey, H. Polymerization of Ethylene Oxide, Propylene Oxide, and Other Alkylene Oxides: Synthesis, Novel Polymer Architectures, and Bioconjugation. Chem. Rev. 2016, 116, 2170–2243.
6. Nagasaki, Y. Construction of a Densely Poly (Ethylene Glycol)-Chain-Tethered Surface and Its Performance. Polym. J. 2011, 43, 949–958.
7. Pasut, G.; Veronese, F.M. State of the Art in PEGylation: The Great Versatility Achieved after Forty Years of Research. J. Control. release 2012, 161, 461–472.
8. Ishii, T.; Wada, A.; Tsuzuki, S.; Casolaro, M.; Ito, Y. A New Nonbiofouling Polyzwitterion Including L-Histidine. Biomacromolecules 2007, 8, 3340–3344.
9. Schlenoff, J.B. Zwitteration: Coating Surfaces with Zwitterionic Functionality to Reduce Nonspecific Adsorption. Langmuir 2014, 30, 9625–9636.
10. He, M.; Gao, K.; Zhou, L.; Jiao, Z.; Wu, M.; Cao, J.; You, X.; Cai, Z.; Su, Y.; Jiang, Z. Zwitterionic Materials for Antifouling Membrane Surface Construction. Acta Biomater. 2016, 40, 142–152.
11. Jiang, S.; Ishihara, K.; Ji, J. Special Issue on Zwitterionic Materials. Acta Biomater. 2016, 40, 4.
12. Sakala, G.P.; Reches, M. Peptide‐based Approaches to Fight Biofouling. Adv. Mater. Interfaces 2018, 5, 1800073.
13. Leng, C.; Buss, H.G.; Segalman, R.A.; Chen, Z. Surface Structure and Hydration of Sequence-Specific Amphiphilic Polypeptoids for Antifouling/Fouling Release Applications. Langmuir 2015, 31, 9306–9311.

14. Ham, H.O.; Park, S.H.; Kurutz, J.W.; Szleifer, I.G.; Messersmith, P.B. Antifouling Glycocalyx-Mimetic Peptoids. J. Am. Chem. Soc. 2013, 135, 13015–13022.
15. Cui, M.; Wang, Y.; Wang, H.; Wu, Y.; Luo, X. A Label-Free Electrochemical DNA Biosensor for Breast Cancer Marker BRCA1 Based on Self-Assembled Antifouling Peptide Monolayer. Sensors Actuators B Chem. 2017, 244, 742–749.
16. Jiang, C.; Alam, M.T.; Parker, S.G.; Darwish, N.; Gooding, J.J. Strategies to Achieve Control over the Surface Ratio of Two Different Components on Modified Electrodes Using Aryldiazonium Salts. Langmuir 2016, 32, 2509–2517.
17. Riedel, T.; Hageneder, S.; Surman, F.; Pop-Georgievski, O.; Noehammer, C.; Hofner, M.; Brynda, E.; Rodriguez-Emmenegger, C.; Dostálek, J. Plasmonic Hepatitis B Biosensor for the Analysis of Clinical Saliva. Anal. Chem. 2017, 89, 2972–2977.
18. Kitano, H.; Kondo, T.; Kamada, T.; Iwanaga, S.; Nakamura, M.; Ohno, K. Anti-Biofouling Properties of an Amphoteric Polymer Brush Constructed on a Glass Substrate. Colloids Surfaces B Biointerfaces 2011, 88, 455–462.
19. Kallitsis, K.; Thuau, D.; Soulestin, T.; Brochon, C.; Cloutet, E.; Dos Santos, F.D.; Hadziioannou, G. Photopatternable High-k Fluoropolymer Dielectrics Bearing Pendent Azido Groups. Macromolecules 2019, 52, 5769–5776.
20. Ito, Y.; Hasuda, H.; Sakuragi, M.; Tsuzuki, S. Surface Modification of Plastic, Glass, and Titanium by Photoimmobilization of Polyethylene Glycol for Antibiofouling. Acta Biomater. 2007, 3, 1024–1032.
21. Akimoto, J.; Park, S.J.; Obuse, S.; Kawamoto, M.; Tamura, M.; Nandakumar, A.; Kobatake, E.; Ito, Y. Synthesis of Photoreactive Poly (Ethylene Oxide) s for Surface Modification. ACS Appl. Bio Mater. 2020, 3, 5941–5947.
22. Konno, T.; Hasuda, H.; Ishihara, K.; Ito, Y. Photo-Immobilization of a Phospholipid Polymer for Surface Modification. Biomaterials 2005, 26, 1381–1388.
23. Lin, X.; Fukazawa, K.; Ishihara, K. Photoreactive Polymers Bearing a Zwitterionic Phosphorylcholine Group for Surface Modification of Biomaterials. ACS Appl. Mater. Interfaces 2015, 7, 17489–17498.
24. Fukazawa, K.; Tsuji, K.; Inoue, Y.; Ishihara, K. Direct Photoreactive Immobilization of Water-Soluble Phospholipid Polymers on Substrates in an Aqueous Environment. Colloids Surfaces B Biointerfaces 2021, 199, 111507.
25. Sakuragi, M.; Tsuzuki, S.; Obuse, S.; Wada, A.; Matoba, K.; Kubo, I.; Ito, Y. A Photoimmobilizable Sulfobetaine-Based Polymer for a Nonbiofouling Surface. Mater.

Sci. Eng. C 2010, 30, 316–322.

26. Sakuragi, M.; Tsuzuki, S.; Hasuda, H.; Wada, A.; Matoba, K.; Kubo, I.; Ito, Y. Synthesis of a Photoimmobilizable Histidine Polymer for Surface Modification. J. Appl. Polym. Sci. 2009, 112, 315–319.
27. Hasuda, H.; Kwon, O.H.; Kang, I.-K.; Ito, Y. Synthesis of Photoreactive Pullulan for Surface Modification. Biomaterials 2005, 26, 2401–2406.
28. Chen, G.; Ito, Y.; Imanishi, Y.; Magnani, A.; Lamponi, S.; Barbucci, R. Photoimmobilization of Sulfated Hyaluronic Acid for Antithrombogenicity. Bioconjug. Chem. 1997, 8, 730–734.
29. Ito, Y.; Nogawa, M.; Takeda, M.; Shibuya, T. Photo-Reactive Polyvinylalcohol for Photo-Immobilized Microarray. Biomaterials 2005, 26, 211–216.
30. Ito, Y.; Nogawa, M. Preparation of a Protein Micro-Array Using a Photo-Reactive Polymer for a Cell-Adhesion Assay. Biomaterials 2003, 24, 3021–3026.
31. Ito, Y. Photoimmobilization for Microarrays. Biotechnol. Prog. 2006, 22, 924–932.
32. Ito, Y. Microarray Chips (in Vitro Diagnosis). In Photochemistry for Biomedical Applications; Springer, 2018; pp. 85–106.
33. Matsudaira, T.; Tsuzuki, S.; Wada, A.; Suwa, A.; Kohsaka, H.; Tomida, M.; Ito, Y. Automated Microfluidic Assay System for Autoantibodies Found in Autoimmune Diseases Using a Photoimmobilized Autoantigen Microarray. Biotechnol. Prog. 2008, 24, 1384–1392.
34. Tsuzuki, S.; Wada, A.; Ito, Y. Photo‐immobilization of Biological Components on Gold‐coated Chips for Measurements Using Surface Plasmon Resonance (SPR) and a Quartz Crystal Microbalance (QCM). Biotechnol. Bioeng. 2009, 102, 700–707.
35. Sivakumar, P.M.; Moritsugu, N.; Obuse, S.; Isoshima, T.; Tashiro, H.; Ito, Y. Novel Microarrays for Simultaneous Serodiagnosis of Multiple Antiviral Antibodies. PLoS One 2013, 8, e81726.
36. Kashiwagi, H.; Morishima, N.; Obuse, S.; Isoshima, T.; Akimoto, J.; Ito, Y. SARS-CoV-2 Proteins Microarray by Photoimmobilization for Serodiagnosis of the Antibodies. Bull. Chem. Soc. Jpn. 2021, 94, 2435–2443.
37. Akimoto, J.; Kashiwagi, H.; Morishima, N.; Obuse, S.; Isoshima, T.; Kageyama, T.; Nakajima, H.; Ito, Y. Rapid and Quantitative Detection of Multiple Antibodies against SARS-CoV-2 Mutant Proteins by Photo-Immobilized Microarray. Anal. Sci. 2022, 38,

1313–1321.

38. Ito, Y.; Moritsugu, N.; Matsue, T.; Mitsukoshi, K.; Ayame, H.; Okochi, N.; Hattori, H.; Tashiro, H.; Sato, S.; Ebisawa, M. An Automated Multiplex Specific IgE Assay System Using a Photoimmobilized Microarray. J. Biotechnol. 2012, 161, 414–421.
39. Ohyama, K.; Omura, K.; Ito, Y. A Photo-Immobilized Allergen Microarray for Screening of Allergen-Specific IgE. Allergol. Int. 2005, 54, 627–631.

CHAPTER V

Conclusions and Future perspectives

1. Conclusions

In order to develop devices for biomedical applications, various functional polymers are required. This thesis describes the development of polymeric materials based on temperature-responsive and photo-reactive polymers. Newly designed functional polymers were synthesized, and their properties were evaluated for biomedical applications.

Chapter I describes the general introduction to stimuli-responsive polymers. Stimuli-responsive polymers have attracted significant attention in digital technology, sensors, and biomedical applications. Upon response to external stimuli, they exhibit a drastic change in their physical or chemical properties, which can be used in smart materials. Temperature is the most common and well-studied stimulus in the fields of bioengineering and biotechnology. Several systems comprising temperature-responsive polymers that are sensitive to a small change in the human body temperature have been developed. This property can be used to develop a more delicate and accurate responsive system. On the other hand, light is not only noncontact and noninvasive stimulus but also induces covalent bonding using photo-reactive species. Photo-reactive polymers have been widely investigated in numerous applications varying from lithography to *in-vivo* polymerized biomedical applications. In this thesis, new types of temperature-sensitive polymers and photo-reactive polymers were designed to be used for a variety of purposes, including medication delivery, tissue engineering, biosensing, and the creation of hydrogels for wound healing.

Chapter II describes the design and production of a novel type of temperature-responsive polymer system using dynamic covalent bonds (DCBs) for the biomaterials. I investigated the thermal control of hydrogel crosslinking by DCBs of boronic ester formation between phenylboronic acid (PBA) and diol of poly(vinyl alcohol) (PVA) at temperatures close to body temperature. Diblock copolymers comprising hydrophobic poly(n-butyl methacrylate) and hydrophilic poly(N,N-dimethylaminopropylacrylamide) were synthesized and conjugated with PBA. The polymers were self-assembled in water to form reactive phenylboronic nanoparticles (PBA-NPs). With the use of a transmission electron microscope, dynamic light scattering, and zeta potential, the produced PBA-NPs were characterized. The boronic ester completely dissociated above 60 °C and did so at a lower temperature than other DCBs. PBA-NPs displayed a reversible gel–sol phase transition at 39.7 °C after three-dimensional (3D) crosslinking with PVA to create a hydrogel. The bonding/dissociation of the boronic-ester-based crosslinking points by the application of heat produced a change in viscoelasticity.

Therefore, easy recombination of the crosslinking points in the hydrogel was achieved via mild temperature changes in order to avoid potential water evaporation during high-temperature treatment. When the temperature was lowered from 45 to 25 °C, PBA-NPs crosslinked hydrogels also exhibited self-healing properties. These boronic-ester-DCB functionalized nanoparticles can enable the recombination of crosslinking sites in hydrogels for use in biomedical applications.

Chapter III discusses the design and evaluation of tough hydrogel using the template polymerization technique. The performance of the hydrogel in terms of recovery is greatly influenced by molecular diffusion. The molecular weight of the polymer is too high to contact DCB-derived functional groups each other because of the lower diffusivity of the polymers than that of small molecules. Furthermore, DCB formation has strong limitations due to the steric hindrance of the polymers. High hydrogel hysteresis could not only be produced by combining the polymers and PBA-NPs crosslinkers. Therefore, template polymerization was used to create a robust hydrogel (TempGel). Actually, PBA-NPs were cemented inside the hydrogel and enhanced its temperature-dependent viscoelasticity. The backbone polymer of N-[Tris(hydroxymethyl)methyl] acrylamide (THMAAm) was used to create the PBA-NPs crosslinker with extremely effective conjugation. For the recombination of crosslinking points of self-healing and thermoplastic properties, the template polymerization method was useful. By changing the temperature, the TempGel was able to alter the bonding state of the boronic ester and exhibited a complete recovery rate to examine how the temperature change affected their thermal viscoelastic characteristics. In this study, the PBA-NPs were successfully used as a template to formulate the smart hydrogel, which has high hysteresis, effective thermal plasticity, and self-healing capabilities.

Chapter IV describes the design and synthesis of photo-reactive polymers for their anti-biofouling applications. Antibiofouling means suppression of nonspecific interactions with the surfaces. Polyethylene glycols (PEGs) are flexible, highly hydrophilic, and exhibit nonadherent and non-biofouling properties. The immobilization of PEGs on the surfaces is common for the preparation of antibiofouling surfaces. However, specific treatments of surfaces were usually required for the chemically covalent immobilization of PEGs on the surfaces. Therefore, the photo-immobilization method was employed as a convenient and applicable method for any materials. I designed photo-reactive PEG-grafted polyethylene glycols (AzPEGs) as antibiofouling surface modifiers. 4-(Glycidyloxymethyl)azidobenzene was copolymerized

with methoxy-PEG epoxide (mPEG-EPO) and ethylene oxide (EO) for AzPEGs. AzPEGs were found to be highly soluble in water and showed photo-reactivity. UV exposure induced nitrene production from azidophenyl groups in the side chain, and the polymer crosslinked each other and with the polystyrene surface. On the polystyrene substrate, the prepared AzPEG layers prevented nonspecific interactions between proteins and cells. AzPEGs can be employed for various surface modifications in biomedical applications due to the applicability of photo-immobilization.

Chapter V concluded the thesis and discussed future perspectives.

This work suggested new designs for fabricating mild or tough temperature-responsive and self-healing hydrogel systems. The photo-reactive PEG can be employed for various surface treatments for antibiofouling. These studies on functional polymer designs can be extended to other medical applications, such as tissue engineering, controlled drug delivery, sensors, and diagnostics.

2. Future perspectives

Stimuli-responsive polymeric materials have gained significant momentum in highly developed industries such as biomaterials, automobiles, electronics, aerospace, and construction. Biotechnology has been continuously developing toward integrating nanoscale, sophisticated, and more complicated systems in recent times. Consequently, industries need to be reliable, sensitive, and efficient. However, rapid technological and industrial advances have led to some problems that cannot be solved using current technologies and materials. Therefore, the demand for smart and intelligent materials, devices, and technologies is continuously increasing. The stimuli-responsive polymer is a powerful tool to overcome the limitations and challenges of the current systems. The current technological problems or limitations can be solved by applying well-controlled polymers. In this regard, stimuli-responsive and stimuli-reactive polymers can be powerful tools for providing solutions. Because such polymers are highly versatile, they can be tailored depending on the target application, such as for developing intelligent biomaterials and smart drug-delivery systems. Temperature- or light-responsive polymer materials can also be utilized as smart sensors and actuators. polymers with well-controlled properties owing to minor environmental variations have great potential in the development of innovative systems to resolve the current technological limitations. In this thesis, I describe stimuli-responsive and stimuli-reactive polymers, the preparation of polymeric materials, and their potential biomedical applications.

As mentioned in chapter II, I explored a new thermal cleavage system that controls the equilibrium state of dynamic covalent bonds (DCB) by utilizing the dynamics and physicochemical properties of polymers. I designed and prepared a thermo-responsive hydrogel using dynamic covalent bonding by mixing three-dimensional crosslinking PBA-NPs with PVA. The thermo-responsive hydrogel was successfully prepared and exhibited a reversible gel−sol phase transition at 39.7 °C. The developed hydrogel can be utilized for a variety of biomedical applications, including medication delivery, tissue engineering [1–3], biosensing [4,5], and the creation of hydrogels for wound healing [6,7].

Additionally, the prepared hydrogel can incorporate epidermal growth factor (EGF) and fibroblast growth factor-2 (FGF-2) to be applied as a transdermal drug delivery system. By the effect of body temperature, the release of the incorporated growth factors can be controlled and can conduct an accelerated wound healing effect [8,9].

Injectable hydrogels have aroused much attention for their advantages such as minimally invasive surgery, avoidance of surgical trauma, and filling and repairing irregularly

shaped tissue defects [10]. Because of its simplicity of administration and low level of invasiveness, which improve patient compliance, the injectable hydrogel has attracted a lot of attention as one of the most successful approaches in the biomedical field, particularly for embolic agents [11–13]. DCB significantly improves the DCB hydrogel's capacity for self-healing, making it injectable given its biomedical applications. The injectability increases the DCB-based hydrogels' delivery options and creates the possibility of biomedical applications [14,15].

I think my prepared hydrogel can be easily injected so it might have great potential as tissue repair material and ease of administration to suit different shapes and this can be utilized for wound care management and articular cartilage repair.

Despite these advantages and promising applications, these hydrogels still require additional studies. For example, the mechanism of thermal cleavage of PBA-diol is not clear. One possibility for checking the mechanism is the conjugation of the diblock copolymer (PBMA-*b*-PDMAPAAm-PBA) with a conventional thermo-responsive polymer as poly(N-isopropyl acrylamide) (PNIPAm). PNIPAm drastically changes the conformation of the polymer in response to the applied heat across the phase transition temperature [16]. By controlling the exposure and shielding of dynamic covalent functional groups through conformation changes in the polymer, the formation of DCBs can be physically disturbed in response to temperature signals. Thus, the equilibrium state of DCB can be actively and sensitively controlled compared with normal DCBs.

Additionally, several factors affect sol-gel behavior and should be further studied. For example, more PVA to PBA-NPs crosslinker ratio should be considered. Moreover, the preparation of the hydrogel should be further studied by using different molecular weights of PVA (1000Da was used in this study), several sizes of the PBA-NP crosslinkers, and chain lengths of PDMAPAAm polymers (74 units were used in this study). The effects of all these parameters on sol-gel transition temperature should be further verified.

As mentioned in chapter III, I designed and prepared a robust and tough DCB-based thermo-responsive hydrogel. The prepared hydrogel can undergo shape re-modeling by temperature changes. The dynamic covalent nature of boronic acid-based hydrogels would allow for 3D cell culture within this synthetic matrix to proliferate. The ability of boronic acid-based hydrogels to dissociate by mild temperature could allow for the construction of more complex material geometries for creating 3D cultures. I contend that these hydrogels made of

boronic acid are appropriate for dynamic 3D cell culture and the development of intricate material geometries. Future research examining the role of cell-matrix and cell-cell interactions in more complicated biological processes or even the delivery of cells *in-vivo* could make use of the approaches established here [17,18].

Additionally, thermo-responsive gels work well as scaffolds for tissue regeneration and stem cell encapsulation. This strategy is becoming one of the potential treatments for cartilage defects, which is still an issue due to the low vascularization and poor chondrocyte migration ability. As a result, cell therapies using mesenchymal stem cells with the ability to produce chondrocytes have been successful in repairing cartilage [19].

With the development of this thermos-responsive hydrogel, upcoming research tracking the movement of cells or cell-cell signaling molecules within these materials may be able to learn interesting things about the mechanisms and regulators of cell migration as well as other functions that are important for the investigation of disease or regenerative processes. Analyzing mechanotransduction and related cell responses in this temporally evolving hydrogel structure for comparison to its physically or irreversibly degradable hydrogel counterparts could be one of the fundamental studies of cell response to cell-matrix interactions within this dynamic covalent system. This dynamic covalent chemistry and cell-degradable cross-links could be combined to create new types of material systems that have emergent properties for a range of applications.

However, some other further studies are required for this hydrogel. For example, the safety and cytotoxicity of the hydrogel should be confirmed. Additionally, stress relaxation of that synthetic extracellular matrices, in addition to other matrix properties, is emerging as an important regulator of cell fate [20,21]. Moreover, fundamental studies of cell response to cell-matrix interactions within this dynamic covalent hydrogel could be intuitive.

To meet the practical requirements in biomedical applications such as drug delivery, wound dressing, tissue engineering, cell culture, biosensors, and so forth, DCB hydrogels are being built. As a result, the next paragon might be the demand-oriented design of DCB hydrogels [22].

Because template polymerization is a general method, other DCBs can also be used to prepare high-efficient hydrogels. In addition, my study is focused on controlling the equilibrium of the DCBs through temperature. The equilibrium of other DCBs can be controlled by other stimuli such as pH and light. Thus, the method proposed in this study can be widely applied to prepare stimuli-responsive smart hydrogels. The factors that are necessary

to induce high hysteresis in a hydrogel are the equilibrium of DCBs, three-dimensional crosslinker with multivalent conjugation, and densely packed structure with template polymerization.

In chapter IV the photo-induced reactive polymer was developed into a polymeric surface coating by using photo-stimuli, and the prepared coated pattern showed excellent nonspecific suppression ability, which is attributed to its PEG backbone chain. When the novel PEG chain was used as the main backbone structure combined with grafted PEG side chain, the photoreactive polymer showed significant improvement in its solubility than that shown by the conventional azide photoreactive polymer. However, some other concentrations of the AzPEG (0.25 wt.% used in this study), as well as some other grafted-PEG molecular weights (350 and 750 used in this study), should be considered in future studies.

Despite these encouraging results, it is important to keep in mind that PEG may cause immunogenicity and ultimately lead to the production of anti-PEG antibodies, which may limit the use of PEG coatings for *in-vivo* sensing or drug delivery and force the investigation of alternative antifouling chemistries [23–25].

Finally, this thesis suggests new designs for fabricating stimuli-induced reactive polymers and provides useful information for the preparation of novel polymeric materials with a combination of stimuli systems. This study can also be extended to other research fields, such as controlled drug delivery, sensors, and diagnostics.

3. Reference

1. Galperin, A.; Long, T.J.; Ratner, B.D. Degradable, Thermo-Sensitive Poly (N-Isopropyl Acrylamide)-Based Scaffolds with Controlled Porosity for Tissue Engineering Applications. Biomacromolecules 2010, 11, 2583–2592.
2. Van Vlierberghe, S.; Dubruel, P.; Schacht, E. Biopolymer-Based Hydrogels as Scaffolds for Tissue Engineering Applications: A Review. Biomacromolecules 2011, 12, 1387–1408.
3. Tan, H.; Marra, K.G. Injectable, Biodegradable Hydrogels for Tissue Engineering Applications. Materials (Basel). 2010, 3, 1746–1767.
4. Yang, W.; Xue, H.; Carr, L.R.; Wang, J.; Jiang, S. Zwitterionic Poly (Carboxybetaine) Hydrogels for Glucose Biosensors in Complex Media. Biosens. Bioelectron. 2011, 26, 2454–2459.
5. Khimji, I.; Kelly, E.Y.; Helwa, Y.; Hoang, M.; Liu, J. Visual Optical Biosensors Based on DNA-Functionalized Polyacrylamide Hydrogels. Methods 2013, 64, 292–298.
6. Yang, J.-A.; Yeom, J.; Hwang, B.W.; Hoffman, A.S.; Hahn, S.K. In Situ-Forming Injectable Hydrogels for Regenerative Medicine. Prog. Polym. Sci. 2014, 39, 1973–1986.
7. Zhao, X.; Wu, H.; Guo, B.; Dong, R.; Qiu, Y.; Ma, P.X. Antibacterial Anti-Oxidant Electroactive Injectable Hydrogel as Self-Healing Wound Dressing with Hemostasis and Adhesiveness for Cutaneous Wound Healing. Biomaterials 2017, 122, 34–47.
8. Smithmyer, M.E.; Deng, C.C.; Cassel, S.E.; LeValley, P.J.; Sumerlin, B.S.; Kloxin, A.M. Self-Healing Boronic Acid-Based Hydrogels for 3D Co-Cultures. ACS Macro Lett. 2018, 7, 1105–1110.
9. Kitajima, T.; Sakuragi, M.; Hasuda, H.; Ozu, T.; Ito, Y. A Chimeric Epidermal Growth Factor with Fibrin Affinity Promotes Repair of Injured Keratinocyte Sheets. Acta Biomater. 2009, 5, 2623–2632.
10. Yan, S.; Wang, W.; Li, X.; Ren, J.; Yun, W.; Zhang, K.; Li, G.; Yin, J. Preparation of Mussel-Inspired Injectable Hydrogels Based on Dual-Functionalized Alginate with Improved Adhesive, Self-Healing, and Mechanical Properties. J. Mater. Chem. B 2018, 6, 6377–6390.
11. Zhou, F.; Chen, L.; An, Q.; Chen, L.; Wen, Y.; Fang, F.; Zhu, W.; Yi, T. Novel Hydrogel Material as a Potential Embolic Agent in Embolization Treatments. Sci. Rep. 2016, 6, 1–11.

12. Patenaude, M.; Campbell, S.; Kinio, D.; Hoare, T. Tuning Gelation Time and Morphology of Injectable Hydrogels Using Ketone–Hydrazide Cross-Linking. Biomacromolecules 2014, 15, 781–790.
13. Yoshida, Y.; Kawahara, K.; Inamoto, K.; Mitsumune, S.; Ichikawa, S.; Kuzuya, A.; Ohya, Y. Biodegradable Injectable Polymer Systems Exhibiting Temperature-Responsive Irreversible Sol-to-Gel Transition by Covalent Bond Formation. ACS Biomater. Sci. Eng. 2017, 3, 56–67.
14. Jiang, Y.; Upputuri, P.K.; Xie, C.; Zeng, Z.; Sharma, A.; Zhen, X.; Li, J.; Huang, J.; Pramanik, M.; Pu, K. Metabolizable Semiconducting Polymer Nanoparticles for Second Near-infrared Photoacoustic Imaging. Adv. Mater. 2019, 31, 1808166.
15. Wang, L.; Zhou, W.; Wang, Q.; Xu, C.; Tang, Q.; Yang, H. An Injectable, Dual Responsive, and Self-Healing Hydrogel Based on Oxidized Sodium Alginate and Hydrazide- Modified Poly (Ethyleneglycol). Molecules 2018, 23, 546.
16. Sponchioni, M.; Palmiero, U.C.; Moscatelli, D. Thermo-Responsive Polymers: Applications of Smart Materials in Drug Delivery and Tissue Engineering. Mater. Sci. Eng. C 2019, 102, 589–605.
17. Tang, S.; Ma, H.; Tu, H.; Wang, H.; Lin, P.; Anseth, K.S. Adaptable Fast Relaxing Boronate-Based Hydrogels for Probing Cell–Matrix Interactions. Adv. Sci. 2018, 5, 1800638.
18. Chen, Y.; Diaz-Dussan, D.; Wu, D.; Wang, W.; Peng, Y.-Y.; Asha, A.B.; Hall, D.G.; Ishihara, K.; Narain, R. Bioinspired Self-Healing Hydrogel Based on Benzoxaborole-Catechol Dynamic Covalent Chemistry for 3D Cell Encapsulation. ACS Macro Lett. 2018, 7, 904–908.
19. Zhang, Y.; Zhang, J.; Chang, F.; Xu, W.; Ding, J. Repair of Full-Thickness Articular Cartilage Defect Using Stem Cell-Encapsulated Thermogel. Mater. Sci. Eng. C 2018, 88, 79– 87.
20. Chaudhuri, O.; Gu, L.; Darnell, M.; Klumpers, D.; Bencherif, S.A.; Weaver, J.C.; Huebsch, N.; Mooney, D.J. Substrate Stress Relaxation Regulates Cell Spreading. Nat. Commun. 2015, 6, 1–7.
21. Chaudhuri, O.; Gu, L.; Klumpers, D.; Darnell, M.; Bencherif, S.A.; Weaver, J.C.; Huebsch, N.; Lee, H.; Lippens, E.; Duda, G.N. Hydrogels with Tunable Stress Relaxation Regulate Stem Cell Fate and Activity. Nat. Mater. 2016, 15, 326–334.

22. Ye, J.; Fu, S.; Zhou, S.; Li, M.; Li, K.; Sun, W.; Zhai, Y. Advances in Hydrogels Based on Dynamic Covalent Bonding and Prospects for Its Biomedical Application. Eur. Polym. J. 2020, 139, 110024, DOI:https://doi.org/10.1016/j.eurpolymj.2020.110024.
23. Lila, A.S.A.; Kiwada, H.; Ishida, T. The Accelerated Blood Clearance (ABC) Phenomenon: Clinical Challenge and Approaches to Manage. J. Control. Release 2013, 172, 38–47.
24. Schellekens, H.; Hennink, W.E.; Brinks, V. The Immunogenicity of Polyethylene Glycol- ol: Facts and Fiction. Pharm. Res. 2013, 30, 1729–1734.
25. Herzenberg, L.A.; Tokuhisa, T. Epitope-Specific Regulation. I. Carrier-Specific Induct- ion of Suppression for IgG Anti-Hapten Antibody Responses. J. Exp. Med. 1982, 155, 1730– 1740.

List of Publications

Original papers for this thesis

1. **Mahmoud H. Othman,** Yoshihiro Ito, Jun Akimoto, "Mild-Temperature-Induced Recombination of Crosslinking Structures in Hydrogels Using Phenylboronic-Acid-Functionalized 3D Nanoparticle Crosslinkers". *ACS Appl. Polym. Mater*., 2022, 4(7), 5047–5055, DOI: 10.1021/acsapm.2c00581.

2. **Mahmoud H. Othman,** Yoshihiro Ito, Jun Akimoto, "Highly Efficient and Rapid Recombination of Crosslinking Points in Hydrogels Through Template Polymerization of Dynamic Covalent Three-Dimensional Nanoparticle Crosslinkers". (In preparation).

3. **Mahmoud H. Othman,** Yoshihiro Ito, Jun Akimoto, "Synthesis and Characterization of Polyethylene Glycol-Grafted and Photoreactive Polyethylene Glycols for Anti-biofouling Applications". *Polymers.*, 2023, 15(1), 184–193, DOI: 10.3390/polym15010184.

Other papers

1. Naveen Nagiah, Raven El Khoury, **Mahmoud H. Othman**, Jun Akimoto, Yoshihiro Ito, David A. Roberson, and Binata Joddar, "Development and Characterization of Furfuryl-Gelatin Electrospun Scaffolds for Cardiac Tissue Engineering". *ACS Omega.*, 2022, 7(16), 13894–13905, DOI: 10.1021/acsomega.2c00271.

Conferences:

1. **Mahmoud H. Othman,** Yoshihiro Ito, Jun Akimoto, "Synthesis of thermally degradable and highly efficient self-healing hydrogel using dynamic covalent 3D nanoparticle crosslinkers". *71st Symposium on Macromolecules,* Sapporo, Japan (Oral presentation, 2022).

2. **Mahmoud H. Othman,** Yoshihiro Ito, Jun Akimoto, "Development of thermoresponsive smart hydrogels using dynamic covalent bonds for dissociating near body temperature". *the 43rd Annual Meeting of the Japanese Society for Biomaterials and The 8th Asian Biomaterials Congress,* Nagoya, Japan (Oral presentation, 2021).

3. **Mahmoud H. Othman,** Yoshihiro Ito, Jun Akimoto, "Development of drug release control device using heat dissociative smart hydrogel". *Tokyo Metropolitan University Bio-conference,* Tokyo, Japan (Oral presentation, 2021).

4. **Mahmoud H. Othman,** Yoshihiro Ito, Jun Akimoto, "Development of shape rewritable self-healing hydrogel using the mild thermoresponsive property of phenylboronic acid dynamic covalent bond". *4th G'L'owing Polymer Symposium in KANTO*, Tokyo, Japan (Oral presentation, 2021).

5. **Mahmoud H. Othman,** Yoshihiro Ito, Jun Akimoto, "Synthesis of Smart Hydrogel for Biomedical Applications using Thermal Cleavage techniques". *Tokyo Metropolitan University - Seoul City University Bio conference,* South Korea (Oral presentation, 2021).

6. **Mahmoud H. Othman,** Yoshihiro Ito, Jun Akimoto, "Development of thermoresponsive smart hydrogels for dissociating near body temperature". *Tokyo Metropolitan University Bio-conference,* Tokyo, Japan (Poster presentation, 2021).

Acknowledgments

Foremost, all praise and glory to Almighty Allah (Subhanahu Wa Ta'ala) who gave me the courage and patience to carry out this work and complete this thesis.

This doctoral thesis summarizes the studies during 2020-2023 under the direction of Professor Yoshihiro Ito at Emergent Bioengineering Materials Research Team, RIKEN, Wako city, Japan.

To Professor Yoshihiro Ito, I would like to express my sincere gratitude and thanks for giving me the chance to pursue a Ph.D. at Tokyo Metropolitan University. He provided me with invaluable professional advice, intellectual input, time, encouragement, scientific support, and helpful criticism throughout the research, for which I am incredibly grateful. I feel fortunate to have had the opportunity to work in his lab at RIKEN.

I am deeply grateful to Dr. Jun Akimoto, the friendly mentor who supported and trusted my research for his optimistic, constant advice and valuable discussions throughout this work. Great thanks for his continuous guidance, suggestions, and encouragement throughout this work.

I am greatly thankful to Professor Hiroyuki Kawahara, Professor Kotohiro Nomura, and Professor Toshiro Aigaki, my Ph.D. committee members for their professional discussions, intellectual guidance, and valuable advice on my Ph.D. progress.

Many thanks to my dear friends and co-graduate students at Nano Medical Engineering Laboratory and Emergent Bioengineering Materials Research Team, who made my life easy and enjoyable, and for their instructive comments.

I am very grateful for the financial assistance provided by the Junior Research Associate (JRA) program for graduate students by the Global Relation Office, RIKEN's research personnel support section.

I would also like to express my sincere gratitude to my loving parents, for their continuous understanding, helpful support, and deep affection. I am extremely thankful for the patience, support, and understanding of my loving wife and my children, who kept me sane even in times of happiness or stress in my research.

January, 2023
Mahmoud Othman
Wako, Japan

Appendix

Published papers

ACS APPLIED POLYMER MATERIALS

pubs.acs.org/acsapm Article

Mild-Temperature-Induced Recombination of Crosslinking Structures in Hydrogels Using Phenylboronic-Acid-Functionalized 3D Nanoparticle Crosslinkers

Mahmoud H. Othman, Yoshihiro Ito,* and Jun Akimoto*

Cite This: ACS Appl. Polym. Mater. 2022, 4, 5047−5055 Read Online

ACCESS | Metrics & More | Article Recommendations | Supporting Information

ABSTRACT: Self-healing properties can be bestowed to hydrogels by recombination of crosslinking points. This study was aimed at controlling these crosslinking points using the dynamic covalent bonds (DCBs) of a boronic ester formed by phenylboronic acid (PBA) and the diols of poly(vinyl alcohol) (PVA) under temperature changes. Interestingly, boronic ester dissociated at a lower temperature than that of other DCBs and completely dissociated above 60 °C. PBA-incorporated nanoparticles underwent three-dimensional (3D) crosslinking with PVA to form a hydrogel and exhibited a reversible gel−sol phase transition at 39.7 °C. The viscoelasticity changed in response to the bonding/dissociation of the boronic-ester-based crosslinking points. The viscoelasticity of the hydrogel decreased rapidly upon heating at 50 °C and recovered to 82% of the original value after 10 min of cooling. Therefore, facile recombination of the crosslinking points in the hydrogel was achieved via mild temperature changes to avoid possible water evaporation in high-temperature treatment. Additionally, hydrogels crosslinked with glutaraldehyde showed self-healing properties upon lowering the temperature from 45 to 25 °C. These boronic-ester-DCB-functionalized nanoparticles can enable the recombination of crosslinking points in hydrogels for biomedical applications.

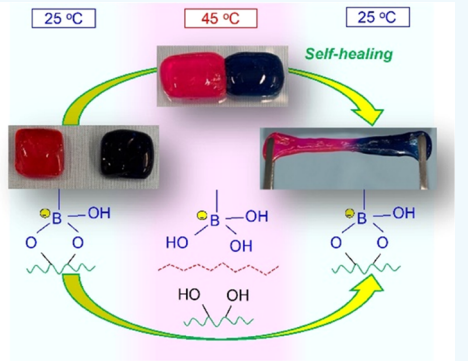

KEYWORDS: *dynamic covalent bonds, hydrogels, thermal cleavage, self-healing, phenylboronic acid*

1. INTRODUCTION

Smart hydrogels exhibit controllable physical properties in response to external environmental changes, such as various physical and chemical stimuli, and have been applied in several areas involving biomaterials, polymeric actuators, energy devices, and molecular sensing.[1−4] Recently, smart gels based on dynamic covalent bonds (DCBs) that exhibit reversible bond dissociation in response to changes in the surrounding environment have been developed.[5,6] DCBs exhibit highly stable covalent properties; moreover, they achieve equilibrium and partially dissociate upon external stimulation (e.g., heat and light) and subsequently reform bonds upon removal of the stimulus.[7,8] The internal structure of hydrogels can be transformed using DCBs as crosslinkers because external stimuli can promote their dissociation. These DCB-derived nonbonding free functional groups can randomly recombine with their counterpart functional groups in the gel upon removal of the stimulus, thereby permitting the recombination of the crosslinking points, which enables adhesion between gels owing to a self-healing function.[9,10]

Several stimuli such as light and temperature enable cleavage of DCBs, with temperature being a particularly common stimulus in the biomedical field because of the ease of external temperature control that can be achieved using various heating devices. DCBs that dissociate with heat are typically considered, such as imine bonds and those in Schiff bases (amine−aldehyde),[11,12] acylhydrazone (hydrazine−aldehyde),[13] the Diels−Alder reaction (ene−diene),[14,15] dithioesters (thiol−thiol),[16] and alkoxyamines (styryl-radical−nitroxy-radical).[17] The physical properties and structure of a gel can be drastically altered using these DCBs because the crosslinking points that support its morphology can be directly cleaved by heating. Controlling the binding and dissociation due to thermal stimuli can enable recombination of the functional groups that form the DCBs, thereby imparting self-healing characteristics to the gel.[18] However, high-temperature treatment is generally required to dissociate these bonds and facilitate polymer chain mobility in the gel to enable recombination of the crosslinking structure. For instance, Schiff bases are dissociated via heating at 67 °C or higher, which are considered relatively low temperatures, to control the functionality of the hydrogel.[8,12]

Received: April 5, 2022
Accepted: June 8, 2022
Published: June 28, 2022

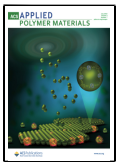

The high-temperature treatments adopted for preparing smart hydrogels significantly affect their physical properties in terms of surface drying and water evaporation. Therefore, hydrogels that exhibit self-healing properties under ambient conditions are being synthesized using DCBs that exist in equilibrium at room temperature and passively exchange their functional groups.[19,20] DCBs should be stable at room temperature and dissociate at mild temperatures to actively induce the exchange of DCB-derived functional groups. However, these DCBs have been rarely reported. Therefore, controlling the bonding of DCB-type smart hydrogels at ambient temperatures can significantly facilitate their biomedical applications.

Phenylboronic acid (PBA), which forms boronic ester DCBs with diol compounds,[21,22] is extensively used in biomedical applications, especially as a glucose sensor owing to its high binding affinity to sugars.[23,24] Additionally, PBA can form a hydrogel with diol-containing polymers, such as poly(vinyl alcohol) (PVA), at high concentrations; the resulting hydrogel has biomedical applications as a cell-coating material, for instance.[25]

Owing to the high biocompatibility of PBA, the DCBs of boronic esters are extensively applied in the biomedical field; however, the influence of temperature on these boronic esters has yet to be reported. Although temperature responsiveness has been imparted to PBA using thermoresponsive polymers, the thermal properties of these boronic esters have not been elucidated because the phase transition of the thermoresponsive polymers occurs at temperatures close to room temperature or higher, hindering analysis of the thermal effects of boronic esters under ambient conditions.[26,27]

Therefore, the thermochemical properties of a boronic ester were clarified in this study to determine the possibility of exploiting the thermal dissociation of its bonds in the preparation of functional hydrogels. In particular, PBA was used in combination with cationic poly(*N*,*N*-dimethylaminopropyl acrylamide) (PDMAPAAm) because the dissociation constant of boronic esters considerably increases in the presence of cationic polymers.[28]

Furthermore, PBA was introduced to the surface of cationic nanoparticles to bind with diol compounds in a multivalent manner. This multivalence effect enabled control of the dissociation and bonding states of the DCBs via a thermal stimulus, thus permitting recombination of hydrogel samples in terms of crosslink density and position to impart self-healing properties.

2. MATERIALS AND METHODS

2.1. Materials. *n*-Butyl methacrylate (BMA), *N*,*N*-dimethylaminopropyl acrylamide (DMAPAAm), and 4-acryloylmorpholine (ACMO) were purchased from FUJIFILM Wako Pure Chemicals (Tokyo, Japan) and were purified by distillation under reduced pressure. PVA (polymerization degree: 1000), 2,2′-azobisisobutyronitrile (AIBN), 2-ethanolamine, alizarin red S (ARS), acetone, hexane, 1,4-dioxane, sodium hydroxide, hydrochloric acid, sulforhodamine B, methylene blue, and glutaraldehyde were also purchased from FUJIFILM Wako Pure Chemicals. Tris(2-carboxyethyl) phosphine hydrochloride (TCEP; Tokyo Chemical Industry, Tokyo, Japan), 3-(acrylamido) phenylboronic acid (APBA; Combi-Blocks, San Diego, CA), and 2-cyano-2-propyl dodecyl trithiocarbonate (CPDT; Sigma-Aldrich, St. Louis, MO) were used as received.

2.2. Synthesis of PBA-Terminated Block Copolymer. BMA (75 mmol), CPDT (3 mmol), and AIBN (0.3 mmol) were dissolved in 1,4-dioxane (100 mL) and bubbled with nitrogen gas for 30 min at 25 °C. Polymerization was subsequently performed at 80 °C for 24 h. The resulting solution was dissolved in acetone, and the unreacted monomer was completely evaporated under vacuum at 100 °C for 1 h. The obtained PBMA was dissolved in 1,4-dioxane for use in the subsequent copolymerization. Next, PBMA (0.1 mmol), DMAPAAm (10 mmol) or ACMO (10 mmol), and AIBN (0.01 mmol) were dissolved in 1,4-dioxane (10 mL). The solution was bubbled with nitrogen gas for 20 min and subsequently reacted at 80 °C for 24 h under a nitrogen atmosphere. The reactant solution was added dropwise to an excess amount of hexane, and the obtained yellow compound was dialyzed against water using a dialysis membrane (Spectra/Por 6, MWCO 3500, Spectrum Laboratories, Rancho Dominguez, CA) for 2 days. A block copolymer was recovered by lyophilization. Subsequently, the diblock copolymer, APBA (10 molar equivalents of the diblock copolymer), and TCEP were dissolved in 1,4-dioxane (10 mL), and 2-aminoethanol (10 molar equivalents of the diblock copolymer) was slowly added to the preceding solution to convert the dodecyl trithiocarbonate (DTC) group into APBA on the terminus of the block copolymer. The solution was stirred at 25 °C for 12 h. After the reaction, the reactant solution was dialyzed against water for 72 h using a dialysis membrane (MWCO 3500), yielding polymers upon freeze-drying. The DTC- and PBA-terminated block polymers possessing cationic PDMAPAAm or nonionic PACMO are denoted as PBMA-*b*-PDMAPAAm-DTC, PBMA-*b*-PDMAPAAm-PBA, and PBMA-*b*-PACMO-PBA (Figure S1). The obtained polymers were characterized by ^{1}H NMR spectroscopy (JNM-ECZ400R, 400 MHz, JEOL, Tokyo, Japan) and a gel permeation chromatography (GPC; JASCO) system equipped with a refractive index detector (RI-2032, JASCO, Tokyo, Japan) and two columns (SB-803 HQ and SB804 HQ; Showa Denko, Tokyo, Japan). Ultraviolet (UV) absorbance was recorded using a UV−vis spectrometer (V−750, JASCO).

2.3. Preparation of Nanoparticles. Each block copolymer (1−100 mg) was dissolved in acetone (1 mL), followed by the addition of water (1 mL). The acetone was completely removed under vacuum at room temperature using a rotary evaporator at 100 hPa. The polymer concentration was adjusted to 0.1−100 mg/mL by adding water to the block copolymer solution. Nanoparticles prepared using PBMA-*b*-PDMAPAAm-PBA, PBMA-*b*-PDMAPAAm-DTC, and PBMA-*b*-PACMO-PBA are denoted as NP(PDMAPAAm)-PBA, NP(PDMAPAAm)-DTC, and NP(PACMO)-PBA, respectively.

2.4. Transmission Electron Microscopy (TEM). One drop of each nanoparticle solution (1 mg/mL) was placed on a carbon-coated TEM grid (COL-C10, 100 μm grid pitch, Okenshoji, Tokyo, Japan). Subsequently, the samples were negatively stained with 2% samarium acetate, and excess liquid was removed with filter paper. The samples were dried for 1 h and examined by TEM (JEM-1230, JEOL).

2.5. Dynamic Light Scattering (DLS) and ζ-Potential Measurements. The NP(PDMAPAAm)-PBA solution was diluted to 1.0 and 0.5 mg/mL for the DLS and ζ-potential measurements, respectively. The pH of the solution was adjusted using a NaOH solution (1 mol/L). Measurements were performed using an ELSZ-2PL instrument (Otsuka Electronics, Osaka, Japan).

2.6. Fluorescence Measurements. An equimolar ratio of ARS to PBMA-*b*-PDMAPAAm-PBA was added to the NP(PDMAPAAm)-PBA solution. Fluorescence intensities were recorded in the 480−650 nm range using a fluorimeter (FP-6500, JASCO, Tokyo, Japan) at an excitation wavelength of 468 nm. The temperature of the solution was controlled using a sample-cell thermostat (ETC-717, JASCO).

2.7. Differential Scanning Calorimetry (DSC). NP(PDMAPAAm)-PBA (5 mg/mL) and PVA (5 mg/mL) were mixed, and the pH of the solution was adjusted by adding HCl or NaOH solutions. Water and the sample were placed in the reference and sample-cell holder of the micro-CAL VP DSC apparatus, respectively (GE Healthcare, Chicago, IL). The DSC peaks were recorded in the 15−70 °C range.

2.8. Changes in Thermo-Viscoelasticity of the PBA-Modified-Nanoparticle/PVA System. NP(PDMAPAAm)-DTC, NP(PDMAPAAm)-PBA, or NP(PACMO)-PBA (1−5 wt %) was placed in a vial, and the pH of the solution was adjusted using NaOH

https://doi.org/10.1021/acsapm.2c00581
ACS Appl. Polym. Mater. 2022, 4, 5047−5055

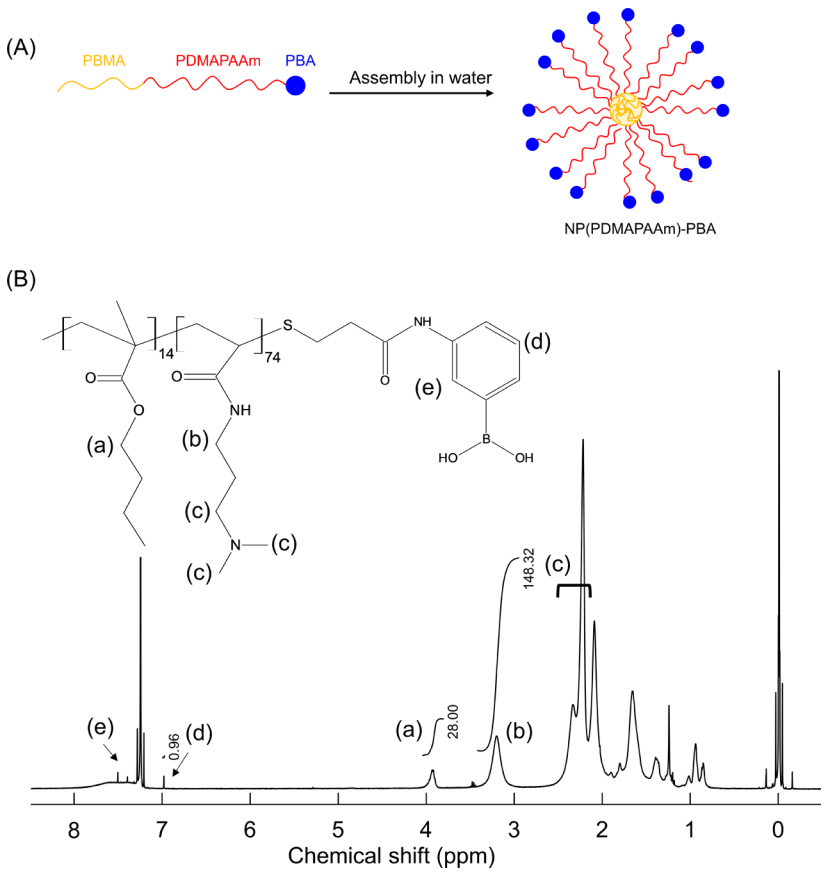

Figure 1. (A) Preparation of NP(PDMAPAAm)-PBA and (B) the ^{1}H NMR spectrum of PBMA-*b*-PDMAPAAm-PBA (solvent: $CDCl_3$).

or HCl solutions. Subsequently, an identical volume of 10 wt % PVA solution was added and gently mixed at 25 °C. Changes in viscosity of the PBMA-*b*-PDMAPAAm-PBA/PVA mixtures were examined at 25 and 45 °C by inverting the vial.

The thermo-viscoelastic changes in NP(PDMAPAAm)-PBA/PVA were measured using a rheometer (AR-G2, TA Instruments, New Castle, DE). After mixing NP(PDMAPAAm)-PBA and PVA, the solution or hydrogel was placed on the rheometer plate. Silicone oil was placed on the solution to prevent water evaporation, and time sweep measurements were performed at a fixed frequency (ω = 1 Hz) and strain (γ = 1%).

The self-healing properties of the hydrogel were investigated after fixing it with 0.3% glutaraldehyde, which was added to the PVA solution to crosslink the PVAs. NP(PDMAPAAm)-PBA and sulforhodamine B or methylene blue were subsequently added to the solution to prepare colored cubic hydrogels. These hydrogels were reintegrated at 45 °C on a hot plate, and the heated hydrogels were cooled thereafter to room temperature. The hydrogel connections were visually confirmed for each process.

3. RESULTS AND DISCUSSION

3.1. Synthesis of PBA-Terminated Block Copolymer. PBMA-*b*-PDMAPAAm-DTC was synthesized by sequential reversible addition−fragmentation chain-transfer (RAFT) polymerization. Hydrophobic PBMA was synthesized using CPDT as the RAFT agent. The average molecular weight of PBMA was determined to be 2600 g/mol from the UV absorbance of the trithiocarbonate unit at 310 nm (ε = 11 000 L/mol/cm).[29] Subsequently, DMAPAAm was propagated from PBMA to yield PBMA-*b*-PDMAPAAm-DTC. The DMAPAAm unit in the block copolymer was confirmed using ^{1}H NMR spectra by comparing the proton intensity of the methylene protons of BMA (−OCH_2−, 2H, 3.84−4.05 ppm) with that of the methylene protons of DMAPAAm (−N−CH_2−, 2H, 2.94−3.42 ppm). The number of BMA and DMAPAAm monomers in the block copolymer was determined to be 14 and 74, respectively. Additionally, the GPC chart showed a monomodal peak derived from the block copolymer, indicating the formation of the PBMA-*b*-PDMAPAAM-DTC diblock polymer (Figure S2).

The DTC group on the terminus of the diblock copolymer was converted into the PBA unit by its aminolysis, followed by the Michael addition of APBA. From the ^{1}H NMR spectrum, the aromatic protons of PBA in PBMA-*b*-PDMAPAAm-PBA were confirmed at 6.98 and 7.51 ppm, and the terminal conversion was determined to be greater than 95% by comparing the aromatic protons of PBA at 6.98 ppm and the methylene protons of BMA at 3.84−4.05 ppm (Figure 1). The GPC chart of PBMA-*b*-PDMAPAAm-PBA showed a monomodal peak similar to that of PBMA-*b*-PDMAPAAm-DTC (Figure S2). Additionally, the PBA-derived UV absorbance after the terminal conversion was confirmed (Figure S3). The UV absorbance of the PBA-free diblock copolymer, which was synthesized without APBA in the terminal conversion reaction, was low in the 280−330 nm range, which corresponded to the absorbance of PBA. Thus, the substitution of PBA at the terminus of the block copolymer was successfully confirmed.

Nonionic PBMA-*b*-PACMO-PBA was synthesized similar to PBMA-*b*-PDMAPAAm-PBA. The number of BMA and ACMO monomers in the block copolymer were 14 and 89, respectively, and the block copolymer showed a monomodal peak in the GPC profile (Figure S2).

https://doi.org/10.1021/acsapm.2c00581
ACS Appl. Polym. Mater. 2022, 4, 5047−5055

3.2. Preparation and Characterization of Synthesized Nanoparticles. Nanoparticles with a PBA surface, hydrophobic core, and hydrophilic corona [NP(PDMAPAAm)-PBA] were prepared by the assembly of PBMA-*b*-PDMAPAAm-PBA in water (Figure 1). Although PBMA-b-PDMAPAAm-PBA was soluble in water, it did not readily dissolve at a higher concentration (5 wt %). Therefore, PBMA-*b*-PDMAPAAm-PBA was first completely dissolved in acetone, and water was subsequently added to the solution. The acetone was evaporated from the solution under reduced pressure, followed by the preparation of the polymer solution.

DLS analysis showed that NP(PDMAPAAm)-PBA exhibited a unimodal peak, with a volume-average diameter of 54 ± 0.16 nm (Figure S4). The morphology of the nanoparticles was confirmed by TEM, which revealed uniformly dispersed ~30-nm-sized spherical dots (Figure S4).

The influence of pH on the ζ-potential of NP(PDMAPAAm)-PBA was investigated to determine the optimal pH range for ionization of PBA and PDMAPAAm in the formation of the boronic ester (Figure 2). The ζ-potential

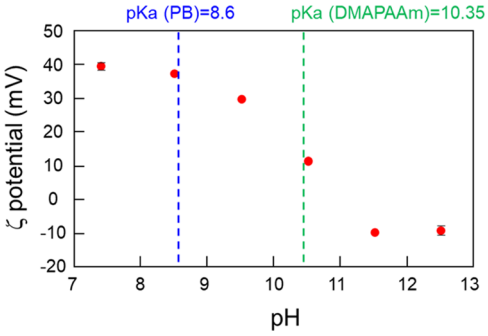

Figure 2. ζ-potentials of NP(PDMAPAAm)-PBA at different pH values (n = 3).

of NP(PDMAPAAm)-PBA at pH 7.4 (39.5 ± 1.1 mV) decreased with increasing pH and became negative at pH > 11.5. NP(PDMAPAAm)-PBA contains two pH-dependent molecules: PBA and DMAPAAm. The dissociation constant, pK_a, of PBA is 8.6, and boron atoms form tetrahedral negative ions at higher pH values.[30] However, DMAPAAm has a pK_a of 10.35, and deprotonation proceeds above this pH. Because NP(PDMAPAAm)-PBA has a PDMAPAAm chain, protonation of DMAPAA is suppressed due to the adjunct protonated DMAPAAm unit, and the pK_a of PDMAPAAm decreases by ~1 compared to that of the DMAPAAm monomer (10.35).[31] Therefore, the ionization of PBA on the particle surface and deprotonation of PDMAPAAm proceeded simultaneously when the pH was 8.6 or higher, resulting in a decreased ζ-potential. As the pH increased to above 11, the effect of protonated PDMAPAAm was hardly observed; moreover, the influence of boronate ions on the surface increased, resulting in a negative shift in the ζ-potential.

3.3. Thermal Properties of Boronic Ester. PBA forms boronic esters with diols and is used to prepare various biomedical materials. However, the temperature responses of these boronic esters have not been comprehensively analyzed, except for the temperature-response behavior of PBA-incorporated thermoresponsive polymers for glucose sensing. Therefore, the thermal properties of the boronic ester investigated in this study were determined using a catechol-functionalized fluorescent molecule ARS, which demonstrates a high affinity for PBA. As a fluorescent reporter, ARS becomes fluorescent upon binding to a PBA and enables the determination of binding constants with ARS.[28,32]

Temperature-dependent fluorescence changes in ARS and NP(PDMAPAAm)-PBA were observed from 20 to 50 °C (Figure S5). Strong fluorescence was observed from the PBA-conjugated ARS at 20 °C. The fluorescence intensity of ARS decreased with increasing temperature and was hardly observed above 40 °C. These results indicate that the boronic ester gradually dissociated in a mild environment from room temperature to body temperature.

DSC measurements were performed using the PBA-modified nanoparticles and PVA at different pH values to investigate the thermal sensitivity of the DCBs constructed by NP(PDMAPAAm)-PBA and PVA diols (Figure 3) because the

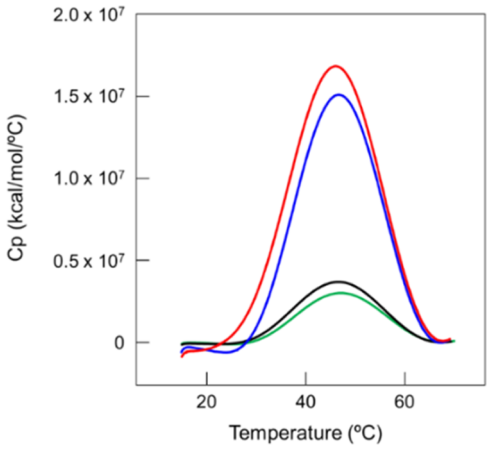

Figure 3. DSC thermograms of NP(PDMAPAAm)-PBA/PVA and NP(ACMO)-PBA/PVA at different pH values. Green, red, and blue profiles represent data of NP(PDMAPAAm)-PBA/PVA at pH 7.4, 9.5, and 11.5, respectively. The black profile represents NP(ACMO)-PBA/PVA data at pH 9.5. A nanoparticle/PVA system concentration of 0.5 wt % was used.

dissociation constant of the boronic ester was affected by pH (Figure 4A). At pH 7.4, the solution containing NP(PDMAPAAm)-PBA and PVA showed a small exothermal peak that started at 25−30 °C and peaked at ~46 °C. In contrast, the heat capacities of the NP(PDMAPAAm)-PBA and PVA solutions at pH 9.5 and 11.5 were 6 times greater than that at pH 7.4. Additionally, the peaks terminated at 65−70 °C. However, the DSC curves were almost identical except for the value regardless of pH. Additional DSC measurements were performed using the nonionic NP(PACMO)-PBA/PVA system at pH 9.5 to confirm the influence of PDMAPAAm on PBA. Interestingly, the resulting exothermic peak was almost identical to that of the NP(PDMAPAAm)-PBA/PVA system at pH 7.4. Moreover, the DSC analysis indicated that the boronic ester could be thermally dissociated and the DCB dissociation was initiated from 25 to 30 °C, regardless of the change in pH. In particular, the appearance of almost identical peak temperatures regardless of the pH and the presence or absence of cationic segments indicate that, in general, the boronic ester readily dissociated by heating.

However, the stability of the bonds was found to be highly dependent on pH; DSC analysis revealed the higher diol binding strength of PBA ionized at a high pH and the high thermodynamic stability in the high-pH region.

https://doi.org/10.1021/acsapm.2c00581
ACS Appl. Polym. Mater. 2022, 4, 5047−5055

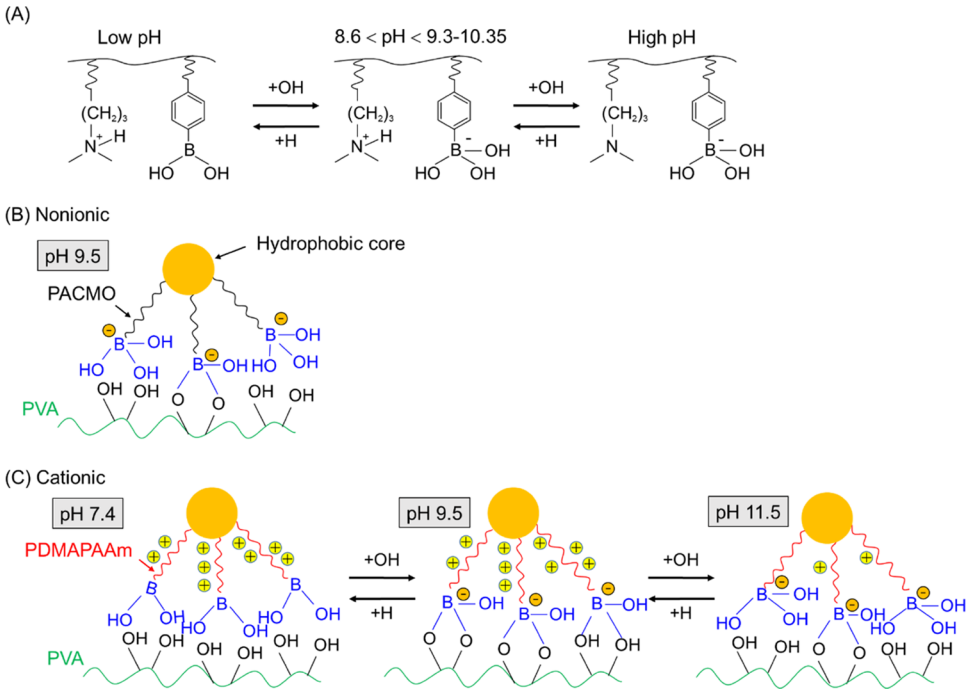

Figure 4. (A) Influence of pH on the charge of DMAPAAm and PBA. Illustration of possible changes in interactions of PVA with (B) nonionic NP(PACMO)-PBA and (C) cationic NP(PDMAPAAm)-PBA at different pH values.

PBA is strongly ionized in the presence of amines, which stabilizes the ionic state of boron (Figure 4). The family of boronic acids containing an adjacent coordinating amine center is characterized by the coordination between the nitrogen center and boron to form a tetrahedral boronate.[33] Additionally, the presence of an amino group increases the water solubility of the polymer and facilitates complex formation with PVA; moreover, the amino group coordinates to boronate to stabilize its ionized form, leading to strong boronate−diol complexation.[34] The presence of NP-(PDMAPAAm)-PBA involving a PBA unit on the nanoparticle surface decreased the polymer chain density at the outermost layer. However, PBA was connected to the PDMAPAAm chain, and numerous DMAPAAm units surrounded the PBA unit. Consequently, the PBA and DMAPAAm units efficiently formed coordination bonds between boron and nitrogen atoms.

The optimal pH of boronic esters is between the pK_a values of PBA and diols [$pH_{optimal} = (pK_{a\text{-acid}} + pK_{a\text{-diol}})/2$];[35−37] therefore, the optimal pH was assumed to be 12.6 in the present study. Therefore, the ionic boron was stabilized in NP(PDMAPAAm)-PBA and showed the high thermochemical stability of the boronic ester in the high-pH region.

In contrast, PBA did not sufficiently form the boronic ester in the absence of the cationic segment on the particles at pH 9.0, which was slightly higher than the pK_a of PBA. Therefore, changes in the ionization state of boron possibly had a significant effect on bond stability.

3.4. Preparation and Characterization of PBA-nanoparticle/PVA Hydrogel. Based on the fluorescence and DSC results, the DCBs of the boronic ester initiated temperature-responsive binding and dissociation under mild conditions from room temperature to near body temperature. The conditions for hydrogel formation using NP(PDMAPAAm)-PBA and PVA were subsequently explored. First, 1−5 wt % NP(PDMAPAAm)-PBA and PVA were mixed at pH 9.5 to ionize the PBA, and the viscosity of the solution was monitored. NP(PDMAPAAm)-DTC and PVA were mixed and prepared as a control; the viscosity of this solution did not increase, regardless of the solution concentration or the mixing ratio of NP(PDMAPAAm)-DTC and PVA. In contrast, the viscosity of the solution containing NP(PDMAPAAm)-PBA and PVA increased upon mixing, and gelation occurred at a solution concentration of 5 wt % (Table 1). The concentration of NP(PDMAPAAm)-PBA was higher than that of conventional PBA and PVA hydrogels[25] because of the presence of the PBA unit only at the terminus of the block copolymer, which decreased the molar concentration of PBA compared to that of other PBA and PVA hydrogels.

Table 1. Viscoelastic Properties of Synthesized Nanoparticle/PVA Mixtures at 25 °C (pH 9.5)

NP	[NP] (wt %)	[PVA] (wt %)	G' (Pa)	G'' (Pa)
NP(PDMAPAAm)-PBA	5	1	4.75	5.89
	5	2.5	14.4	19.3
	5	5	68.4	50.4
	2.5	5	30.0	21.1
NP(PACMO)-PBA	5	5	0.114	1.20
NP(PDMAPAAm)-DTC	5	5	5.48	8.17

A glucose solution (1 mol/L) was used to confirm the bonding enabled by the boronic ester between PBA on the nanoparticles and the PVA diols in the hydrogel. After the addition of the glucose solution, the hydrogel rapidly decomposed because the PBA of the boronic ester is exchanged from bonding with PVA to bonding with glucose.[38] Thus, the crosslinking points of the boronic ester between PBA on the nanoparticles and PVA were dissociated, indicating hydrogel formation by the DCBs of the boronic ester (Figure S6).

https://doi.org/10.1021/acsapm.2c00581
ACS Appl. Polym. Mater. 2022, 4, 5047−5055

The pH dependence of the hydrogel viscoelasticity was subsequently investigated (Figure 5). At pH 7.4, the mixture remained in the sol form. The viscoelasticity of the gel increased with increasing pH, yielding hydrogels, and peaked upon hydrogel formation at pH 9.5. However, its viscoelasticity gradually decreased from pH 9.5 onward, yielding a sol at pH > 11. These results indicate that a stable hydrogel can be prepared using PVA and the PDMAPAAm nanoparticles if the pH of the solution is higher than the pK_a of PBA and lower than the pK_a of PDMAPAAm, with PBA being ionized and further stabilized by protonated DMAPAAm.

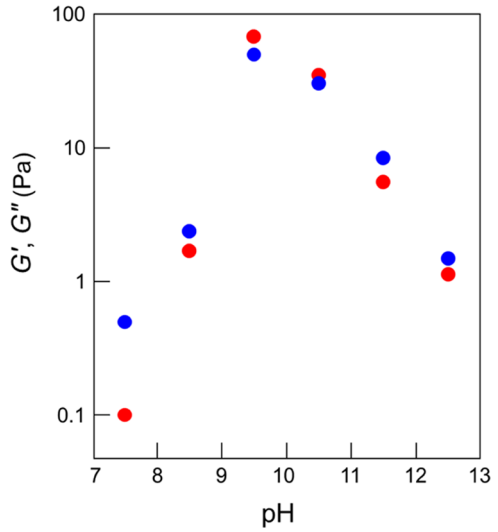

Figure 5. Effect of pH on the viscoelasticity of the NP-(PDMAPAAm)-PBA/PVA hydrogel. Red and blue circles indicate G' and G'', respectively.

Multivalent binding between the PVA diols and PBA on the nanoparticles was achieved by the introduction of PBA to the nanoparticle surface. This multivalent binding effect was evaluated by synthesizing linear P(DMAPAAm-*co*-PBA) (DMAPAAm/PBA = 475/25 (unit) as determined by ^{1}H NMR spectroscopy) and mixing with PVA. The mixture of linear P(DMAPAAm-*co*-PBA) and PVA exhibited the highest G' and G'' values in a region with values higher than the pK_a of PBA, similar to the mixture of NP(PDMAPAAm)-PBA and PVA, although it did not form a hydrogel (Table S1). These results suggest that the introduction of PBA to the nanoparticle surface is critical to the preparation of stable hydrogels because of the multivalent-bond-formation characteristic of the boronic ester; furthermore, the formation of the boronic ester on the nanoparticle surface in three dimensions enables efficient nanoparticle−PVA bonding.

3.5. Thermally Induced Formation and Dissociation of Crosslinking Points in Hydrogel. The thermal properties of the NP(PDMAPAAm)-PBA/PVA hydrogel at pH 9.5 were subsequently investigated using a rheometer (Figure 6). The viscoelasticity of the gel gradually decreased as the temperature increased from 25 °C. G'' overtook G' at 39.7 °C, indicating gel−sol phase transition. Conversely, the viscoelasticity gradually increased as the solution temperature decreased from 50 °C; moreover, G' overtook G'' at 21.3 °C and gelation occurred, confirming the reversibility of the sol−gel transition of the PBA-nanoparticle/PVA mixture. The DSC measurements suggested that the bond dissociation was almost complete at 65 °C. Thus, the solution temperature was increased to more than 50 °C to investigate the viscoelasticity of the sol phase. As the temperature increased to above 50 °C, the viscoelasticity gradually decreased, resulting in G' and G'' values of less than 1 Pa above 65 °C. These results indicate that the PBA−PVA bonds, which were the crosslinking points of the hydrogel, gradually dissociated with increasing temperature. DSC analysis of the hydrogel containing 5 wt % NP(PDMAPAAm)-PBA at pH 9.5 indicated that the gel structure collapsed at a temperature below that at which half of the bonds dissociated, resulting in the hydrogel becoming a sol. A further increase in temperature to 65 °C or higher led to the dissociation of almost all of the PBA−diol bonds, and the PBA particles and PVA molecules were considered to exist independently. Consequently, the dissociation of the PBA−diol bonds proceeded at mild temperatures, and the crosslinking state of the gel could be readily controlled by altering the temperature. Finally, the restoration efficiency of the hydrogel was confirmed by changing the temperature (25 and 50 °C). At 25 °C, the G' and G'' values of the hydrogel were 145 and 82 Pa, respectively. The sample was subsequently heated at 50 °C for 10 min and cooled thereafter at 25 °C for 10 min, which resulted in G' values of 119 and 66 Pa, respectively, for the hydrogel. The restoration efficiency, which was estimated to be ∼82%, gradually decreased with repeated heating and cooling and became ∼70% after the fifth cycle.

The self-healing property of the hydrogel was investigated by crosslinking it with glutaraldehyde. Because the NP-(PDMAPAAm)-PBA/PVA hydrogel transformed into a solution at temperatures over 39 °C, the hydrogel was crosslinked with glutaraldehyde to maintain its structure at higher temperatures. As shown in Figure 7, the hydrogel retained its structure at 45 °C. The Young's moduli of the hydrogel before and after thermal cycling were determined using the following equation

$$E = 2G'(1 + \nu)$$

where E and ν represent the Young's modulus and Poisson's ratio, respectively.

The Young's moduli of the unheated, heat-treated (50 °C), and cooled (25 °C) hydrogel were determined to be 321, 33, and 119 Pa, respectively. As shown in Figure 6D, the stiffness of the hydrogel was not sufficiently restored after 10 min of cooling. However, the boronic ester was gradually formed at the low temperature, which increased the stiffness of the hydrogel.

To confirm the self-healing property of the hydrogel, its ability to reestablish connections was investigated using colored hydrogel specimens. The prepared hydrogels were formed into cubes, and adhesion tests of the gels were conducted by changing the temperature (Figure 7B). Initially, the surfaces of the gels were brought into contact with each other at 25 °C; however, no adhesion was observed. Subsequently, the hydrogel cubes were heated on a hot plate at 45 °C, which led to their softening and a significant increase in G''; the G' and G'' values changed from 128 and 81 Pa, respectively, at 25 °C to 7 and 11 Pa at 50 °C. Moreover, no adhesion was observed between the gel surfaces under heated conditions. However, adhesion was observed when these gels were cooled to room temperature with the surfaces in contact. The strong connections due to the self-healing ability of the NP(PDMAPAAm)-PBA/PVA hydrogel were confirmed by stretching it to (Figure 7) more than 2-fold.

https://doi.org/10.1021/acsapm.2c00581
ACS Appl. Polym. Mater. 2022, 4, 5047−5055

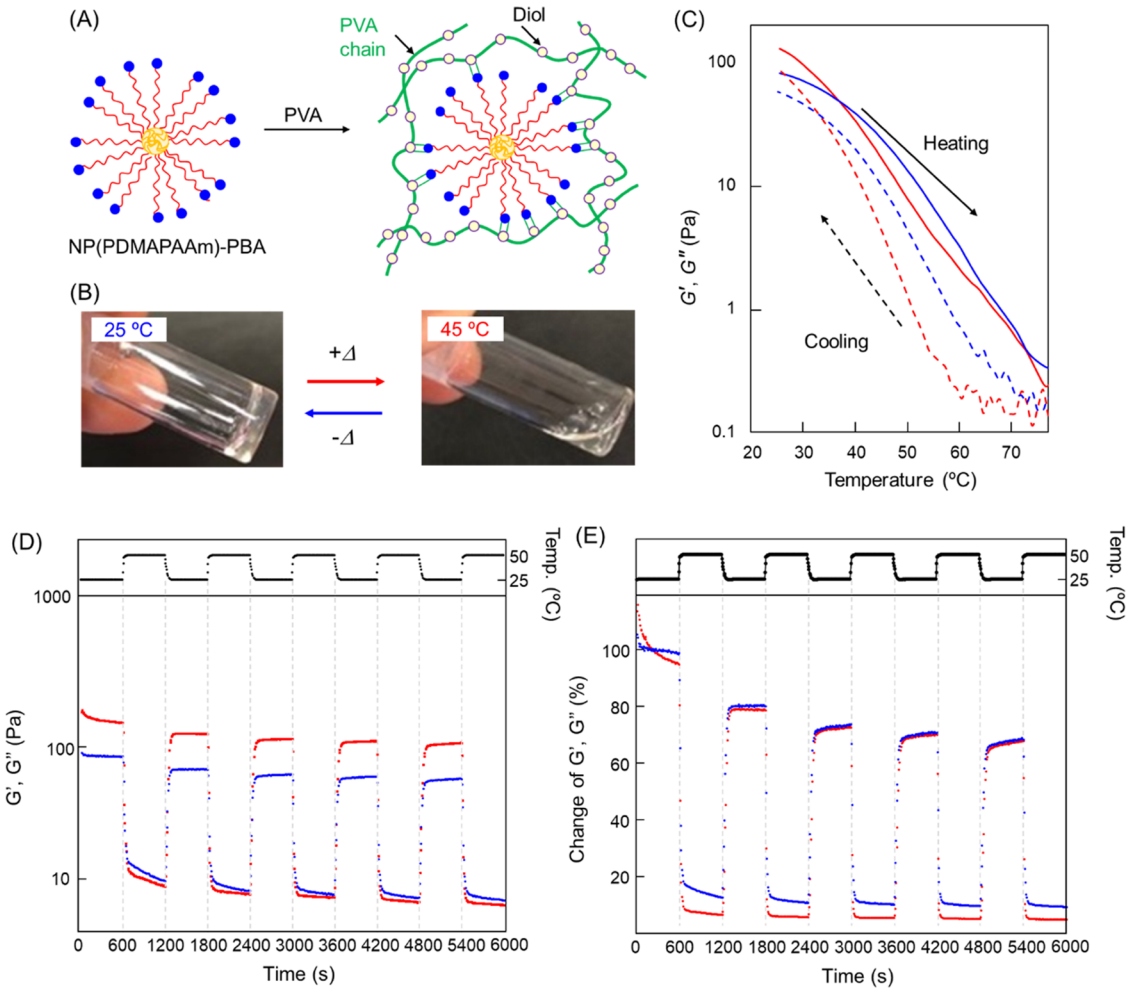

Figure 6. Changes in thermo-viscoelasticity of NP(PDMAPAAm)-PBA/PVA. (A) Preparation of hydrogel using NP(PDMAPAAm)-PBA and PVA. (B) Images of a mixture of NP(PDMAPAAm)-PBA (5 wt %) and PVA at 25 and 50 °C. Sol−gel phase transition occurred reversibly in response to temperature variations. (C) Changes in viscoelasticity of NP(PDMAPAAm)-PBA (5 wt %) and PVA (5 wt %) at pH 9.5. Red and blue profiles indicate G' and G'', respectively. Solid and dashed profiles indicate heating and cooling processes (5 °C/min), respectively. (D) G' and G'' data and (E) restoration efficiency of NP(PDMAPAAm)-PBA (5 wt %) and PVA (5 wt %) at 25 and 50 °C. The temperature was alternated between 25 and 50 °C every 10 min.

Overall, a hydrogel capable of undergoing sol−gel transition under extremely mild conditions was successfully synthesized by clarifying the thermochemical properties of PBA−diol bonds. The thermal dissociation of various DCBs is known to induce thermal properties in gels. However, even Schiff bases, which are typical thermally dissociable DCBs, are subjected to temperatures above 67 °C for thermal dissociation.[8] High temperatures strongly influence this property of hydrogels via evaporation of water and drying of the surface. However, compared to other DCBs, the PBA−diol bonds can be dissociated from 30 °C and are completely dissociated above 60 °C. Consequently, self-healing characteristics can be readily imparted to the hydrogel using mild-temperature treatments. Moreover, functional control of this boronic-ester-based hydrogel was demonstrated under conditions close to body temperature. This hydrogel is expected to be highly versatile and applicable as a medical material on skin surfaces, although a high pH is required for its preparation. Essentially, this boronic-ester-DCB-based hydrogel can be used as a material that can express its functions in ambient environments such as body surfaces because of its functions under mild temperature changes.

4. CONCLUSIONS

Thermal cleavage of the DCBs of a boronic ester was found to begin from a low temperature of 25−30 °C and dissociate (half of the DCBs) at ∼46 °C, which is lower than that of other temperature-responsive DCBs. The viscoelasticity of the hydrogel containing a boronic ester for crosslinking changed drastically with increasing temperature. In particular, the hydrogel transformed into a sol at temperatures over 39.7 °C because of the dissociation of its boronic-ester-based cross-linking points. The boronic ester was reconstructed upon cooling at 25 °C, which led to the re-emergence of the hydrogel. The thermally cleaved boronic ester on the surface or inside the hydrogel could be randomly reconjugated by decreasing the temperature. Consequently, exchange between the boronic ester on the surface of the hydrogel samples enabled their connection, indicating its self-healing ability. The boronic ester could be controlled under gentle conditions at temperatures slightly higher than body temperature, and the self-healing property was demonstrated without changing the properties of the hydrogel derived via water evaporation, for instance. Thus, the boronic-ester-based NP(PDMAPAAm)-

https://doi.org/10.1021/acsapm.2c00581
ACS Appl. Polym. Mater. 2022, 4, 5047−5055

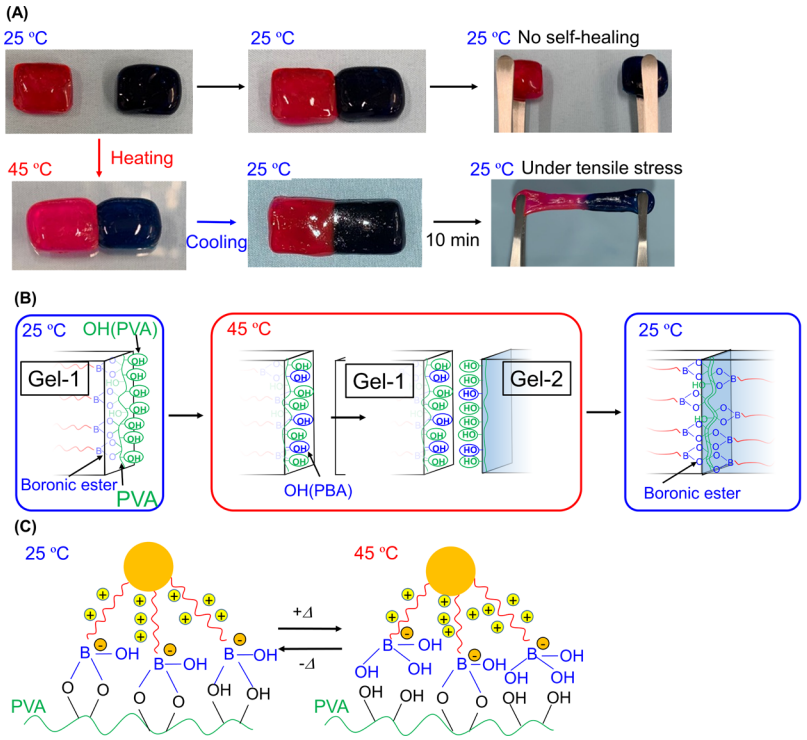

Figure 7. Self-healing properties of NP(PDMAPAAm)-PBA/PVA hydrogel. (A) Photos of hydrogels at each step of the thermal investigation. Red and blue hydrogels were stained with sulforhodamine B and methylene blue, respectively. (B) Possible changes in surface chemistry of the NP(PDMAPAAm)-PBA/PVA hydrogel at each investigated temperature. (C) Illustration of possible changes in interactions between PVA and NP(PDMAPAAm)-PBA at different temperatures.

PBA system can be a promising hydrogel crosslinker for the development of smart hydrogels for biomedical applications.

■ ASSOCIATED CONTENT

Supporting Information

The Supporting Information is available free of charge at https://pubs.acs.org/doi/10.1021/acsapm.2c00581.

GPC charts and UV spectra of diblock copolymers; DLS charts and TEM images of nanoparticles; changes in fluorescence intensity of ARS and NP(PDMAPAAm)-PBA; photographs of NP(PDMAPPAm)-PBA/PVA before and after the addition of glucose; and changes in viscoelasticity of P(DMAPAAm-co-APBA)/PVA (PDF)

■ AUTHOR INFORMATION

Corresponding Authors

Yoshihiro Ito − *Emergent Bioengineering Materials Research Team, RIKEN Center for Emergent Matter Science, Wako, Saitama 351-0198, Japan; Department of Biological Sciences, Graduate School of Science, Tokyo Metropolitan University, Hachioji, Tokyo 192-0397, Japan; Nano Medical Engineering Laboratory, RIKEN Cluster for Pioneering Research, Wako, Saitama 351-0198, Japan;* orcid.org/0000-0002-1154-253X; Email: y-ito@riken.jp

Jun Akimoto − *Emergent Bioengineering Materials Research Team, RIKEN Center for Emergent Matter Science, Wako, Saitama 351-0198, Japan;* orcid.org/0000-0003-1554-6869; Email: jun.akimoto@a.riken.jp

Author

Mahmoud H. Othman − *Emergent Bioengineering Materials Research Team, RIKEN Center for Emergent Matter Science, Wako, Saitama 351-0198, Japan; Department of Biological Sciences, Graduate School of Science, Tokyo Metropolitan University, Hachioji, Tokyo 192-0397, Japan*

Complete contact information is available at: https://pubs.acs.org/10.1021/acsapm.2c00581

Notes

The authors declare no competing financial interest.

■ ACKNOWLEDGMENTS

The authors are grateful to Masamichi Nakayama (Tokyo Women's Medical University, TWIns) for the DSC measurements and members of the Materials Characterization Support Unit of the RIKEN Center for Emergent Matter Science (CEMS) for the TEM imaging. M.H.O. acknowledges partial financial support from The Otsuka Toshimi Scholarship Foundation.

■ REFERENCES

(1) Zhang, Y.; Xie, S.; Zhang, D.; Ren, B.; Liu, Y.; Tang, L.; Chen, Q.; Yang, J.; Wu, J.; Tang, J.; Zheng, J. Thermo-Responsive and Shape-Adaptive Hydrogel Actuators from Fundamentals to Aapplications. *Eng. Sci.* **2019**, *6*, 1−11.

(2) Zhang, D.; Ren, B.; Zhang, Y.; Xu, L.; Huang, Q.; He, Y.; Li, X.; Wu, J.; Yang, J.; Chen, Q.; et al. From Design to Applications of Stimuli-Responsive Hydrogel Strain Sensors. *J. Mater. Chem. B* **2020**, *8*, 3171−3191.

(3) Mai, W.; Yu, Q.; Han, C.; Kang, F.; Li, B. Self-Healing Materials for Energy-Storage Devices. *Adv. Funct. Mater.* **2020**, *30*, No. 1909912.

(4) Li, S.; Wang, L.; Zheng, W.; Yang, G.; Jiang, X. Rapid Fabrication of Self-Healing, Conductive, and Injectable Gel as Dressings for Healing Wounds in Stretchable Parts of the Body. *Adv. Funct. Mater.* **2020**, *30*, No. 2002370.
(5) Chen, Y.; Tan, Z.; Wang, W.; Peng, Y.-Y.; Narain, R. Injectable, Self-Healing, and Multi-Responsive Hydrogels via Dynamic Covalent Bond Formation between Benzoxaborole and Hydroxyl Groups. *Biomacromolecules* **2019**, *20*, 1028−1035.
(6) Perera, M. M.; Ayres, N. Dynamic Covalent Bonds in Self-Healing, Shape Memory, and Controllable Stiffness Hydrogels. *Polym. Chem.* **2020**, *11*, 1410−1423.
(7) Habault, D.; Zhang, H.; Zhao, Y. Light-Triggered Self-Healing and Shape-Memory Polymers. *Chem. Soc. Rev.* **2013**, *42*, 7244−7256.
(8) Miao, J.-T.; Ge, M.; Peng, S.; Zhong, J.; Li, Y.; Weng, Z.; Wu, L.; Zheng, L. Dynamic Imine Bond-Based Shape Memory Polymers with Permanent Shape Reconfigurability for 4D Printing. *ACS Appl. Mater. Interfaces* **2019**, *11*, 40642−40651.
(9) Taylor, D. L.; in het Panhuis, M. Self-Healing Hydrogels. *Adv. Mater.* **2016**, *28*, 9060−9093.
(10) Wu, G.; Jin, K.; Liu, L.; Zhang, H. A Rapid Self-Healing Hydrogel Based on PVA and Sodium Alginate with Conductive and Cold-Resistant Properties. *Soft Matter* **2020**, *16*, 3319−3324.
(11) Zhang, H.; Wang, D.; Wu, N.; Li, C.; Zhu, C.; Zhao, N.; Xu, J. Recyclable, Self-Healing, Thermadapt Triple-Shape Memory Polymers Based on Dual Dynamic Bonds. *ACS Appl. Mater. Interfaces* **2020**, *12*, 9833−9841.
(12) de Hatten, X.; Bell, N.; Yufa, N.; Christmann, G.; Nitschke, J. R. A Dynamic Covalent, Luminescent Metallopolymer that Undergoes Sol-to-Gel Transition on Temperature Rise. *J. Am. Chem. Soc.* **2011**, *133*, 3158−3164.
(13) Folmer-Andersen, J. F.; Lehn, J.-M. Thermoresponsive Dynamers: Thermally Induced, Reversible Chain Elongation of Amphiphilic Poly(Acylhydrazones). *J. Am. Chem. Soc.* **2011**, *133*, 10966−10973.
(14) Bapat, A. P.; Ray, J. G.; Savin, D. A.; Hoff, E. A.; Patton, D. L.; Sumerlin, B. S. Dynamic-Covalent Nanostructures Prepared by Diels-Alder Reactions of Styrene-Maleic Anhydride-Derived Copolymers Obtained by One-Step Cascade Block Copolymerization. *Polym. Chem.* **2012**, *3*, 3112−3120.
(15) Liu, Y.-L.; Chuo, T.-W. Self-Healing Polymers Based on Thermally Reversible Diels-Alder Chemistry. *Polym. Chem.* **2013**, *4*, 2194−2205.
(16) Tuten, B. T.; Chao, D.; Lyon, C. K.; Berda, E. B. Single-Chain Polymer Nanoparticles via Reversible Disulfide Bridges. *Polym. Chem.* **2012**, *3*, 3068−3071.
(17) Otsuka, H.; Aotani, K.; Higaki, Y.; Takahara, A. A Dynamic (Reversible) Covalent Polymer: Radical Crossover Behaviour of TEMPO−Containing Poly(Alkoxyamine Ester)s. *Chem. Commun.* **2002**, 2838−2839.
(18) Chen, Q.; Zhu, L.; Chen, H.; Yan, H.; Huang, L.; Yang, J.; Zheng, J. A Novel Design Strategy for Fully Physically Linked Double Network Hydrogels with Tough, Fatigue Resistant, and Self-Healing Properties. *Adv. Funct. Mater.* **2015**, *25*, 1598−1607.
(19) Cai, Y.; Zou, H.; Zhou, S.; Chen, Y.; Liang, M. Room-Temperature Self-Healing Ablative Composites via Dynamic Covalent Bonds for High-Performance Applications. *ACS Appl. Polym. Mater.* **2020**, *2*, 3977−3987.
(20) Xu, J.; Guo, Z.; Chen, Y.; Luo, Y.; Xie, S.; Zhang, Y.; Tan, H.; Xu, L.; Zheng, J. Tough, Adhesive, Self-healing, Fully Physical Crosslinked κ-CG-K+/pHEAA Double-Network Ionic Conductive Hydrogels for Wearable Sensors. *Polymer* **2021**, *236*, No. 124321.
(21) Bapat, A. P.; Sumerlin, B. S.; Sutti, A. Bulk Network Polymers with Dynamic B−O Bonds: Healable and Reprocessable Materials. *Mater. Horiz.* **2020**, *7*, 694−714.
(22) Cho, S.; Hwang, S. Y.; Oh, D. X.; Park, J. Recent Progress in Self-Healing Polymers and Hydrogels Based on Reversible Dynamic B−O Bonds: Boronic/Boronate Esters, Borax, and Benzoxaborole. *J. Mater. Chem. A* **2021**, *9*, 14630−14655.
(23) Anzai, J.-i. Recent Progress in Electrochemical Biosensors Based on Phenylboronic Acid and Derivatives. *Mater. Sci. Eng.: C* **2016**, *67*, 737−746.
(24) Matsumoto, A.; Yoshida, R.; Kataoka, K. Glucose-Responsive Polymer Gel Bearing Phenylborate Derivative as a Glucose-Sensing Moiety Operating at the Physiological pH. *Biomacromolecules* **2004**, *5*, 1038−1045.
(25) Konno, T.; Ishihara, K. Temporal and Spatially Controllable Cell Encapsulation using a Water-Soluble Phospholipid Polymer with Phenylboronic Acid Moiety. *Biomaterials* **2007**, *28*, 1770−1777.
(26) Kataoka, K.; Miyazaki, H.; Okano, T.; Sakurai, Y. Sensitive Glucose-Induced Change of the Lower Critical Solution Temperature of Poly[*N, N*-(Dimethylacrylamide)-*co*-3-(Acrylamido)-Phenylboronic Acid] in Physiological Saline. *Macromolecules* **1994**, *27*, 1061−1062.
(27) Hoare, T.; Pelton, R. Charge-Switching, Amphoteric Glucose-Responsive Microgels with Physiological Swelling Activity. *Biomacromolecules* **2008**, *9*, 733−740.
(28) Yan, J.; Springsteen, G.; Deeter, S.; Wang, B. The Relationship Among pKa, pH, and Binding Constants in the Interactions between Boronic Acids and Diols—It is not as Simple as it Appears. *Tetrahedron* **2004**, *60*, 11205−11209.
(29) Akimoto, J.; Nakayama, M.; Sakai, K.; Okano, T. Temperature-Induced Intracellular Uptake of Thermoresponsive Polymeric Micelles. *Biomacromolecules* **2009**, *10*, 1331−1336.
(30) Shno, D.; Kubo, A.; Murata, Y.; Koyama, Y.; Kataoka, K.; Kikuchi, A.; Sakurai, Y.; Okano, T. Amine Effect on Phenylboronic Acid Complex with Glucose under Physiological pH in Aqueous Solution. *J. Biomater. Sci., Polym. Ed.* **1996**, *7*, 697−705.
(31) Brilmayer, R.; Hess, C.; Andrieu-Brunsen, A. Influence of Chain Architecture on Nanopore Accessibility in Polyelectrolyte Block-co-Oligomer Functionalized Mesopores. *Small* **2019**, *15*, No. 1902710.
(32) Mulla, H. R.; Agard, N. J.; Basu, A. 3-Methoxycarbonyl-5-Nitrophenyl Boronic Acid: High Affinity Diol Recognition at Neutral pH. *Bioorg. Med. Chem. Lett.* **2004**, *14*, 25−27.
(33) Wulff, G.; Lauer, M.; Böhnke, H. Rapid Proton Transfer as Cause of an Unusually Large Neighboring Group Effect. *Angew. Chem., Int. Ed.* **1984**, *23*, 741−742.
(34) Kitano, S.; Hisamitsu, I.; Koyama, Y.; Kataoka, K.; Okano, T.; Sakurai, Y. Effect of the Incorporation of Amino Groups in a Glucose-Responsive Polymer Complex Having Phenylboronic Acid Moieties. *Polym. Adv. Technol.* **1991**, *2*, 261−264.
(35) Sienkiewicz, P. A.; Roberts, D. C. Chemical Affinity Systems-I: pH Dependence of Boronic Acid-Diol Affinity in Aqueous Solution. *J. Inorg. Nucl. Chem.* **1980**, *42*, 1559−1575.
(36) Liu, X.-C.; Scouten, W. H. New Ligands for Boronate Affinity Chromatography. *J. Chromatogr. A* **1994**, *687*, 61−69.
(37) Van Duin, M.; Peters, J.; Kieboom, A.; Van Bekkum, H. Studies on Borate Esters 1: The pH Dependence of the Stability of Esters of Boric Acid and Borate in Aqueous Medium as Studied by 11B NMR. *Tetrahedron* **1984**, *40*, 2901−2911.
(38) Nakahata, M.; Mori, S.; Takashima, Y.; Hashidzume, A.; Yamaguchi, H.; Harada, A. pH-and Sugar-Responsive Gel Assemblies Based on Boronate−Catechol Interactions. *ACS Macro Lett.* **2014**, *3*, 337−340.

https://doi.org/10.1021/acsapm.2c00581
ACS Appl. Polym. Mater. 2022, 4, 5047−5055

Supporting information for

Mild-temperature-induced recombination of crosslinking structure in hydrogel using phenylboronic-acid-functionalized 3D nanoparticle crosslinkers

Mahmoud H. Othman[1,2,4], Yoshihiro Ito[1,2,3], Jun Akimoto[1*]*

[1] Emergent Bioengineering Materials Research Team, RIKEN Center for Emergent Matter Science, 2-1 Hirosawa, Wako, Saitama 351-0198, Japan

[2] Department of Biological Sciences, Graduate School of Science, Tokyo Metropolitan University, 1-1 Minami-Osawa, Hachioji, Tokyo 192-0397, Japan

[3] Nano Medical Engineering Laboratory, RIKEN Cluster for Pioneering Research, 2-1 Hirosawa, Wako, Saitama 351-0198, Japan

[4] Department of Pharmaceutics and Pharmaceutical Technology, Faculty of Pharmacy, Al-Azhar University, Assiut 71524, Egypt

Corresponding Authors

*E-mail: jun.akimoto@a.riken.jp (J.A.)

*E-mail: y-ito@riken.jp (Y.I.)

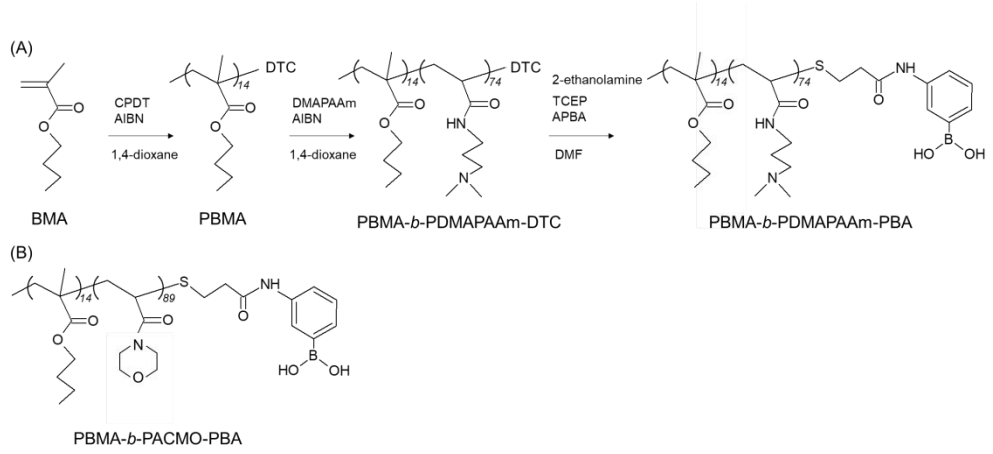

Figure S1. (A) Scheme for preparing PBMA-*b*-PDMAPAAm-PBA and (B) chemical structure of PBMA-*b*-PACMO-PBA

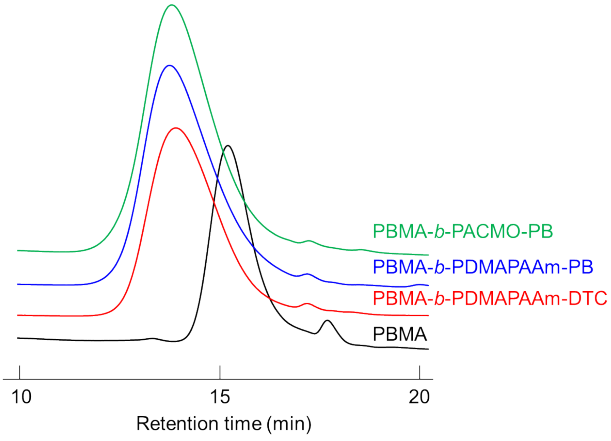

Figure S2. GPC charts of polymers. Eluent: *N,N*-dimethylformamide continuing 10 mmol/L lithium bromide, flow rate: 1 mL/min.

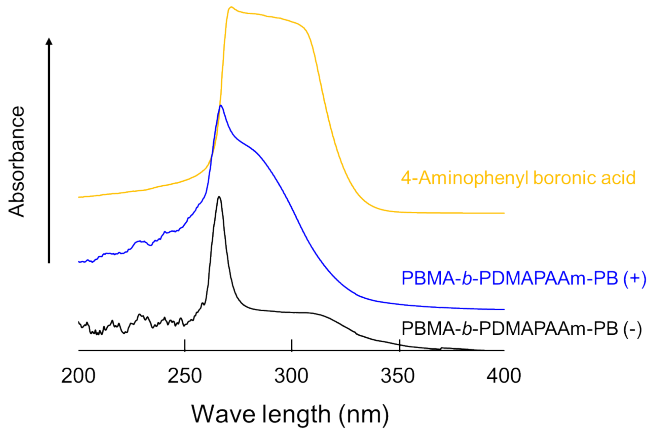

24

25 **Figure S3.** UV spectra of block copolymers and 4-aminophenyl boronic acid in water.

26

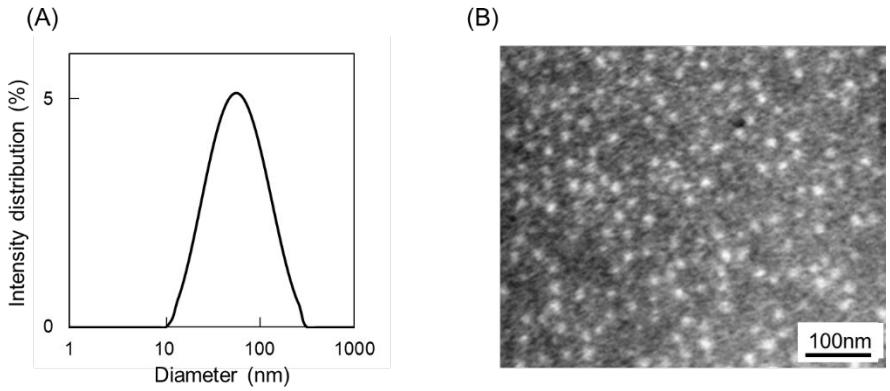

27

28 **Figure S4.** (A) DLS chart and (B) TEM image of NP(PDMAPAAm)-PBA.

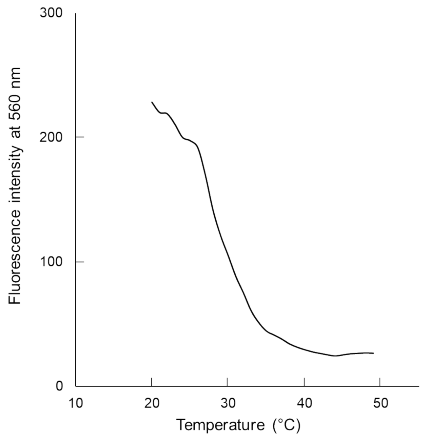

29

30 **Figure S5.** Fluorescence intensity changes of ARS and NP(PDMAPAAm)-PBA.

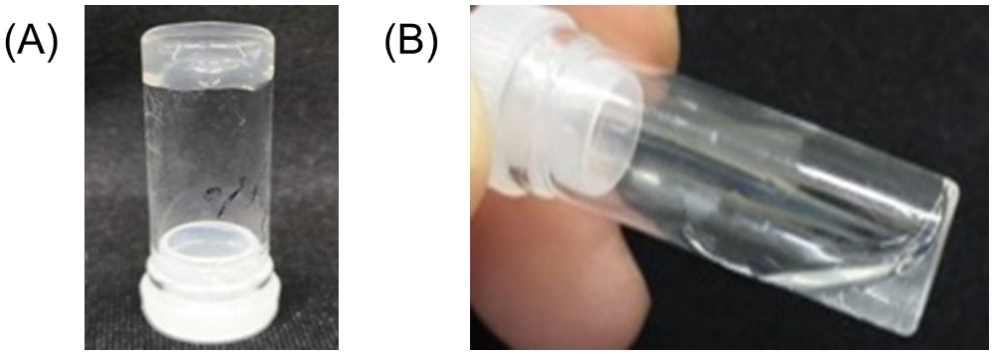

Figure S6. Photos of NP(PDMAPPAm)-PBA/PVA (A) before and (B) 30 s after adding 1 mg/mL glucose solution.

Table S1. Viscoelasticity change of P(DMAPAAm-*co*-APBA)/PVA(5 wt.%/5 wt.%) solution

pH	G′ (Pa)	G″ (Pa)
8.5	1.9	2.7
9.5	2.7	4.2
10.5	2.9	4.6

polymers

MDPI

Article

Synthesis and Characterization of Polyethylene Glycol-Grafted Photoreactive Polyethylene Glycols for Antibiofouling Applications

Mahmoud H. Othman [1,2], Yoshihiro Ito [1,2,3,*] and Jun Akimoto [1,*]

[1] Emergent Bioengineering Materials Research Team, RIKEN Center for Emergent Matter Science, 2-1 Hirosawa, Wako 351-0198, Saitama, Japan
[2] Department of Biological Sciences, Graduate School of Science, Tokyo Metropolitan University, 1-1 Minami-Osawa, Hachioji 192-0397, Tokyo, Japan
[3] Nano Medical Engineering Laboratory, RIKEN Cluster for Pioneering Research, 2-1 Hirosawa, Wako 351-0198, Saitama, Japan
* Correspondence: y-ito@riken.jp (Y.I.); jun.akimoto@a.riken.jp (J.A.)

Abstract: Notably, antibiofouling is an important and predominant technique adopted to improve the surfaces of biomaterials. In this study, polyethylene glycol-grafted polyethylene glycols bearing azidophenyl groups were synthesized and immobilized on polystyrene surfaces via photoirradiation. The prepared polymers were found to be highly soluble in water, and photoimmobilization with fluorescent proteins was confirmed based on micropatterning using a photomask. These polymers suppressed nonspecific interactions between proteins and cells on the substrate. Considering that photoimmobilization can be adopted for the covalent bond modification of various surfaces, the developed water-soluble and highly antibiofouling polymers appear to be useful in biomaterial preparation.

Keywords: photoreactive; azidophenyl; polyethylene glycol; photoimmobilization; cell adhesion; protein adsorption; antibiofouling

Citation: Othman, M.H.; Ito, Y.; Akimoto, J. Synthesis and Characterization of Polyethylene Glycol-Grafted Photoreactive Polyethylene Glycols for Antibiofouling Applications. *Polymers* **2023**, *15*, 184. https://doi.org/10.3390/polym15010184

Academic Editor: Ivan Gitsov

Received: 23 November 2022
Revised: 26 December 2022
Accepted: 27 December 2022
Published: 30 December 2022

1. Introduction

Typically, surface functionalization can facilitate the control of interactions between target materials while simultaneously suppressing nonspecific interactions with the surfaces. In particular, non-biofouling surfaces resist the adsorption of proteins and/or cell adhesion. This is because proteins generally have a strong tendency to adsorb on almost all surfaces, leading to cell adhesion. Therefore, surfaces that resist protein adsorption also resist cell adhesion [1,2].

There have been many recent advances in the construction of anti-biofouling surfaces for preventing nonspecific binding (fouling) in biomedical fields. For example, a microelectrode coated with a polyethylene glycols (PEG) methacrylate polymer (anti-biofouling layer) was developed to facilitate its implantation into the rat brain for electrophysiological recordings [3,4].

A nanosensor coated with a PEG–lipid was shown to minimize protein fouling and to prolong nanoparticle blood circulation for the monitoring of histamines [5,6]. Nanoparticles coated with a PEG polymer network (subsequently an antifouling shell) are capable of the in vivo detection of hydrogen peroxide (H_2O_2) that indicates many pathological processes including chronic diseases such as cancer. PEG was shown to endow the particles with good fouling resistance, water solubility, and biocompatibility [7].

The development of anti-biofouling membranes for inhibiting membrane biological contamination in the field of water purification was also established. The coated

membranes were shown to inhibit the initial attachment or deposition of biological macromolecules/microorganisms and to prevent the subsequent growth and multiplication of adhered microbes [8].

To date, various polymers have been used to suppress nonspecific interactions in cells; these include polyethylene glycol (PEG) [9–13], zwitterionic species [14–17], peptides [18], polypeptides [19], and glycocalyx [20]. These polymers are highly hydrophilic and flexible, and they exhibit nonadherent and nonbiofouling properties. Furthermore, the immobilization of these polymers on antibiofouling surfaces has been achieved with various methods, including self-assembly [21], electro-grafting [22], and polymerization; in this regard, atom transfer radical polymerization [23] and reversible addition–fragment chain transfer polymerization have also recently been employed [24]. Among these methods, photoimmobilization is interesting because it enables the covalent immobilization of the antibiofouling layer [25]. Therefore, some types of photoimmobilizable (reactive) polymers containing PEG [26,27], zwitterions (such as phosphorylcholine) [28–30], sulfobetaine [31], carbobetaine [32], pullulan [33], sulfated hyaluronic acid [34], polyvinyl alcohol [35] and polyacrylate derivatives [36] have been used for the preparation of antibiofouling surfaces.

Among the photoreactive polymers, photoreactive antifouling acrylic polymers grafted with PEG have been used as microarray matrixes [37–43] and are now commercially employed in allergy diagnosis (DropScreen^{R}) [44,45]. In a previous study, photoreactive PEG was synthesized via the copolymerization of methacrylate-PEG and acryloyl 4-azidobenzene. The photoreactive polymer was photoimmobilized on plastic, glass, and titanium surfaces for antibiofouling surface modification [26]. This immobilization technique is indeed extremely useful for surface antibiofouling modification due to its convenience. The modified surface significantly reduces interactions with proteins and can be used for protein immobilization via photo-induced crosslinking [26].

However, owing to the low hydrophilicity of the polymethacrylate backbone, the water solubility of these polymers is relatively low and further decreases following an increase in the number of azidophenyl groups [13,27]. To enhance water solubility, we synthesized a PEG-based photoreactive polymer composed of ethylene oxide and azidophenyl-coupled ethylene oxide. However, its water solubility was still low. Therefore, in this study, co-immobilization with PEG-carrying ethylene oxide was performed to enhance its water solubility and photoreactivity, and the resulting antibiofouling properties were investigated.

2. Materials and Methods

2.1. Materials

4(Glycidyloxymethyl)azidobenzene (AzPheEO) was prepared according to our previous report [21]. Methoxy-PEG epoxide (mPEG-EPO, Mn = 350 and 750) was purchased from Biochempeg Scientific (Boston, MA, USA). Tetrabutylammonium bromide (TBAB), ethanol, methanol, *n*-hexane, and *N*,*N*-dimethylformamide were purchased from FUJIFILM Wako Pure Chemical (Osaka, Japan). Ethylene oxide (EO, 1.0 mmol/L toluene solution), 4-azidobenzoic acid, lithium bromide, and triisobutyl aluminum (i-Bu_3Al, 1.0 mol/L toluene solution) were purchased from Tokyo Chemical Industry (Tokyo, Japan). Tissue culture polystyrene dishes were purchased from Iwaki (Tokyo, Japan). Alexa488-conjugated immunoglobulin G (Alexa488–IgG), fetal bovine serum (FBS), and trypsin were purchased from Thermo Fisher Scientific (Waltham, MA, USA). A penicillin–streptomycin solution was purchased from Nacalai Tesque (Kyoto, Japan).

2.2. Copolymerization of EO, AzPheEO, and mPEG-EPO

First, EO was copolymerized with AzPheEO and mPEG-EPO (Scheme 1). For this, TBAB, AzPheEO, and mPEG-EPO were dried under vacuum for 2 h, after which they were exposed to dry nitrogen. Toluene was added to the flask to dissolve mPEG-EPO. Subsequently, the EO solution and i-Bu_3Al were added to the flask in an ice bath. The solution was stirred for copolymerization at 25 °C in the dark for 18 h. Methanol was added to the solution, and the solvent was removed under reduced pressure. The crude

compound was dissolved in acetone, and the solution was dialyzed against water for three days. The resulting polymer was then freeze-dried and is referred to as AzPEGx [y], where x and y represent the Mn and feed ratio of mPEG-EO, respectively. The obtained AzPEGx [y] polymer was characterized via ^{1}H-nuclear magnetic resonance (NMR) spectroscopy (JNM-ECZ400R, 400 MHz, JEOL, Tokyo, Japan) in chloroform, as well as via gel permeation chromatography (GPC; JASCO, Tokyo, Japan). The system was equipped with a refractive index detector (RI-2032, JASCO, Tokyo, Japan) and two columns (SB-803 HQ and SB804 HQ; Showa Denko, Tokyo, Japan) in dimethylformamide (DMF) containing 10 mM lithium bromide.

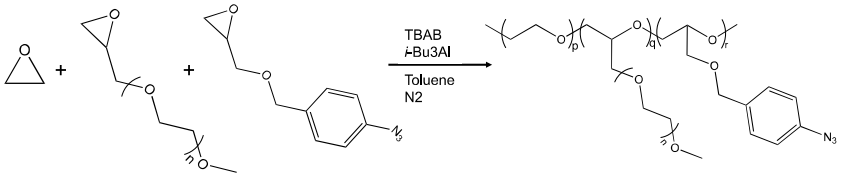

Scheme 1. Preparation of photoreactive polyethylene glycol-grafted polyethylene glycol.

Furthermore, the ultraviolet (UV) absorbance spectra (V−750, JASCO, Tokyo, Japan) of the polymers and 4-azidobenzoic acid were obtained. The polymer and 4-azidobenzoic acid were dissolved in a mixture of ethanol/water (0.1 wt.%). The UV absorbance of each solution was measured between 200 and 400 nm.

2.3. Contact Angle Measurements

An unpatterned AzPEGx [y]-coated plate was placed on the stage of a CA−W Automatic Contact Angle Meter (Kyowa Interface Science, Saitama, Japan), and a drop of water (0.1 µL) was placed on the sample surface. The contact angle of the drop with respect to the surface was measured at room temperature. At least 10 angles were measured in different areas, and the results are expressed as the average values with the standard deviation.

2.4. Photoimmobilization of AzPEGx [y]

The photoimmobilization procedure is illustrated in Scheme 2a. The prepared AzPEGx [y] polymer (0.25 wt.% in water, 100 µL) was placed on polystyrene dishes (for tissue culture, Iwaki, Tokyo, Japan). These dishes were then dried at 40 °C under vacuum. A stainless steel punch sheet with 500 µm holes (Yasutoyo Trading, Tokyo, Japan) was placed on the substrate as a photomask, and the surface was exposed to UV light for 20 s using a photoirradiator (45 mW/cm^2 at 270 nm, L5662 UV spotlight source, Hamamatsu photonics, Hamamatsu, Japan). The surface was then washed with water and subsequently immersed in water for one day. The plates were dried under vacuum and stored in a dark desiccator until further use. To confirm the photoimmobilization of the polymer on polystyrene, the AzPEGx [y] (0.25 wt.%, 90 µL) solution was mixed with Alexa488–IgG (0.25 wt.%, 10 µL) and co-immobilized on the plate (Scheme 2b). Furthermore, fluorescence images were obtained using a fluorescence microscope (Olympus, Tokyo, Japan).

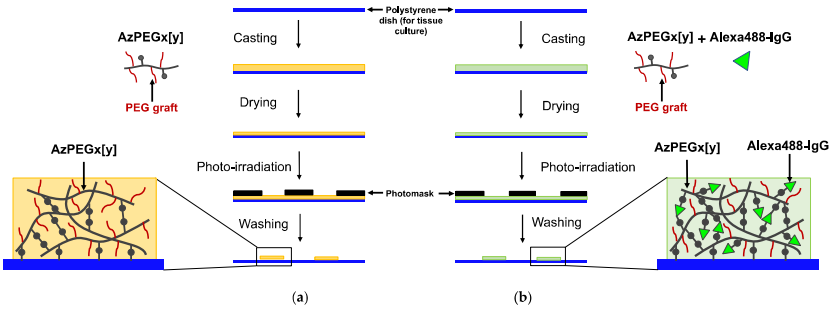

Scheme 2. Micropatterning of the prepared AzPEGx [y] polymer (**a**) without and (**b**) with fluorescent-labeled IgG. The circular micropattern was identical to the diameter of the photomask holes.

2.5. Protein Adsorption

A solution of Alexa488–IgG (0.25 wt.%, 100 μL) was placed onto the AzPEGx [y]-coated surfaces and allowed to stand for 2 h at 25 °C. The substrates were then washed with water and immersed in water overnight. The substrates were then dried under vacuum, and fluorescence images were acquired using a fluorescence microscope (Olympus).

2.6. Cell Adhesion

Mouse fibroblast (3T3) cells (Japanese Collection of Research Bioresources, Osaka, Japan) were cultured in Dulbecco's Modified Eagle's Medium (Sigma-Aldrich, St. Louis, MO, USA) supplemented with 10% FBS and antibiotics (penicillin (100 units/mL) and streptomycin (100 μg/mL)). The cells were harvested using a 0.25% trypsin–ethylenediaminetetraacetic acid solution. The cell suspension (1.0×10^6 cells) was seeded onto the AzPEGx [y]-coated dishes and incubated at 37 °C in a humidified atmosphere with 5% CO_2 for 24 h. After incubation, the dishes were washed thrice with phosphate-buffered saline, and the cells were observed using a phase-contrast microscope (Olympus, Tokyo, Japan).

3. Results and Discussion

3.1. Synthesis of Photoreactive PEG (AzPEGx [y])

EO was copolymerized with AzPheEO and mPEG-EPO via activated ring-opening polymerization. TBAB was used as an initiator and i-Bu_3Al as the monomer activator to generate polymers with various PEG chain lengths and azidophenyl group contents.

Table 1 summarizes the AzPEGx [y] polymers synthesized via the copolymerization of AzPheEO with EO and two different molecular weights of mPEG-EPO. The azidophenyl group content was confirmed via UV absorbance spectroscopy. The molecular weights and polydispersity indices (PDIs) of the polymers were analyzed using GPC. The AzPheEO and mPEG-EPO contents in the copolymers were found to be lower than those in the feed. The decrease in the ratio of mPEG-EPO was greater than that of AzPheEO. This can be attributed to the high steric hindrance of the PEG moiety in mPEG-EPO. The PDI increased at a lower proportion of the azidophenyl group due to the steric hindrance of mPEG-EPO. In the absence of mPEG-EPO, the polymer did not dissolve in pure water. Therefore, Az [10] was not used for further investigations.

Table 1. Characterization of the prepared polymers.

Code	Feed (mol/%)				Composition (mol%) [a]			Mw [b]	PDI [b]
–	AzPhe-EO	EO	mPEG-EPO	mPEG-EPO MW	AzPhe-EO	EO	mPEG-EPO	–	–
Az [10] [c]	10	90	0	–	9.6	90.4	0	8700	1.6
AzEG350 [10]	10	80	10	350	8.4	85.8	5.8	7800	1.7
AzPEG750 [5]	10	85	5	750	7.4	89.8	2.8	13,000	1.9
AzPEG750 [1]	10	89	1	750	9.9	89.5	0.6	12,000	1.7

[a] Determined via ^{1}H NMR. [b] Determined via GPC. [c] No PEG-grafted polymer.

The ^{1}H NMR spectrum of the synthesized AzPEG750 [5] is presented in Figure 1. Peaks corresponding to the protons of the PEG ethylene group units and methyl protons of the grafted PEG chain were observed at 3.6 and 3.35 ppm, respectively. In addition, peaks corresponding to benzylic protons, aromatic protons, and azidophenyl units were observed at 4.54, 7.37, and 7.05 ppm, respectively.

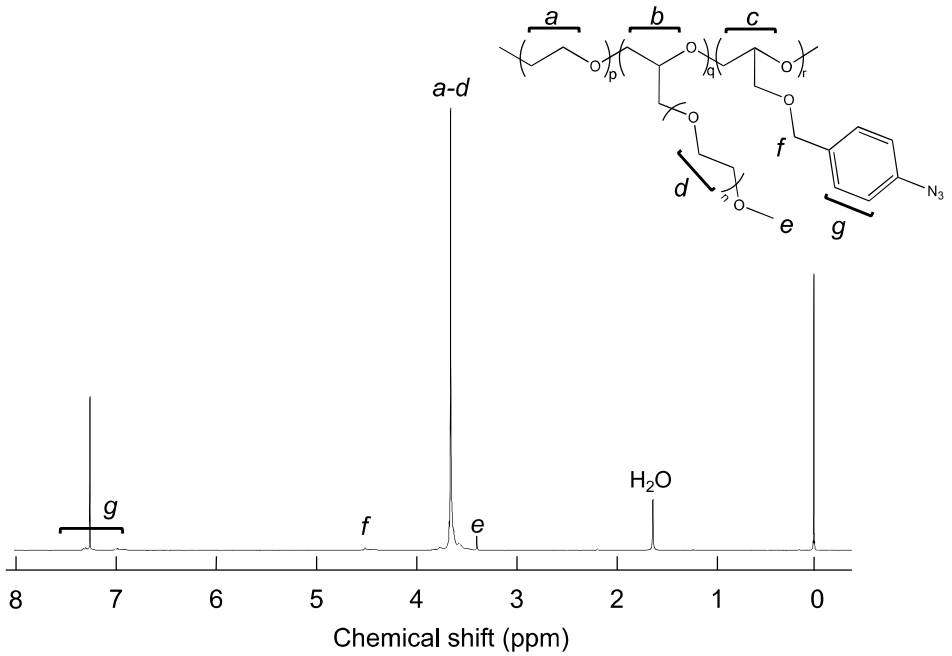

Figure 1. ^{1}H NMR spectrum of AzPEG750 [5] (solvent: chloroform–d).

The UV absorbance spectrum of AzPEG750 [5] and 4-azidobenzoic acid is presented in Figure 2. The peak of the azidophenyl group slightly shifted to a lower wavelength. The azidophenyl group was considered to be in the hydrophobic region of the polymer.

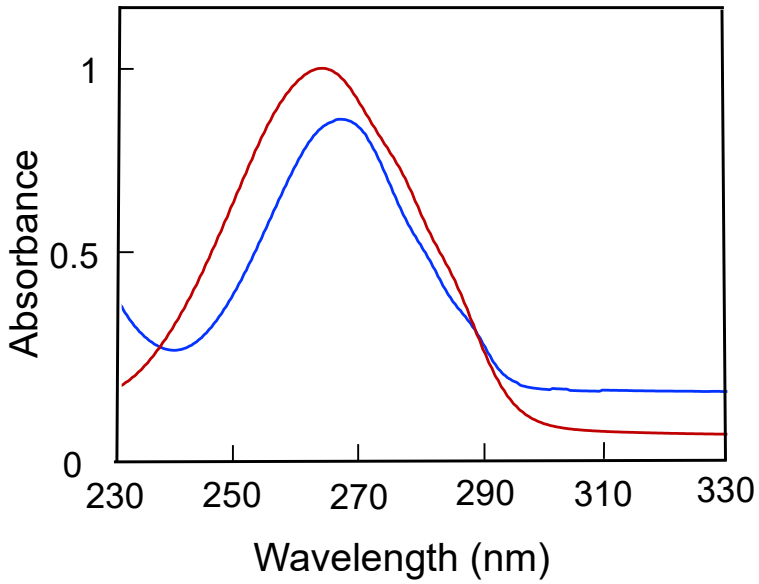

Figure 2. UV absorbance spectra of AzPEG750 [5] (red) and 4-azidobenzoic acid (blue) in ethanol/water (0.1 wt.%).

The molecular weight and distribution of AzPEGx [y] were determined via GPC (Figure 3). The prepared AzPEGx [y] polymer appeared as a unimodal trace. This revealed an almost complete polymerization between mPEG-EPO and AzPheEO.

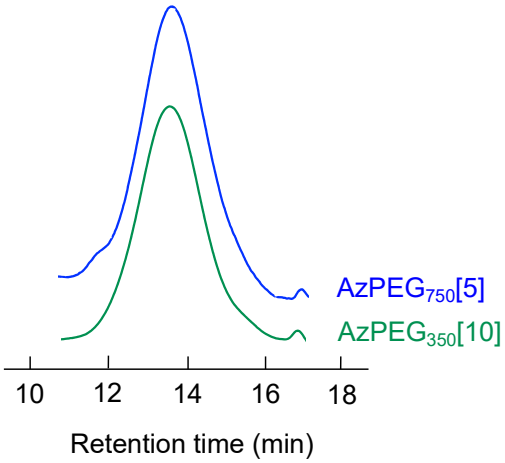

Figure 3. GPC charts of AzPEG350 [10] (green) and AzPEG750 [5] (blue), proving that the azidophenyl group was successfully synthesized via the copolymerization of AzPheEO with EO and mPEG-EPO. Eluent: DMF containing 10 mmol/L LiBr. Flow rate (1 mL/min).

3.2. Contact Angle Measurements

Water contact angle measurements were performed to investigate the surface properties of AzPEGx [y] immobilized without a photomask (unpatterned surfaces). As indicated in Table 2, the contact angle on the photoimmobilized surface was lower than that on the non-immobilized surface. This alteration in the contact angle was assumed to be caused by PEG coverage. The hydrophilicity of the immobilized surface was almost independent of the copolymer.

Table 2. Contact angles on different surfaces.

Surface	Contact Angle (°) ± Standard Deviation
Polystyrene (for tissue culture)	70.7 ± 2.1
Polystyrene with AzPEG350 [10]	41.1± 1.8
Polystyrene with AzPEG750 [5]	41.2 ± 1.6

3.3. Formation of Micropatterns

According to Scheme 2b, AzPEGx [y] was micropatterned on the polystyrene surface, as presented in Figure 4. Mixed Alexa488–IgG was co-immobilized with AzPEGx [y] after UV exposure, and the immobilized pattern was the same as that on the photomask. Notably, upon UV irradiation, the highly active nitrenes produced from the azidophenyl moieties randomly attacked the polymer, proteins, and substrate. Consequently, polymer–polymer crosslinks of AzPEGx [y]–AzPEGx [y], AzPEGx [y]–Alexa488–IgG, and AzPEGx [y]–polystyrene substrates were obtained (Scheme 2b).

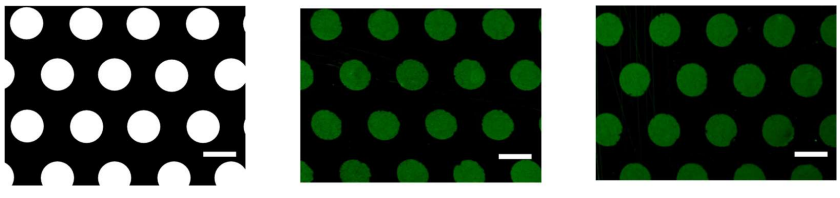

(**a**) (**b**) (**c**)

Figure 4. (**a**) Phase-contrast image of photomask. (**b**) Micropatterning test of AzPEG350 [10] and (**c**) micropatterning test of AzPEG750 [5] performed using photomask. The micropattern plate had two different regions, as indicated by the green and dark sections. In the photomask, the green section allowed UV light to enter the AzPEGx [y]–Alexa488IgG complex, resulting in photoimmobilization, which was not possible in the dark sections. Scale bars: 500 μm.

3.4. Protein Adsorption

To assess the nonspecific adsorption of proteins on immobilized PEG surfaces, a fluorescent protein (Alexa488-conjugated IgG) was added to the surface prepared based on Scheme 2a, and the resulting structure was examined via fluorescence microscopy (Figure 5). The immobilized AzPEGx [y] suppressed the adsorption of the fluorescent-labeled proteins. The suppression effect did not significantly depend on the nature of AzPEGx [y]. These results revealed that the immobilized surface suppressed nonspecific protein adsorption.

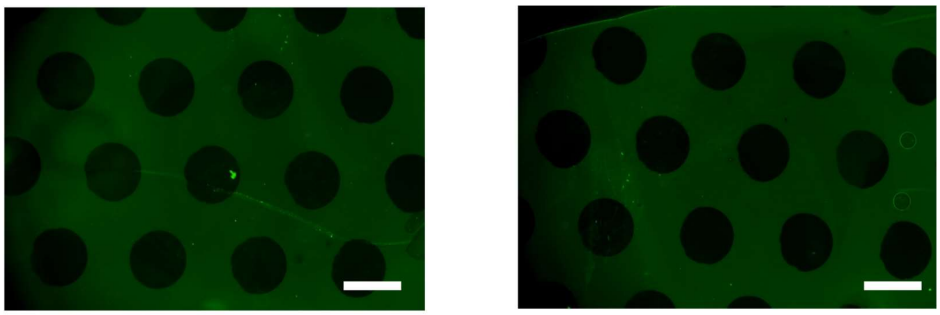

(**a**) (**b**)

Figure 5. Fluorescence microscopy images of (**a**) AzPEG350 [10]– and (**b**) AzPEG750 [5]–coated micropatterned polystyrene plates after the adsorption of Alexa488-conjugated IgG. Scale bars: 500 μm.

3.5. Cell Adhesion

Furthermore, cell adhesion onto the AzPEGx [y]-coated polystyrene substrates was evaluated using 3T3 mouse fibroblast cells (Figure 6). For this, 3T3 cells were cultured on the micropatterned surfaces for 24 h. The non-cell-adhered pattern was found to be identical to the hole pattern on the stainless steel photomask. The cells only adhered to the non-UV-exposed areas. The prepared AzPEGx [y] polymer almost completely suppressed cell adhesion due to the introduction of hydrophilic PEG. The suppressive effect on cell adhesion did not depend on AzPEGx [y].

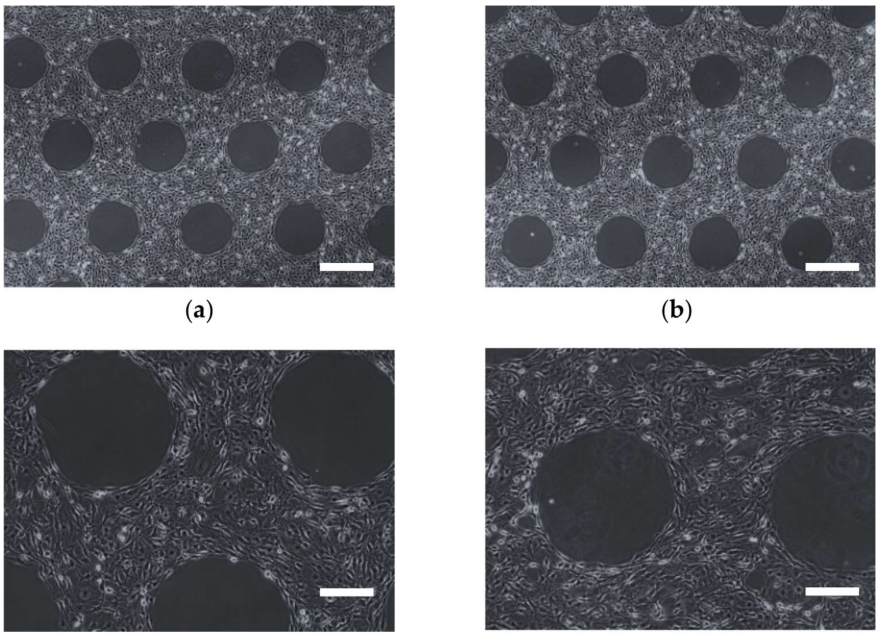

(**a**) (**b**)

(**c**) (**d**)

Figure 6. Phase-contrast images of 3T3 mouse fibroblast cells cultured on the AzPEG350 [10]-coated (**a**,**c**) and AzPEG750 [5]-coated (**b**,**d**) micropatterned polystyrene plates at 0.25 wt.%. Scale bars: (**a**,**b**) 500 μm; (**c**,**d**) 200 μm.

Notably, PEG is a representative antibiofouling polymer. PEG immobilization on biomaterial surfaces is typically conducted for various purposes. Previously, we prepared a PEG-based polymer containing azidophenyl groups in the side chains [21]. However, the polymer was not completely soluble in pure water. Therefore, copolymerization with mPEG-EPO was performed herein, and the resulting copolymer was found to be completely soluble in pure water; it was mixed with a fluorescent protein and immobilized as a mixture on the substrate. The antibiofouling effect was attributed to the hydrophilicity and repulsion of the amphiphilic and flexible grafted polymer chains. Such a copolymer may be useful for micropatterning water-soluble proteins and biomacromolecules with mixing.

Photoreaction is an effective and reasonable method for modifying polymer materials on biomedical devices through covalent binding. The new photoreactive PEG can be coated with water and fixed on the various types of organic substrate by simple photoirradiation. Through the photochemical process, a stable anti-biofouling interface between the polymer and the biomedical devices will be prepared for medical implants, blood contacting tubes, wearable sensors, organ-on-a-chips, microfluidics, and microarray chips.

4. Conclusions

In this study, we designed azidophenyl-modified and PEG-grafted PEG (AzPEGx [y]) as photoreactive polymers for surface antibiofouling modifications. Photoreactive polymers were successfully synthesized using AzPheEO copolymerized with mPEG-EPO and EO. AzPEGx [y] significantly reduced the interactions with biological components, such as proteins and cells. Hence, this polymer, with desirable antibiofouling properties, can be used for surface modifications in biomedical applications.

Author Contributions: Conceptualization, Y.I.; methodology, J.A.; validation, M.H.O. and J.A.; formal analysis, M.H.O. and J.A.; investigation, M.H.O. and J.A.; writing–original draft preparation, M.H.O. and J.A.; writing–review and editing, Y.I.; visualization, Y.I.; supervision, Y.I.; project administration, J.A.; funding acquisition, Y.I. All authors have read and agreed to the published version of the manuscript.

Funding: This research received no external funding.

Institutional Review Board Statement: Not applicable.

Data Availability Statement: All data are available upon reasonable request from the corresponding authors.

Acknowledgments: Mahmoud H. Othman was financially supported by the Junior Research Associate (JRA) program from RIKEN.

Conflicts of Interest: The authors declare no conflict of interest.

References

1. Jiang, C.; Wang, G.; Hein, R.; Liu, N.; Luo, X.; Davis, J.J. Antifouling Strategies for Selective in Vitro and in Vivo Sensing. *Chem. Rev.* **2020**, *120*, 3852–3889. [CrossRef] [PubMed]
2. Zhang, P.; Ratner, B.D.; Hoffman, A.S.; Jiang, S. Nonfouling Surfaces. In *Biomaterials Science*; Elsevier: Amsterdam, The Netherlands, 2020; pp. 507–513.
3. Kozai, T.D.Y.; Langhals, N.B.; Patel, P.R.; Deng, X.; Zhang, H.; Smith, K.L.; Lahann, J.; Kotov, N.A.; Kipke, D.R. Ultrasmall Implantable Composite Microelectrodes with Bioactive Surfaces for Chronic Neural Interfaces. *Nat. Mater.* **2012**, *11*, 1065–1073. [CrossRef]
4. Schwerdt, H.N.; Zhang, E.; Kim, M.J.; Yoshida, T.; Stanwicks, L.; Amemori, S.; Dagdeviren, H.E.; Langer, R.; Cima, M.J.; Graybiel, A.M. Cellular-Scale Probes Enable Stable Chronic Subsecond Monitoring of Dopamine Neurochemicals in a Rodent Model. *Commun. Biol.* **2018**, *1*, 144. [CrossRef] [PubMed]
5. Cash, K.J.; Clark, H.A. Phosphorescent Nanosensors for in Vivo Tracking of Histamine Levels. *Anal. Chem.* **2013**, *85*, 6312–6318. [CrossRef] [PubMed]
6. Dubach, J.M.; Harjes, D.I.; Clark, H.A. Fluorescent Ion-Selective Nanosensors for Intracellular Analysis with Improved Lifetime and Size. *Nano Lett.* **2007**, *7*, 1827–1831. [CrossRef] [PubMed]

7. Zhen, X.; Zhang, C.; Xie, C.; Miao, Q.; Lim, K.L.; Pu, K. Intraparticle Energy Level Alignment of Semiconducting Polymer Nanoparticles to Amplify Chemiluminescence for Ultrasensitive in Vivo Imaging of Reactive Oxygen Species. *ACS Nano* **2016**, *10*, 6400–6409. [CrossRef] [PubMed]
8. Zhang, H.; Zhu, S.; Yang, J.; Ma, A. Advancing Strategies of Biofouling Control in Water-Treated Polymeric Membranes. *Polymers.* **2022**, *14*, 1167. [CrossRef]
9. Lowe, S.; O'Brien-Simpson, N.M.; Connal, L.A. Antibiofouling Polymer Interfaces: Poly (Ethylene Glycol) and Other Promising Candidates. *Polym. Chem.* **2015**, *6*, 198–212. [CrossRef]
10. Emilsson, G.; Schoch, R.L.; Feuz, L.; Höök, F.; Lim, R.Y.H.; Dahlin, A.B. Strongly Stretched Protein Resistant Poly (Ethylene Glycol) Brushes Prepared by Grafting-To. *ACS Appl. Mater. Interfaces* **2015**, *7*, 7505–7515. [CrossRef] [PubMed]
11. Herzberger, J.; Niederer, K.; Pohlit, H.; Seiwert, J.; Worm, M.; Wurm, F.R.; Frey, H. Polymerization of Ethylene Oxide, Propylene Oxide, and Other Alkylene Oxides: Synthesis, Novel Polymer Architectures, and Bioconjugation. *Chem. Rev.* **2016**, *116*, 2170–2243. [CrossRef] [PubMed]
12. Nagasaki, Y. Construction of a Densely Poly (Ethylene Glycol)-Chain-Tethered Surface and Its Performance. *Polym. J.* **2011**, *43*, 949–958. [CrossRef]
13. Pasut, G.; Veronese, F.M. State of the Art in PEGylation: The Great Versatility Achieved after Forty Years of Research. *J. Control. Release* **2012**, *161*, 461–472. [CrossRef] [PubMed]
14. Ishii, T.; Wada, A.; Tsuzuki, S.; Casolaro, M.; Ito, Y. A New Nonbiofouling Polyzwitterion Including L-Histidine. *Biomacromolecules* **2007**, *8*, 3340–3344. [CrossRef] [PubMed]
15. Schlenoff, J.B. Zwitteration: Coating Surfaces with Zwitterionic Functionality to Reduce Nonspecific Adsorption. *Langmuir* **2014**, *30*, 9625–9636. [CrossRef]
16. He, M.; Gao, K.; Zhou, L.; Jiao, Z.; Wu, M.; Cao, J.; You, X.; Cai, Z.; Su, Y.; Jiang, Z. Zwitterionic Materials for Antifouling Membrane Surface Construction. *Acta Biomater.* **2016**, *40*, 142–152. [CrossRef] [PubMed]
17. Jiang, S.; Ishihara, K.; Ji, J. Special Issue on Zwitterionic Materials. *Acta Biomater.* **2016**, *40*, iv. [CrossRef]
18. Sakala, G.P.; Reches, M. Peptide-based Approaches to Fight Biofouling. *Adv. Mater. Interfaces* **2018**, *5*, 1800073. [CrossRef]
19. Leng, C.; Buss, H.G.; Segalman, R.A.; Chen, Z. Surface Structure and Hydration of Sequence-Specific Amphiphilic Polypeptoids for Antifouling/Fouling Release Applications. *Langmuir* **2015**, *31*, 9306–9311. [CrossRef]
20. Ham, H.O.; Park, S.H.; Kurutz, J.W.; Szleifer, I.G.; Messersmith, P.B. Antifouling Glycocalyx-Mimetic Peptoids. *J. Am. Chem. Soc.* **2013**, *135*, 13015–13022. [CrossRef]
21. Cui, M.; Wang, Y.; Wang, H.; Wu, Y.; Luo, X. A Label-Free Electrochemical DNA Biosensor for Breast Cancer Marker BRCA1 Based on Self-Assembled Antifouling Peptide Monolayer. *Sens. Actuators B Chem.* **2017**, *244*, 742–749. [CrossRef]
22. Jiang, C.; Alam, M.T.; Parker, S.G.; Darwish, N.; Gooding, J.J. Strategies to Achieve Control over the Surface Ratio of Two Different Components on Modified Electrodes Using Aryldiazonium Salts. *Langmuir* **2016**, *32*, 2509–2517. [CrossRef] [PubMed]
23. Riedel, T.; Hageneder, S.; Surman, F.; Pop-Georgievski, O.; Noehammer, C.; Hofner, M.; Brynda, E.; Rodriguez-Emmenegger, C.; Dostálek, J. Plasmonic Hepatitis B Biosensor for the Analysis of Clinical Saliva. *Anal. Chem.* **2017**, *89*, 2972–2977. [CrossRef]
24. Kitano, H.; Kondo, T.; Kamada, T.; Iwanaga, S.; Nakamura, M.; Ohno, K. Anti-Biofouling Properties of an Amphoteric Polymer Brush Constructed on a Glass Substrate. *Colloids Surf. B Biointerfaces* **2011**, *88*, 455–462. [CrossRef] [PubMed]
25. Kallitsis, K.; Thuau, D.; Soulestin, T.; Brochon, C.; Cloutet, E.; Dos Santos, F.D.; Hadziioannou, G. Photopatternable High-k Fluoropolymer Dielectrics Bearing Pendent Azido Groups. *Macromolecules* **2019**, *52*, 5769–5776. [CrossRef]
26. Ito, Y.; Hasuda, H.; Sakuragi, M.; Tsuzuki, S. Surface Modification of Plastic, Glass and Titanium by Photoimmobilization of Polyethylene Glycol for Antibiofouling. *Acta Biomater.* **2007**, *3*, 1024–1032. [CrossRef] [PubMed]
27. Akimoto, J.; Park, S.J.; Obuse, S.; Kawamoto, M.; Tamura, M.; Nandakumar, A.; Kobatake, E.; Ito, Y. Synthesis of Photoreactive Poly (Ethylene Oxide) s for Surface Modification. *ACS Appl. Bio Mater.* **2020**, *3*, 5941–5947. [CrossRef]
28. Konno, T.; Hasuda, H.; Ishihara, K.; Ito, Y. Photo-Immobilization of a Phospholipid Polymer for Surface Modification. *Biomaterials.* **2005**, *26*, 1381–1388. [CrossRef] [PubMed]
29. Lin, X.; Fukazawa, K.; Ishihara, K. Photoreactive Polymers Bearing a Zwitterionic Phosphorylcholine Group for Surface Modification of Biomaterials. *ACS Appl. Mater. Interfaces* **2015**, *7*, 17489–17498. [CrossRef]
30. Fukazawa, K.; Tsuji, K.; Inoue, Y.; Ishihara, K. Direct Photoreactive Immobilization of Water-Soluble Phospholipid Polymers on Substrates in an Aqueous Environment. *Colloids Surf. B Biointerfaces* **2021**, *199*, 111507. [CrossRef] [PubMed]
31. Sakuragi, M.; Tsuzuki, S.; Obuse, S.; Wada, A.; Matoba, K.; Kubo, I.; Ito, Y. A Photoimmobilizable Sulfobetaine-Based Polymer for a Nonbiofouling Surface. *Mater. Sci. Eng. C* **2010**, *30*, 316–322. [CrossRef]
32. Sakuragi, M.; Tsuzuki, S.; Hasuda, H.; Wada, A.; Matoba, K.; Kubo, I.; Ito, Y. Synthesis of a Photoimmobilizable Histidine Polymer for Surface Modification. *J. Appl. Polym. Sci.* **2009**, *112*, 315–319. [CrossRef]
33. Hasuda, H.; Kwon, O.H.; Kang, I.-K.; Ito, Y. Synthesis of Photoreactive Pullulan for Surface Modification. *Biomaterials.* **2005**, *26*, 2401–2406. [CrossRef] [PubMed]
34. Chen, G.; Ito, Y.; Imanishi, Y.; Magnani, A.; Lamponi, S.; Barbucci, R. Photoimmobilization of Sulfated Hyaluronic Acid for Antithrombogenicity. *Bioconjug. Chem.* **1997**, *8*, 730–734. [CrossRef] [PubMed]
35. Ito, Y.; Nogawa, M.; Takeda, M.; Shibuya, T. Photo-Reactive Polyvinylalcohol for Photo-Immobilized Microarray. *Biomaterials* **2005**, *26*, 211–216. [CrossRef] [PubMed]

36. Ito, Y.; Nogawa, M. Preparation of a Protein Micro-Array Using a Photo-Reactive Polymer for a Cell-Adhesion Assay. *Biomaterials* **2003**, *24*, 3021–3026. [CrossRef]
37. Ito, Y. Photoimmobilization for Microarrays. *Biotechnol. Prog.* **2006**, *22*, 924–932. [CrossRef]
38. Ito, Y. Microarray Chips (in Vitro Diagnosis). In *Photochemistry for Biomedical Applications*; Springer: Berlin/Heidelberg, Germany, 2018; pp. 85–106.
39. Matsudaira, T.; Tsuzuki, S.; Wada, A.; Suwa, A.; Kohsaka, H.; Tomida, M.; Ito, Y. Automated Microfluidic Assay System for Autoantibodies Found in Autoimmune Diseases Using a Photoimmobilized Autoantigen Microarray. *Biotechnol. Prog.* **2008**, *24*, 1384–1392. [CrossRef]
40. Tsuzuki, S.; Wada, A.; Ito, Y. Photo-immobilization of Biological Components on Gold-coated Chips for Measurements Using Surface Plasmon Resonance (SPR) and a Quartz Crystal Microbalance (QCM). *Biotechnol. Bioeng.* **2009**, *102*, 700–707. [CrossRef]
41. Sivakumar, P.M.; Moritsugu, N.; Obuse, S.; Isoshima, T.; Tashiro, H.; Ito, Y. Novel Microarrays for Simultaneous Serodiagnosis of Multiple Antiviral Antibodies. *PLoS ONE* **2013**, *8*, e81726. [CrossRef]
42. Kashiwagi, H.; Morishima, N.; Obuse, S.; Isoshima, T.; Akimoto, J.; Ito, Y. SARS-CoV-2 Proteins Microarray by Photoimmobilization for Serodiagnosis of the Antibodies. *Bull. Chem. Soc. Jpn.* **2021**, *94*, 2435–2443. [CrossRef]
43. Akimoto, J.; Kashiwagi, H.; Morishima, N.; Obuse, S.; Isoshima, T.; Kageyama, T.; Nakajima, H.; Ito, Y. Rapid and Quantitative Detection of Multiple Antibodies against SARS-CoV-2 Mutant Proteins by Photo-Immobilized Microarray. *Anal. Sci.* **2022**, *38*, 1313–1321. [CrossRef] [PubMed]
44. Ito, Y.; Moritsugu, N.; Matsue, T.; Mitsukoshi, K.; Ayame, H.; Okochi, N.; Hattori, H.; Tashiro, H.; Sato, S.; Ebisawa, M. An Automated Multiplex Specific IgE Assay System Using a Photoimmobilized Microarray. *J. Biotechnol.* **2012**, *161*, 414–421. [CrossRef] [PubMed]
45. Ohyama, K.; Omura, K.; Ito, Y. A Photo-Immobilized Allergen Microarray for Screening of Allergen-Specific IgE. *Allergol. Int.* **2005**, *54*, 627–631. [CrossRef]